AN ABSTRACT OF THE THESIS OF

Gerardo E. Barreda for the degree of Master of Science in Radiation Health Physics presented on December 28, 2010.
Title: An Investigation into the Feasibility of Neutron Activating Holmium-Loaded, Polymeric Microspheres in the Thermal Column of a TRIGA Reactor Using MCNP5 Simulation Models.

Abstract approved:

. _____ .
Jack Higginbotham

In intra-arterial radioembolization, nano- and micro-scaled carriers are used in patients with liver tumors that cannot be removed by surgery to deliver various radioisotopes with the aim of improving the outcome of tumor radiotherapy, of minimizing dose to healthy tissue, and of improving the quality of the diagnosis and imaging. In this technique, radioisotopes are incorporated in either nanospheres or microspheres for delivery. The synthesis of these may be performed either using the isotope in its radioactive form or nonradioactive form; however, if the synthesis is performed using non-radioactive isotopes, a subsequent activation by neutron bombardment in a nuclear reactor is required.

This investigation focused on neutron-activation simulations using computer models of microspheres loaded with a holmium acetylacetonate (HoAcAc) complex in a polymeric matrix that are used for intra-arterial radioembolization therapy of liver cancer. The polymer matrix is made of poly ($_{L}$-lactic acid) (PLLA) which is both biodegradable and biocompatible. In

addition, as a requirement for therapeutic applications of these microspheres, not only their diameter must be within a range between 20 μm and 50 μm, but also before administration to a patient, they must be neutron-activated by turning holmium-165 into holmium-166.

The main objective of this investigation was to minimize the energy deposited by neutrons and gammas produced by fission and both fission and neutron activation reactions, respectively, that would result in damages to both the microsphere's polymeric matrix and holmium complex. To accomplish this objective, Monte Carlo N-Particle models were created to perform the following simulations: (1) microspheres loaded with a HoAcAc complex in a polymeric matrix were exposed to a neutron flux in the thermal column of a TRIGA reactor while arranged in a sheet-shaped packing configuration, and, similarly, (2) while arranged in a pile-shaped packing configuration, microspheres also loaded with a HoAcAc complex in a polymeric matrix were also exposed to the same neutron flux in the thermal column. Then, results from both types of simulations were analyzed and were compared.

An Investigation into the Feasibility of Neutron Activating Holmium-Loaded, Polymeric Microspheres in the Thermal Column of a TRIGA Reactor Using MCNP5 Simulation Models.

By

Gerardo E. Barreda

A THESIS

submitted to

Oregon State University

In partial fulfillment of
the requirements for the
degree of

Master of Science

Presented December 28, 2010
Commencement June 2011

Master of Science thesis of Gerardo E. Barreda presented on December 28, 2010.

APPROVED:

. .

Major Professor, representing Radiation Health Physics

. .

Head of the Department of Nuclear Engineering and Radiation Health Physics

. .

Dean of the Graduate School

I understand that my thesis will become part of the permanent collection of Oregon State University libraries. My signature below authorizes release of my thesis to any reader upon request.

. .

Gerardo E. Barreda, Author

ACKNOWLEDGEMENTS

I would like to thank the following committee members for their knowledge and support: Dr. Steven Reese, Dr. Jack F. Higginbotham, Dr. Kenneth Krane, and Dr. Walter Loveland.

TABLE OF CONTENTS

TABLE OF CONTENTS (Continued)

Page

TABLE OF CONTENTS (Continued)

Page

LIST OF FIGURES

Figure Page

LIST OF FIGURES (Continued)

Figure Page

LIST OF FIGURES (Continued)

Figure Page

LIST OF FIGURES (Continued)

Figure Page

LIST OF TABLES

Table Page

An Investigation into the Feasibility of Neutron-Activating Holmium-Loaded, Polymeric Microspheres in the Thermal Column of a TRIGA Reactor Using MCNP5 Simulation Models.

1.0 Introduction

There are two general types of radiotherapy used to treat tumors: (1) external radiotherapy and (2) radionuclide-based therapies. In external radiotherapy, a beam of radiation, such as protons, neutrons, and electrons, is applied to the tumor; however, this type of treatment may damage healthy tissue, resulting in several side effects and considerable complications (*Ref. 1*). On the other hand, radionuclide-based therapies include intra-arterial radioembolization, metabolic radiotherapy, immunoradiotherapy, and brachytherapy (*Ref. 1*). Among these, both intra-arterial radioembolization and brachytherapy have the advantage of delivering radioisotopes, such as yttrium-90, rhenium-186, and holmium-166, locally in the tumor mass, avoiding healthy tissue by restricting the radiation dose to a defined tumor area (*Ref. 1*).

In intra-arterial radioembolization, nano- and micro-scaled carriers are used in patients with liver tumors that cannot be removed by surgery to deliver various radioisotopes with the aim of improving the outcome of tumor radiotherapy, of minimizing dose to healthy tissue, and of improving the quality of the diagnosis and imaging (*Ref. 1*). In this technique, radioisotopes are incorporated in either nanospheres or microspheres for delivery. The synthesis of these may be performed either using the isotope in its radioactive form or nonradioactive form; however, if the synthesis is performed using non-radioactive isotopes, a subsequent activation by neutron bombardment in a nuclear reactor is required (*Ref. 1*).

Among the most promising radioisotopes for radionuclide therapy applications is holmium-166, which can be obtained from the neutron activation of holmium-165 which has an abundance of 100% and a high neutron capture cross-section of 58 b and achieves high radioactivities in short activation times, as well (*Ref. 1*). Furthermore, among the useful properties of holmium-166 for radiotherapeutic applications include the following: (1) a maximum beta energy of 1.84 MeV, being high and sufficient for radionuclide-based therapy; (2) a physical half-life of 26.8 h, which is suitable for radiotherapy and transport; (3) a maximum radiation tissue diffusion range around 10 mm, satisfying internal radiotherapy applications; and (4) holmium-166 emits photons (81 keV, 6.2%), which are suitable for imaging (*Ref. 2*). Finally, various substances, such as albumin, glass, resin, and poly ($_L$-lactic acid) (PLLA) can be used to synthesize these particles.

This investigation focused on neutron-activation simulations using computer models of microspheres loaded with holmium acetylacetonate (HoAcAc) complex in a polymeric matrix that are used for intra-arterial radioembolization therapy of liver cancer. Treatment with radioactive microspheres is based on the following principle: once administered via a catheter through the hepatic artery, microspheres with a diameter between 20 and 50 μm will lodge themselves in the vascular bed of the liver, restricting the radiation to the tumor (*Ref. 2*). The polymer matrix is made of poly ($_L$-lactic acid) (PLLA) which is both biodegradable and biocompatible. In addition, as a requirement for therapeutic applications of these microspheres, before administration into a patient, they must be neutron-activated by turning holmium-165 into holmium-166, as illustrated in *Fig. 1.1* (*Ref. 1*).

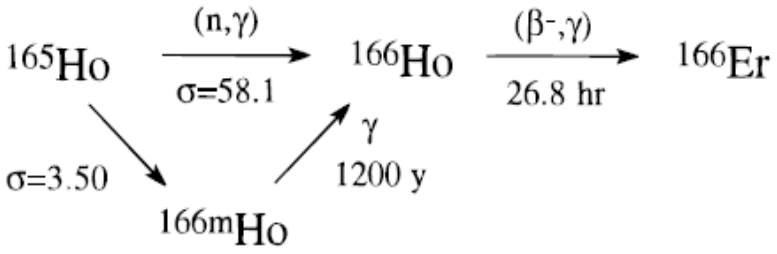

Figure 1.1-Neutron activation and decay path of holmium-165. (This figure was obtained from *Ref. 20*.)

It has been determined that, as a result of the activation of the microspheres in a nuclear reactor, the energy deposited by neutron irradiation, together with simultaneous generated *γ-rays*, as well as secondary *γ-rays* caused by *H(n,γ)* and *Ho(n,γ)* reactions, can result in damage to the PLLA matrix (*Ref. 3*). This damage is in the form of a decrease in the PLLA's molecular weight, caused by chain scission, resulting in changes of the matrix's physical properties. In addition, this damage may result in deformation, cracking, or even melting, increasing the probability of not only causing damage to the holmium acetylacetonate complex in the polymeric matrix, but also preventing the microspheres from lodging themselves around the hepatic tumor (*Ref. 3*).

The main objective of this investigation was to minimize the energy deposited by neutrons and gammas produced by both fission and neutron activation reactions, respectively, that would result in damages to both the microsphere's polymeric matrix and the holmium complex. To accomplish this objective, Monte Carlo N-Particle models were created to perform the following simulations: (1) microspheres loaded with a HoAcAc complex in a polymeric matrix were exposed to a neutron flux in the thermal column of a TRIGA reactor while arranged

in a sheet-shaped packing configuration, and, similarly, (2) while arranged in a pile-shaped packing configuration, microspheres also loaded with a HoAcAc complex in a polymeric matrix were also exposed to the same neutron flux in the thermal column. Then, results from both types of simulations were analyzed and were compared.

In addition to the main objective, results regarding neutron and photon energy depositions, dose, temperature change rates at microspheres' contact points, changes in enthalpy values of crystallization and melting, and melting point temperature changes obtained from both pile-shaped packing configuration simulations and sheet-shaped packing configuration simulations were compared; techniques that provided a uniform exposure of the microspheres to a neutron flux were determined; whether or not the magnitude of the neutron flux produced by a 1 MWt-rated TRIGA reactor was sufficient for neutron activating holmium-loaded microspheres to therapeutic activity levels was determined; and finally, the effects of changing both the material and the location of the activation vials in the thermal column during the neutron activation process were determined.

The motivation behind this investigation was to determine if the activity, the product yield, and the amount of radioactive holmium-loaded microspheres could have been increased by using the thermal column section of a TRIGA reactor instead of conventional ways of neutron activation, such as using either the rabbit pneumatic system or the rotating rack in which both temperature and neutron flux magnitude provide irradiation time and weight limitations, requiring the need for forced cooling.

2.0 Background

Liver metastases frequently occur during the progression of various solid tumors, such as colorectal cancers. External beam radiotherapy used in the treatment of hepatic malignancies is limited by the tolerance of the hepatic cells, which can tolerate doses of only up to 30 Gy for liver irradiation, making this treatment modality ineffective (*Ref. 2*). An alternative mode of therapy is the use of intra-arterially injected radioactive microspheres of a size sufficient to lodge in end-arterioles. The basis for such therapy is that tumors are usually rich in vasculature and that liver metastases are almost exclusively dependent on arterial blood supply, contrasting with a normal liver, which receives most of its flow from the portal vein (*Ref. 2*). This selectivity can also be increased by the use of vasoactive drugs, which cause vasoconstriction of the normal liver arterioles, but to which tumor vessels, lacking smooth muscles, are insensitive (*Ref. 2*).

The intra-arterial radioembolization treatment is based on the following principle: microspheres with a diameter between 20 and 50 μm lodge themselves in the vascular bed of the liver (*Ref. 2)*. The microspheres are delivered via a catheter through the hepatic artery, after the administration of a vasoactive drug. Owing to the high sensitivity of this technique, the radiation is mainly restricted to the tumor, with absorbed radiation doses varying between 50 and 150 Gy (*Ref. 2*).

2.1 Intra-Arterial Radioembolization Procedure

Intra-arterial radioembolization (RE) is a minimally invasive radiotherapy for liver tumors that cannot be removed by surgery. Currently, this type of cancer procedure is performed by injecting radioactive, yttrium-loaded microspheres into the hepatic artery using a catheter

(*Ref. 4*). The high-energy, beta-emitting, radioactive yttrium-loaded microspheres subsequently strand in the arterioles of the tumor, delivering a tumoricidal radiation dose. Currently, the only clinically available microspheres loaded with yittrium-90 for radioembolization are made of either glass or resin (*Ref. 4*). However, in order to eliminate leaching problems, yttrium-containing glass microspheres are preferred (*Ref. 5*).

Although considered a safe and an effective treatment, radioactive yttrium-loaded microspheres have the following disadvantages: their actual biodistribution cannot be accurately visualized, and the density of the microspheres is greater than the blood's, accounting for the considerable toxicity caused by backflow to surrounding tissues (*Ref. 4*). For these reasons, holmium-loaded, poly ($_{L}$-lactic acid) (PLLA) microspheres have been developed which combine the advantages of biocompatibility and of biodegradability with short physical half-life, natural abundance of ^{165}Ho (100%), and near-plasma density. However, the microspheres must be made radioactive by neutron activation of ^{165}Ho to yield ^{166}Ho (*Ref. 5*).

Holmium-166 not only emits high-energy beta particles to eradicate tumor cells, but it also emits low-energy (81 keV) photons, which allows for nuclear imaging, making visualization of the microspheres feasible (*Ref. 5*). This is very useful for the following reasons: prior to administration of the treatment dose, a small scout dose of radioactive, holmium-loaded microspheres can be administered for prediction of the distribution of the treatment dose, providing the theoretical advantage over radioactive yttrium-loaded microspheres for which the distribution assessment depends on a scout dose of technetium-99m albumin macroaggregates (^{99m}Tc-MAA) (*Ref. 4*). In addition, quantitative analysis of nuclear images would allow

assessment of the radiation dose delivered on both the tumor and the normal liver. Furthermore, holmium-166 is highly paramagnetic, making the microspheres capable of being visualized using magnetic resonance imaging (MRI), and it also has a high linear attenuation coefficient, allowing for visualization through *x-ray* computed tomography (CT) (*Ref. 5*). (CT images of bodily structures are formed based on their ability to block *x-ray* beams.) Finally, quantitative analysis of these MRI images is useful for both medium- and long-term monitoring of the intra-hepatic behavior of the microspheres (*Ref. 4*).

2.2 Administration of Radioactive Holmium-Loaded Microspheres

A typical administration system, as illustrated in *Fig. 2.1*, consists of polyethylene tube lines equipped with one-way valves, preventing backflow of microspheres in the lines. The lines are interconnected using a “Y-connector.” The system is connected to a catheter that is used to deliver the microspheres to the tumor area. To reduce the radiation dose to personnel, the vial containing the radioactive holmium-loaded microspheres is placed in a high-density, lead-glass vial shield (*Ref. 6*).

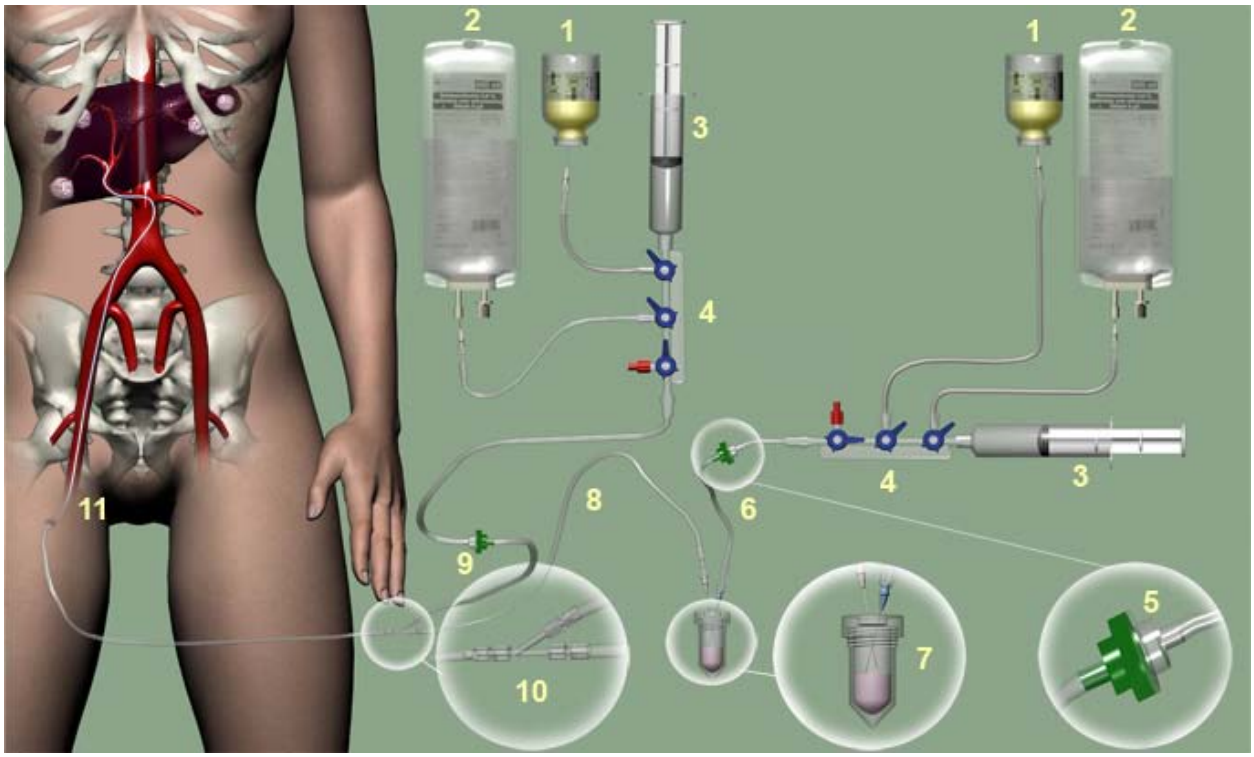

Figure 2.1-Microsphere administration system setup for the intra-arterial radioembolization treatment of hepatic cancer. (This figure was obtained from *Ref. 6*.)

After a right femoral artery puncture is made, an "Avanti+ sheath" is introduced (*Ref. 6*). Under fluoroscopic guidance, the common hepatic artery is catherized, and the exact anatomy of its branches is mapped out (*Ref. 6*). The scout dose and treatment dose of radioactive holmium-loaded microspheres are flushed out of the vial and into the catheter (straight tip), positioned in the proper hepatic artery, by injecting 40 to 60 mL of 50:50 mixture of saline and iodine contrast agent into the vial at a rate of 0.5 to 1.0 mL s^{-1}, under fluoroscopy guidance (*Ref. 6*). Fluoroscopy is a form of diagnostic radiology that enables the radiologist to see the organ or tumor area using x-rays and a contrasting agent; the image can be seen clearly, as the contrasting agent flows.

2.3 Neutron Activation of Microspheres for Radiotherapeutic Applications

In neutron activation, an element is bombarded with neutrons to induce an excited intermediate, which may de-excite by emitting prompt *γ-rays*. The radioactive product then decays via α, β, γ, or delayed neutron emission processes. The *γ-rays* emitted in this latter decay process are known as delayed *γ-rays*, which are detected after activation.

Thermal neutrons are the most commonly used to activating particles. Their velocities are low (2200 m s^{-1}), and their mean energy is only about 0.04 eV (the most probable energy is about 0.025 eV). Neutrons with slightly higher energies (0.1 to 1 eV), called epithermal, serve as the activating particle for epithermal neutron activation. Resonance neutrons in the 1 eV to 1 keV energy region are often grouped with epithermal neutrons, and any neutrons with energies greater than 0.5 MeV are called fast neutrons.

Because not all elements are activated identically, the type, the energy, and the flux of the irradiating particles may be varied, allowing for selective activation of certain elements. The time of activation can be varied, resulting in enhanced degrees of activation of elements with either short or long half-life radionuclides.

A wide range of devices is used to produce the particles or photons needed for activation. For example, a nuclear reactor produces neutrons as a by-product of uranium fission processes occurring within the reactor core. Small reactors, called research reactors, have been designed to provide neutrons needed for physics research and applications such as nuclear activation analysis. Nuclear reactors emit neutrons that have a wide range of energies. The fission process

itself results in the emission of fast neutrons. However, moderation of these fast neutrons produces thermal, epithermal, and resonance neutrons.

The largest research reactors can produce thermal neutron flux densities up to approximately 10^{15} n cm^{-2} s^{-1} and are most often located at national laboratories. Smaller reactors, like the TRIGA and the SLOWPOKE, produce useful flux densities approximately 10^{11} to 10^{15} n cm^{-2} s^{-1} and are found in university and industrial research facilities.

2.4 Determination of the Activation of Product

Calculations of both the products' activation and dose were used to determine the effects of changing the packing arrangement of microspheres from a conventional pile shape to a sheet shape when exposed to a neutron flux. The effects were calculated by determining the following parameters: irradiation times, activation and dose magnitudes, neutron and photon energy depositions, and target atom depletion. Results from both the sheet-shaped and pile-shaped packing arrangements were analyzed and were compared to determine advantages and disadvantages between them.

2.4.1 *Neutron Activation of Target Atoms*

Activation product formation is illustrated in *Fig. 2.3* for a flux (ϕ) of neutrons incident upon a thin target containing N_1 atoms, initially. It is assumed that the target thickness is such that the flux of neutrons remains essentially the same as it passes through. When this condition occurs, absorption reactions produce new atoms of N_2 at the following rate:

$$N_2 = \phi \sigma N_1 \qquad (1)$$

where ϕ is the neutron flux (n cm^{-2} s^{-1}) and σ (cm^2) is the absorption cross-section for projectiles (commonly neutrons) of a given energy (*Ref. 7*).

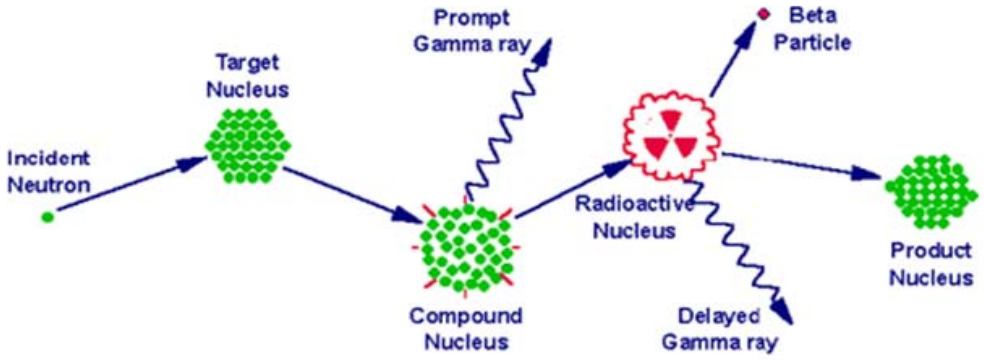

Figure 2.3-Schematic for the activation product formation and decay. (This figure was obtained from *Ref. 8.*)

As soon as atoms of N_2 are formed, they can be removed by radioactive transformation and/or activation to a new product as follows:

$$\text{Removal of } N_2 = \lambda_2 N_2 + \phi \sigma_2 N_2 \qquad (2)$$

If activation can be ignored, the rate of removal of N_2 atoms is due only to radioactive transformations, and for thin foils containing N_1 atoms, the rate of change of new atoms of N_2 with time is the rate of production minus the rate of removal as follows:

$$dN_2/dt = \phi\sigma_1 N_1^\circ - \lambda_2 N_2 \quad (3)$$

which when solved yields

$$N_2(t) = (\phi\sigma_1 N_1^\circ/\lambda_2)(1-e^{-\lambda_2 t}) \quad (4)$$

or in terms of activity

$$A_2(t) = \phi\sigma_1 N_1^\circ (1-e^{-\lambda_2 t}) \quad (5)$$

2.4.2 *Depletion of Target Atoms During Neutron Activation*

Depletion of target atoms is of little concern for short irradiation of most materials because the number of target atoms can be presumed to remain constant (*Ref. 7*). However, since the radioisotope content per microsphere is considerably low and the irradiation time have the potential of being significantly high, a test for target depletion per microsphere is considered (*Ref. 7*). In order to account for target depletion, N_1 is treated as a variable, such that

$$N_1(t) = N_1^\circ e^{-\phi\sigma_1 t} \quad (6)$$

where $N_1(t)$ is the number of target atoms after an irradiation time t; N_o is the initial number of target atoms, and $\phi\sigma_1$ in the exponential term is the depletion constant (*Ref. 7*). The rate of change of atoms of the product N_2 is

$$dN_2/dt = \phi\sigma_1 N_1(t) - \lambda_2 N_2 \quad (7)$$

but since $N_1(t)$ is treated as a variable, then

$$dN_2/dt = \phi\sigma_1 N_1^{\circ} e^{-\phi\sigma_1} - \lambda_2 N_2 \quad (8)$$

which when solved yields

$$N_2 = \phi\sigma_1 N_1^{\circ}/(\lambda_2 - \phi\sigma_1)\,(e^{-\phi\sigma_1 t} - e^{-\lambda_2 t}) \quad (9)$$

Target depletion and product activation may both be significant in special circumstances (*Ref. 7*). In this case, a similar approach can be used to obtain the number of product atoms with time as follows:

$$dN_2/dt = \phi\sigma_1 N_1(t) - \lambda_2 N_2 - \phi\sigma_2 N_2 \quad (10)$$

which when solved yields

$$N_2 = \left[\phi\sigma_1 N_1^{\circ}/(\lambda_2 + \phi\sigma_2 - \phi\sigma_1)\right](e^{-\phi\sigma_1 t} - e^{-(\lambda_2 + \phi\sigma_2)t}) \quad (11)$$

2.4.3 *Calculations of Dose to the Liver and Exposure*

The specific activity of the radioactive holmium-loaded microspheres can be modified by adapting the activation time in the nuclear reactor, causing the dose to which the liver is exposed

to vary (*Ref. 4*). Assuming a homogeneous uptake throughout the liver of a maximum treated weight (inclusive the tumor tissue) of 3 kg, the amount of radioactivity administered to the patient is calculated according to the following formula:

$$Liver\ Dose(Gy) = 15.87 \times 10^{-3}\ (J/MBq) A_{Ho\text{-}166}(MBq)/LW(kg) \qquad (12)$$

where *LW* is the liver weight of the patient which may be determined using *CT*, *MRI*, or ultrasound, and where 15.87 x 10^{-3} (J/MBq) is the activity-to-dose conversion factor for ^{166}Ho (*Ref. 4*).

2.5 Attenuation of Neutron and Photon Fluxes

Because of the packing arrangement of the holmium-loaded microspheres in the activation vials and the direction of the neutron flux in the thermal column, the activation values of each individual microsphere were not uniform throughout the packing arrangement for both the pile- and sheet-shaped configurations. To achieve a uniform activation per microsphere throughout the packing configuration, the neutron flux was manipulated by using flux attenuation principles. Similarly, to minimize both the photon flux and photon energy deposition on the polymeric matrix of the microspheres, flux attenuation principles were used as well, as presented in the following sections.

2.5.1 *Attenuation of the Neutron Flux*

A flux of neutrons (*I)* diminish in a thickness *x* of an absorber proportional to the intensity of the neutron source and the neutron removal coefficient Σ_{nr} of the absorbing material as follows:

$$-dI/dx = \Sigma_{nr} I \qquad (13)$$

which when solved yields

$$I(x) = I_o\, e^{-\Sigma_{nr} x} \qquad (14)$$

where I_o is the initial intensity and *I(x)* refers to those neutrons that penetrate a distance *x* in an absorber without a collision (*Ref. 7*).

Various interactions serve to remove a neutron from the beam such that it does not reach the receptor of interest. In this respect, elastic and inelastic scattering interactions deflect neutrons out of the beam, and $\sum_{nr}$ accounts for all of the process that do so (*Ref. 7*). However, neutrons scattered from the narrow beam are likely to undergo other scattering interactions and be deflected back into the beam and the receptor (*Ref. 7*). These more realistic, or poor geometry conditions, are accounted for with a buildup factor as follows:

$$I(x) = I_o\, B e^{-\Sigma_{nr} x} \qquad (15)$$

When no hydrogenous materials are present, the neutron removal coefficient $\sum_{nr}$ is determined by the macroscopic cross-section, $\sum = N\sigma_t$ where N is the number of target (atoms) in an absorber and σ_t is the total cross-section in barns for each atom in a unit volume of absorber (*Ref. 7*). Therefore, $\sum_{nr}$ has units of cm^{-1}, and it can be converted to a neutron mass coefficient ($cm^2\ g^{-1}$) by dividing by the density (ρ) of the absorber as follows:

$$\textit{Neutron mass coefficient } (cm^2\ g^{-1}) = \sum_{nr} / \rho \qquad (16)$$

2.5.2 *Attenuation of the Photon Flux*

The attenuation of photons by various absorbing materials under ideal narrow-beam conditions satisfies the relationship

$$I(x) = I_o e^{-\mu x} \qquad (17)$$

where I_o is the initial photon intensity; $I(x)$ is the photon intensity after passing through an absorber of thickness x in narrow-beam geometry; and $\mu\ (cm^{-1})$ is the total attenuation coefficient, which accounts for all interaction processes, including scattering reactions that remove photon from the beam (*Ref. 7*). The attenuation coefficient μ is dependent on the particular absorber medium and the photon energy (*Ref. 7*).

When a significant absorbing medium such as a metal shield is placed between a photon and a receptor, the photon flux will be altered significantly because *Compton* scattered photons produced in the absorber, many of which will reach the receptor (*Ref. 7*). The scattered photons

are also reduced in energy, and the flux reaching the receptor becomes a complicated function of beam size, photon energy distribution, absorber material, and geometry (*Ref. 7*). The conditions that include these complexities are called poor geometry and represent most practical situations in radiation protection (*Ref. 16*). A calculated value of *I(x)* based on the attenuation coefficient μ determined in good geometry conditions underestimates the number of photons reaching the receptor which implies that absorption is greater than actually occurs, and a shield designed on this basis will not be thick enough (*Ref. 7*).

The effects of scattered photons, in addition to unscattered primary photons, is best dealt with as a buildup factor (*B*) to account for photons scattered towards the receptor from regions outside the primary beam (*Ref. 7*). When the buildup is included, the radiation intensity is determined as follows:

$$I(x) = I_o B e^{-\mu x} \qquad (18)$$

The buildup factor is dependent on the absorbing medium, the photon energy, the attenuation coefficient for specific energy photons in the medium, and the absorber thickness *x* (*Ref. 7*).

2.6 TRIGA Reactor Background Information

The following sections provide background information regarding the operational parameters, materials, and neutron activation sections of a TRIGA nuclear reactor. This information was used to build various MCNP5 simulation models of the thermal column to investigate the neutron activation of holmium-loaded microspheres.

2.6.1 *Description of a TRIGA Reactor as the Neutron Source*

General Atomics TRIGA reactors are used in many diverse applications, including production of radioisotopes for medicine and industry, treatment of tumors, nondestructive testing, basic research on the properties of matter, and for education and training (*Ref. 9*). These reactors operate at thermal powers levels from less than 0.1 to 16 MWt, and are pulsed to 22,000 MWt (*Ref. 9*). The high power pulsing is possible due to unique properties of General Atomics uranium-ziconium hydride fuel, which provides unrivaled safety characterisitics (*Ref. 9*). The safety features of this fuel also permit flexibility in siting, with minimal environmental effects (*Ref. 9*).

The operational parameters, materials, and dimensions of the MCNP5 model of the thermal column are similar to the thermal column of the TRIGA nuclear reactor at Oregon State University (OSTR). The TRIGA nuclear reactor is a 1 MWt, water-cooled, swimming-pool-type reactor that uses zirconium hydride/uranium fuel elements in a circular grid array (*Ref. 10*). The uranium fuel is enriched to 20% in uranium-235, and there are 88 fuel elements normally in the core (*Ref. 10*). These fuel elements offer a useful lifetime of over 5000 megawatt-days in contrast to just about 100 megawatt-days with conventional TRIGA fuel elements (*Ref. 10*).

The reactor is surrounded by a ring of graphite that serves to minimize neutron leakage by reflecting neutrons back into the core, and the reactor core is situated near the bottom of a 22-foot-deep tank, as illustrated in *Figs. 2.4 and 2.5*, and a concrete monolith surrounding the tank acts as a radiation shield (*Ref. 10*). The OSTR can be operated in three main modes: steady-state mode, pulsing mode, and square-wave mode (*Ref. 10*). The neutron fluxes associated with 1

MW_t, steady-state power for each of the experimental facilities are given in *Table 2.1*. The maximum reactivity insertion for a pulse is $2.55, giving a peak power of approximately 3000 MWt (*Ref. 10*). The three main uses of the OSTR are instruction, research, and radioisotope production.

Figure 2.4-TRIGA reactor and pool structure similar to the research reactor at Oregon State University. (This figure was obtained from *Ref. 11*.)

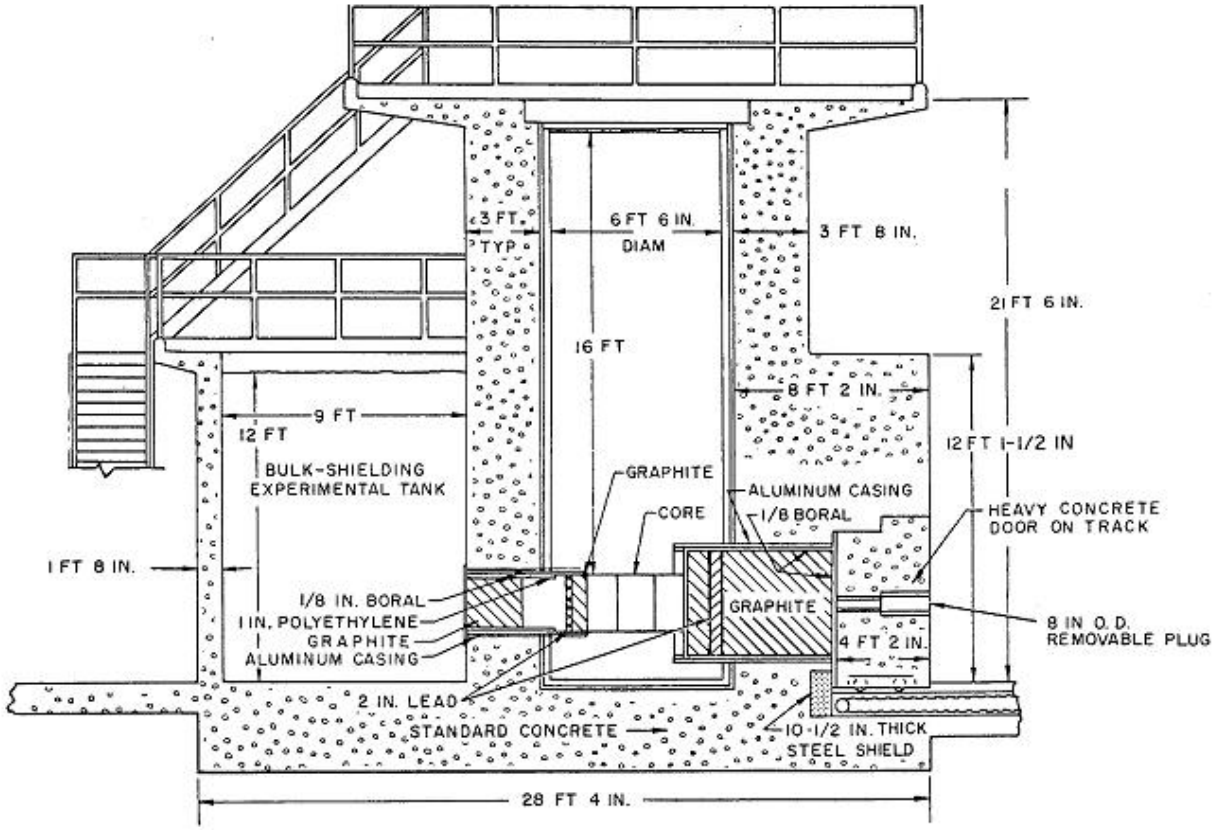

Figure 2.5-Diagram of a TRIGA reactor illustrating the dimensions of both the pool structure and the thermal column similar to the research reactor at Oregon State University. (This figure was obtained from *Ref. 12)*

Table 2.1-Peak Fluxes in HEU and LEU Cores of OSTR

Facility*	HEU Peak Thermal Flux* ($n\ cm^{-2}\ s^{-1}$)	HEU Peak Epithermal Flux* ($n\ cm^{-2}\ s^{-1}$)	LEU Peak Thermal Flux* ($n\ cm^{-2}\ s^{-1}$)	LEU Peak Epithermal Flux* ($n\ cm^{-2}\ s^{-1}$)
ICIT	$1.1 \times 10^{13} \pm 7 \times 10^{11}$	$9 \times 10^{11} \pm 8 \times 10^{10}$	$5.5 \times 10^{12} \pm 3 \times 10^{11}$	$1.0 \times 10^{12} \pm 1 \times 10^{11}$
CLICIT	~0	$1.2 \times 10^{12} \pm 1 \times 10^{11}$	~0	$1.3 \times 10^{12} \pm 1 \times 10^{11}$
GRICIT	$7.2 \times 10^{12} \pm 4 \times 10^{11}$	$4.3 \times 10^{12} \pm 2 \times 10^{10}$	$3.4 \times 10^{12} \pm 2 \times 10^{11}$	$3.3 \times 10^{11} \pm 2 \times 10^{10}$
Lazy Susan	$3.0 \times 10^{12} \pm 2 \times 10^{11}$	$1.2 \times 10^{11} \pm 7 \times 10^{9}$	$2.3 \times 10^{12} \pm 2 \times 10^{11}$	$9.6 \times 10^{12} \pm 1 \times 10^{10}$
Thermal column	$8 \times 10^{10} \pm 1 \times 10^{10}$	~0	$7 \times 10^{10} \pm 9 \times 10^{9}$	~0
Rabbit pneumatic system	$1.0 \times 10^{13} \pm 8 \times 10^{11}$	$4.0 \times 10^{11} \pm 3 \times 10^{10}$	$8.3 \times 10^{12} \pm 8 \times 10^{11}$	$1.2 \times 10^{11} \pm 1 \times 10^{10}$

*These neutron activation facilities and values were obtained from *Ref. 12*

The pneumatic transfer facility consists of an irradiation position in the outer ring of the core, in a high-neutron-flux region, to allow samples to be transferred in and out of the reactor core very rapidly (*Ref. 10*). The flux in the pneumatic transfer terminal in the core is 1.4 x 10^{10} cm^{-2} s^{-1}, as illustrated in *Fig. 6*, and the cadmium ratio is 1.7 when the OSTR is operated at the level of 1 MW_t (*Ref. 10*). A second pneumatic transfer facility in which the irradiation terminal is surrounded with cadmium is also available.

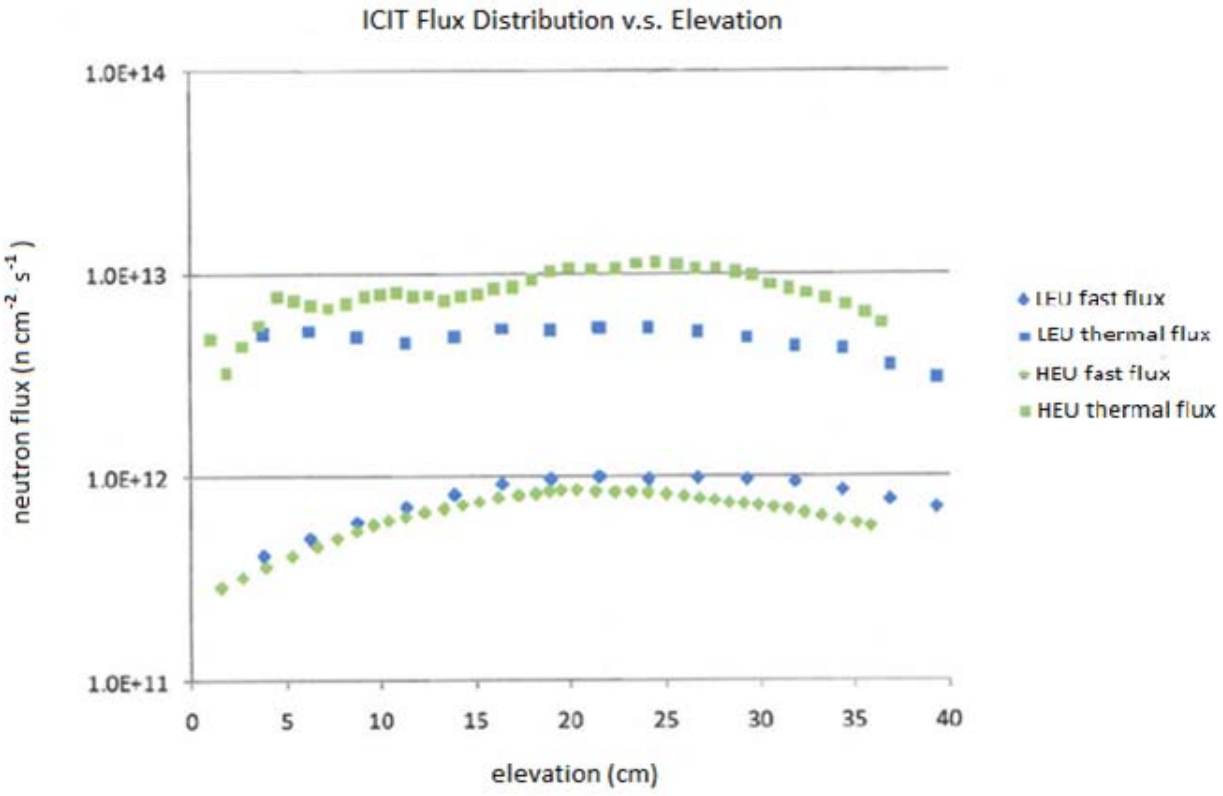

Figure 2.6-Comparison of ICIT flux distribution in the HEU and LEU cores of a TRIGA reactor. (This figure was obtained from *Ref. 12*.)

The rotating specimen rack is located in a position that surrounds the top of the reactor core, inside the graphite reflector, as illustrated in *Figs. 2.7 and 2.8* (*Ref. 10*). The rack consists of a circular array of 40 tubular holders (*Ref. 10*). Each holder can accommodate up to two TRIGA-type, irradiation tubes, so that up to 80-separated samples may be irradiated at any one time in this facility. Typically, researchers use the rotating rack when larger samples, in larger numbers and longer irradiation times (more than two hours), are required.

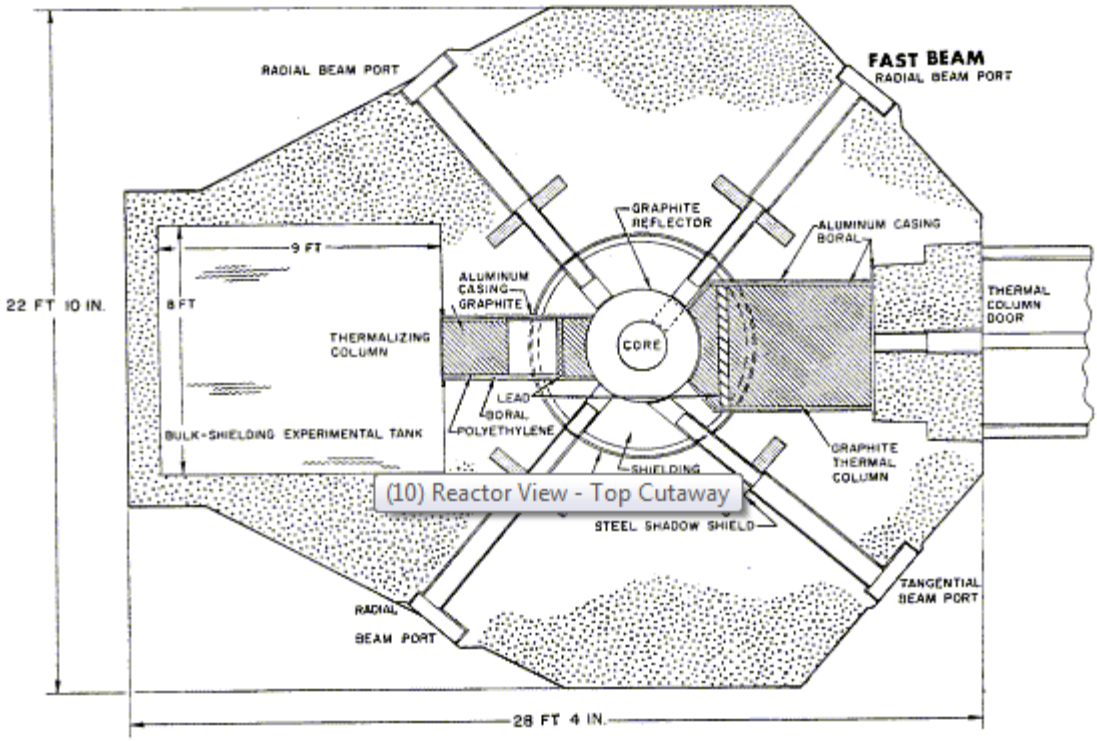

Figure 2.7-Diagram illustrating a "top view" of a TRIGA reactor, beam ports, bulk shield tank, and thermal column. (This figure was obtained from *Ref. 12*)

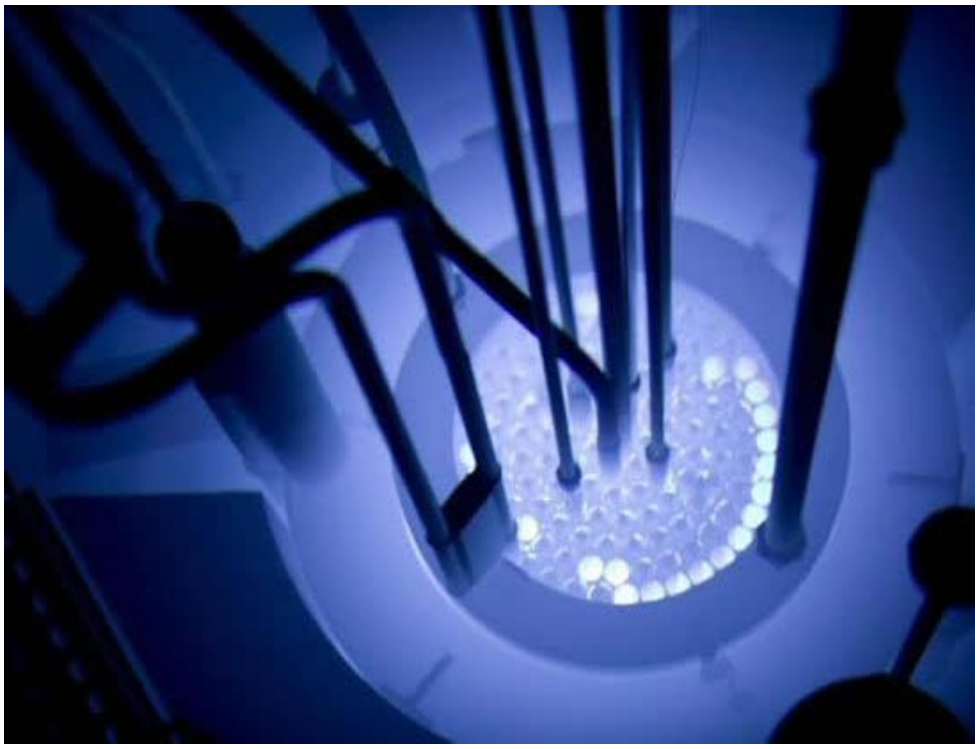

Figure 2.8-TRIGA reactor and rotating specimen rack located in a position surrounding the top of the reactor, inside the graphite reflector. (This figure is a picture of OSTR.)

The average thermal flux in the rotating rack is less than half that of the pneumatic transfer facility, as illustrated in *Fig. 2.9*, and the cadmium ratio is higher (*Ref. 10*). For irradiation experiments requiring the highest possible neutron flux, samples can be placed in three central thimbles or in the dummy-fuel-element position. Sealed experimental samples can also be irradiated by placing them on top of the reactor core itself (*Ref. 10*).

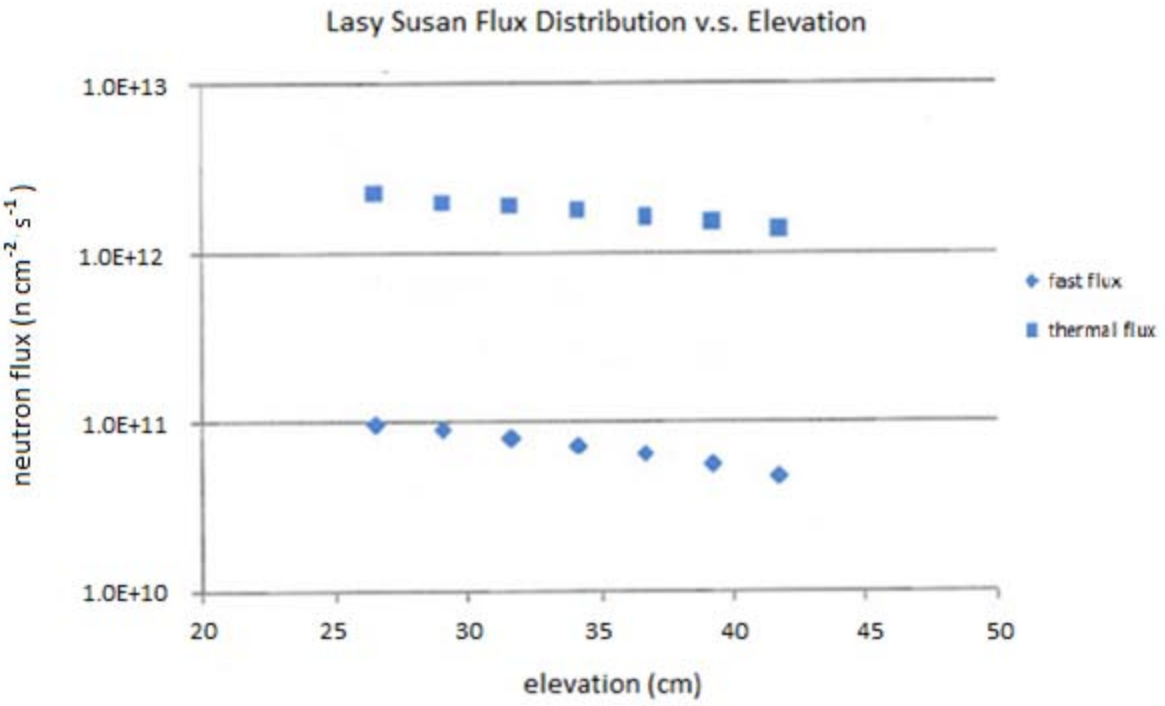

Figure 2.9-Measured flux in the LEU Core Lazy Susan facility of a TRIGA reactor. (This figure was obtained from *Ref. 12*.)

2.6.2 *Description of Thermal Column in TRIGA Reactor*

The following information regarding the thermal column of the TRIGA reactor was obtained from *Ref. 12*: The thermal column, a section of the TRIGA reactor illustrated in *Fig. 2.10*, is a large, boral-lined, graphite-filled aluminum container. Its outside dimensions are 10 cm by 10 cm in cross-section and approximately 125 cm in length. The thermal column liner is a seal-welded container fabricated in two sections from aluminum plate. The outer section is embedded in a concrete shield, and the inner section is welded to and is an integral part of the aluminum tank. The surfaces of the outer section (which are in contact with the concrete) are wrapped with plastic tape for corrosion protection. The inner section (welded to the aluminum tank) extends to the graphite reflector and matches the contour of the reflector. The horizontal

centerline coincides with that of the core centerline. In a vertical plane, the column extends approximately 30 cm. above and below the reflector, with the centerlines of the column and the reflector coinciding.

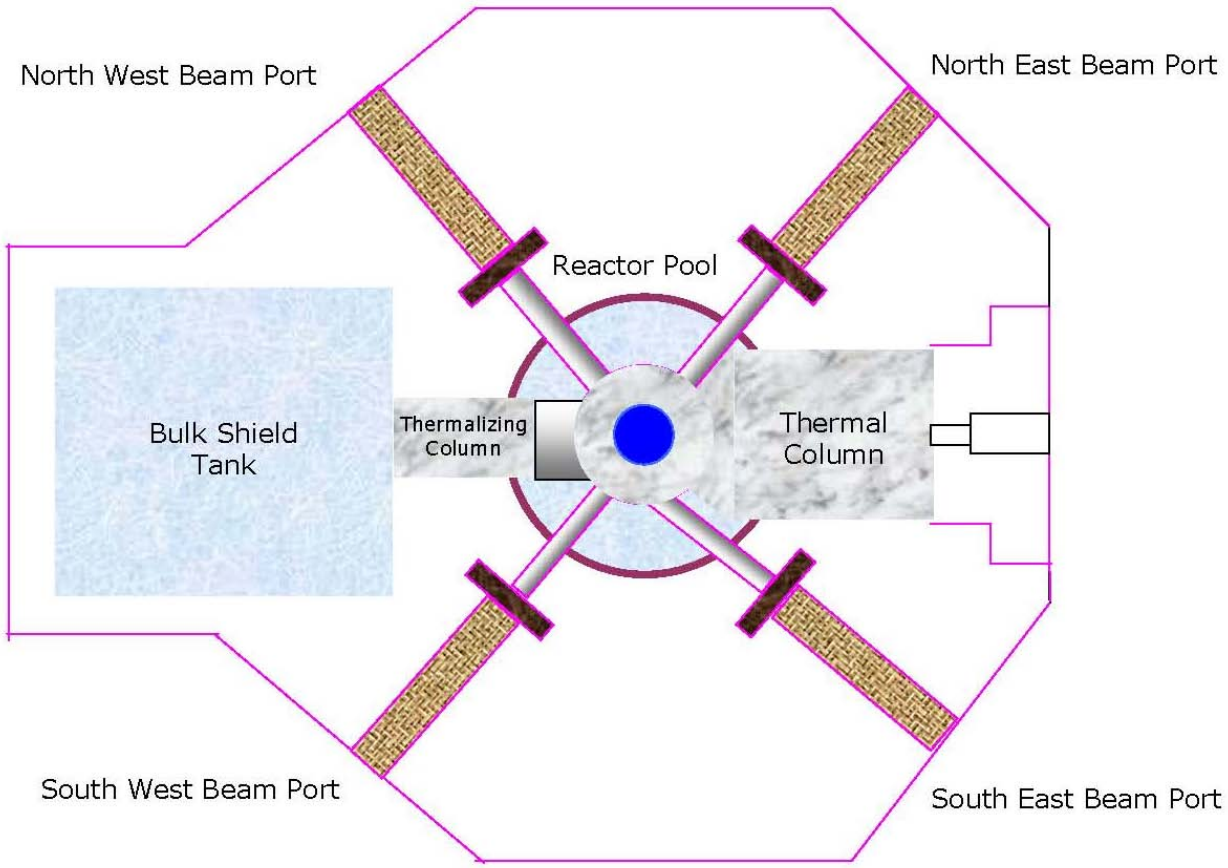

Figure 2.10-Schematic of a TRIGA reactor showing the thermal column section which is used for building the MCNP5 model for simulating the neutron activation of holmium-loaded microspheres. (This figure was obtained from *Ref. 12*.)

The aluminum container is open toward the reactor room. Blocks of AGOT, nuclear-grade graphite occupy the entire volume. The individual blocks are approximately 10 cm by 10

cm in cross-section, the longest being 125 cm in length. All pieces are stamped with identification letters and number. The values for the thermal column neutron flux at different distances are illustrated in *Fig. 2.11*.

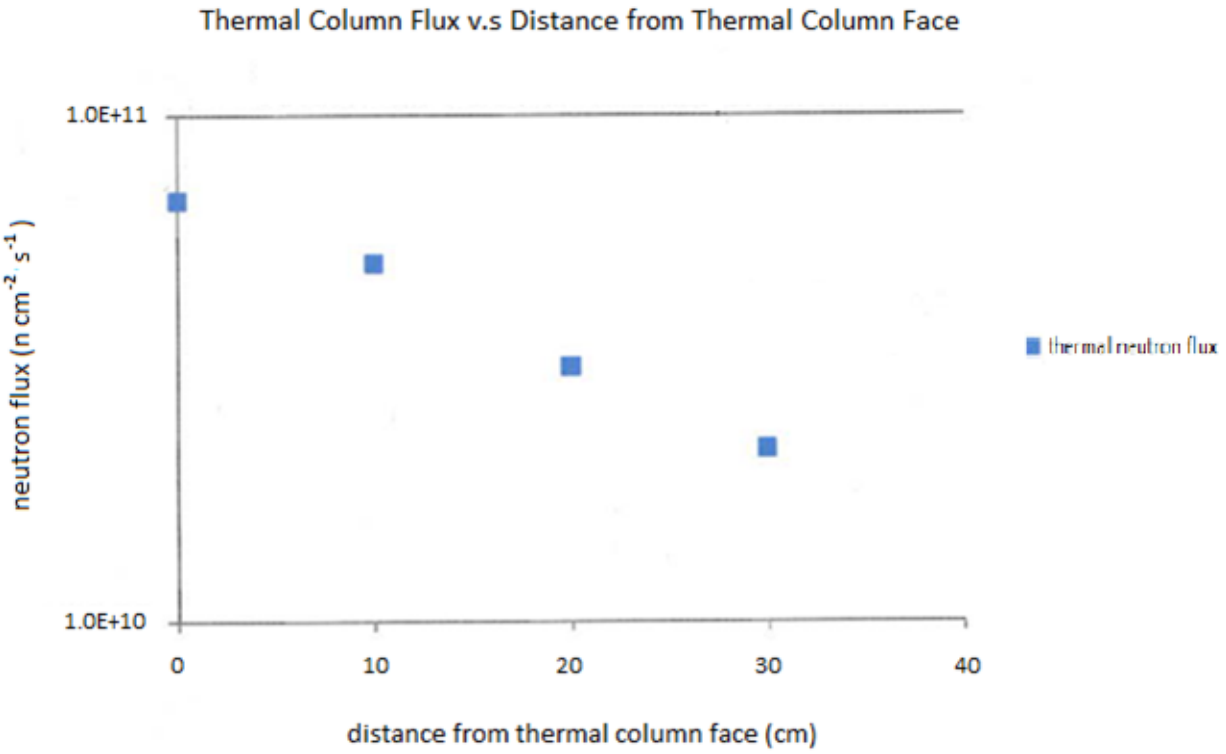

Figure 2.11-Measured flux in the LEU core thermal column of a TRIGA reactor. (This figure was obtained from *Ref. 12.*)

Five graphite blocks serve as removable foil stringers. These five stringers were machined slightly undersize for easy removal and insertion. The central is aligned with an access plug in the thermal column door. The central stringer cold, therefore, can be removed and

inserted without having to move the entire door. To gain access to the other four stringers, the thermal column door must be rolled back on its tracks. Surrounding the graphite on the inside of the aluminum casing (on all four sides) are sheets of boral, which are incorporated in the design to reduce the production of capture gamma by flux in the surrounding concrete shield.

A track-mounted door shields the outer face of the thermal column. The door is recessed into the biological concrete shielding and is flushed with the shield structure when closed. To reduce the radiation streaming, the door configuration is of a stepped design. The door is filled with heavy-aggregate concrete. Its total weight is about 19 tons. A four-heeled carriage supports the door and rolls on two steel rails, which are flush with the door. On the door surface facing the thermal column, a boral sheet is attached to the door.

A plug in the door provides access to the centrally located stringer in the thermal column. This plug is filled with heavy-aggregate concrete and stepped to reduce radiation streaming. The inner section is 20 cm in diameter, and the outer section is 25 cm in diameter. The plug surface facing toward the thermal column is covered with boral sheet.

3.0 Materials and Methods

The following sections describe materials, computer codes, and techniques involved in the creation of simulation models that were used to investigate the possibilities of not only neutron-activating microspheres loaded with holmium-165 in a polymeric matrix made from

poly ($_L$-lactic acid) PLLA, but also to improving the quality and yield of the product and to improving the efficiency of the process.

3.1 Descriptions of Computer Codes and Materials Used for Creating Models

The following materials, as indicated in *Tables 3.1* through *3.3*, were used in the design of MCNP5 neutron-activation simulation models:

Table 3.1-List of materials used for MCNP5 Simulations

Material	Components	Moles	Molecular Weight (g mol^{-1})	Density (g cm^{-3})
Graphite	C	1	12	2.16
Quartz	Si	1	60.08	2.62
	O	2		
Bismuth	Bi	1	208.98	9.78
Aluminum	Al	1	26.98	2.7
Polyethylene	H	4	240000	0.941
	C	2		
Poly($_L$-lactide)	C	3	26000	1.27
	H	4		
	O	2		

Table 3.2-Elemental Analysis of Holmium-Trisacetylacetonate

Element*	Mass Content* (%)	Theoretical Ho-Complex ($3xH_2O$)* (%)	Molecular Weight (g mol^{-1})	Density (g ml^{-3})
C	36.55	34.9	516.3	1.74
H	4.98	5.27		
O	27.12	27.89		
Cl	0	0		
Ho-165	31.19	31.94		

*These components and values were obtained from *Ref. 2*.

Table 3.3-Components in Air used for MCNP5 Simulation Models

Component* (Dry Air)	Volume Ratio*	Molecular Mass* (kg/kmol)	Molecular Mass in Air* (kg/kmol)
Oxygen	2.095×10^{-1}	32	6.704
Nitrogen	7.809×10^{-1}	28.02	21.88
Carbon Dioxide	3×10^{-4}	44.01	0.013
Hydrogen	5×10^{-7}	2.02	0
Argon	9.33×10^{-3}	39.94	0.373
Neon	1.8×10^{-5}	20.18	0
Helium	5×10^{-6}	4	0
Krypton	1×10^{-6}	83.8	0
Xenon	9×10^{-8}	131.29	0
Total Molecular Mass			28.97

*These components and values were obtained from *Ref. 13*.

In addition to the materials presented in *Tables 3.1* through *3.3*, the following three types of computer codes were used: Monte Carlo N-Particle (MCNP5) code, FORTRAN-90, and Visual Editor. The stochastic transport Monte Carlo based code MCNP5 was used to calculate the following values for each microsphere: neutron flux, photon flux, dose, and energy depositions from neutrons and photons on the polymeric matrix (*Ref. 14*). The code can be used in several transport modes: neutron-only, photon-only, or combined neutron-photon transport where the photons are produced by neutron interactions (*Ref. 14*). For this investigation, the combined neutron/photon mode was used. The neutron energy regime specified in the models was from 10^{-11} to 20 MeV for all isotopes, and the photon energy regime was from 1 keV to 100 GeV (*Ref. 14*). It should be noted that MCNP5 only calculated energy depositions from prompt gammas, disregarding energy depositions from delay gammas.

As part of the MCNP5 code, Visual Editor (VisEd) is a graphical user interface, which has powerful capabilities including the ability to display multiple cross-sectional views of the geometry with optional displays of the geometry in 3D, such as the microspheres illustrated in *Figs. 3.1* through *3.6*, using either wire mesh or ray tracing (*Ref. 15*). Additional capabilities include plotting of the source and the display of particle tracks during the random walks. The Visual Editor also includes geometry creation capabilities that allow the user to create MCNP5 geometries directly from the plot window using the mouse, and these capabilities allow the MCNP5 programmer the tools to quickly create complex geometries and display important features of the transport process (*Ref. 15*). Visual Editor's capabilities were applied to creating the simulation models as follows: the code was used to verify the locations of the microspheres arranged in different packing configurations, and it was used to test the geometry of the thermal column structure for particle leakage.

In addition to the MCNP5 and Visual Editor codes, a code written in FORTRAN-90 was used. FORTRAN-90 is a general purpose, procedural, imperative programming language that is especially suited for numeric computation and scientific and engineering computing. The FORTRAN-90 code written for this investigation determined the locations and the amount of microspheres inside an activation vial after specifying the following parameters: diameter of the microspheres, diameter and thickness of the activation vial, size of pile (number of microsphere layers), and shape of the packing arrangement of the microspheres inside the activation vials.

In the simulation models, for microspheres arranged in a "pile-shaped" packing configuration, the layers of the pile were assembled as illustrated in *Fig. 3.1*. Although the shape

of the activation vials was cylindrical, the FORTRAN-90 code generated a cross-section with hexagonal shape for the pile-shaped packing configuration, as illustrated in *Figs. 3.2 and 3.3*.

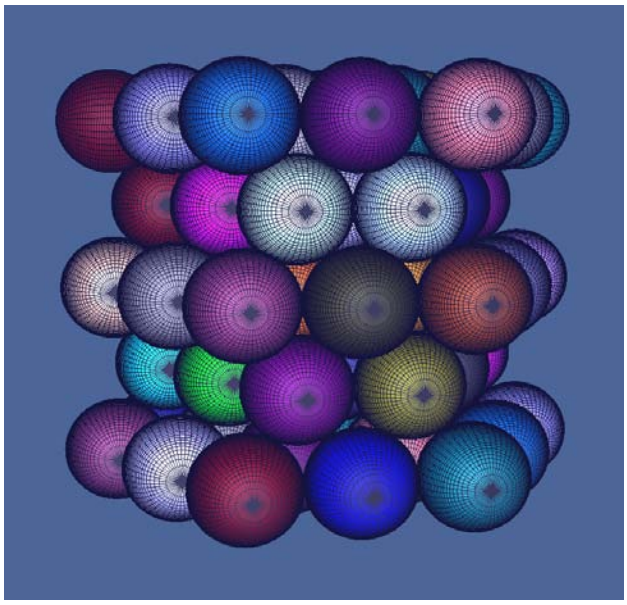

Figure 3.1-A 3D-view of a section of a MCNP5 model showing how layers of holmium-loaded microspheres are arranged in a pile-shaped packing configuration.(This figure was generated using VisEd with FORTRAN-90 output.)

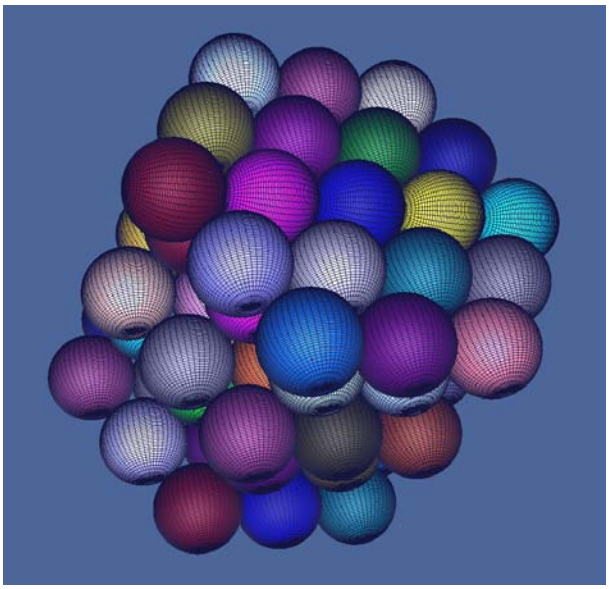

Figure 3.2-A 3D-view of a section of a MCNP5 model showing the cross-section and layers of holmium-loaded microspheres arranged in a pile-shaped packing configuration. (This figure was generated using VisEd with FORTRAN -90 output.)

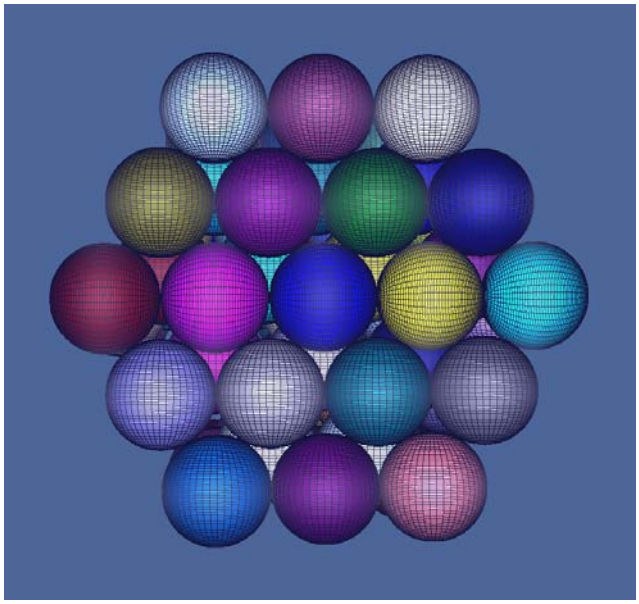

Figure 3.3-A 3D-view of a section of a MCNP5 model showing the cross-section of holmium-loaded microspheres arranged in a pile-shaped packing configuration inside a cylindrical activation vial. (This figure was generated using VisEd with FORTRAN-90 output.)

As part of this investigation for either minimizing or eliminating altogether photon energy deposition or minimizing irradiation time by increasing and providing a uniform neutron flux exposure, microspheres were arranged in a sheet-shaped packing configuration, as illustrated in *Figs. 3.4* through *3.6*. The size of the sheet generated by the FORTRAN-90 code was approximately equivalent to the amount of microspheres used to build the pile, so results can be analyzed and compared to determine any effects caused by modifications made to the packing geometry.

.

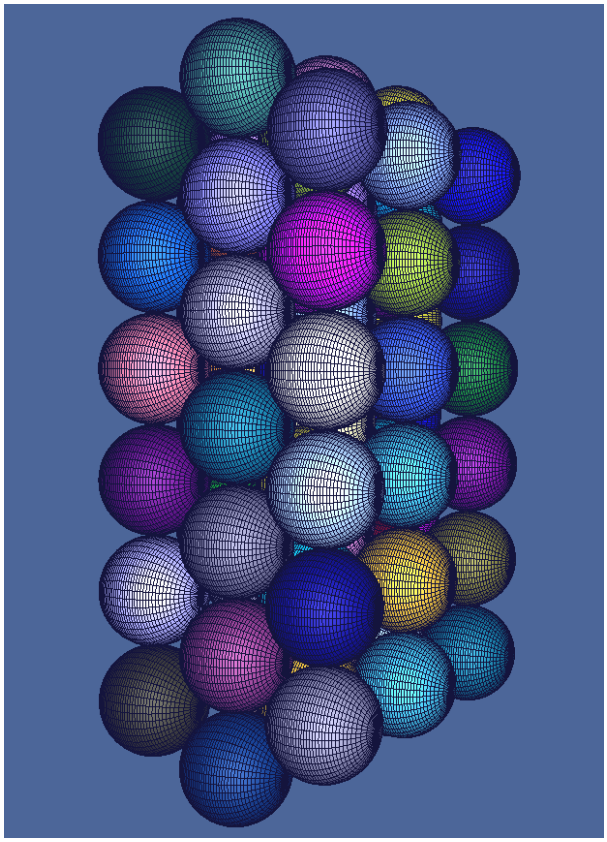

Figure 3.4-A 3D-view of a section of a MCNP5 model showing the cross-section and layers of holmium-loaded microspheres a-rranged in a sheet-shaped packing configuration. (This figure was generated using VisEd with FORTRAN-90 output.)

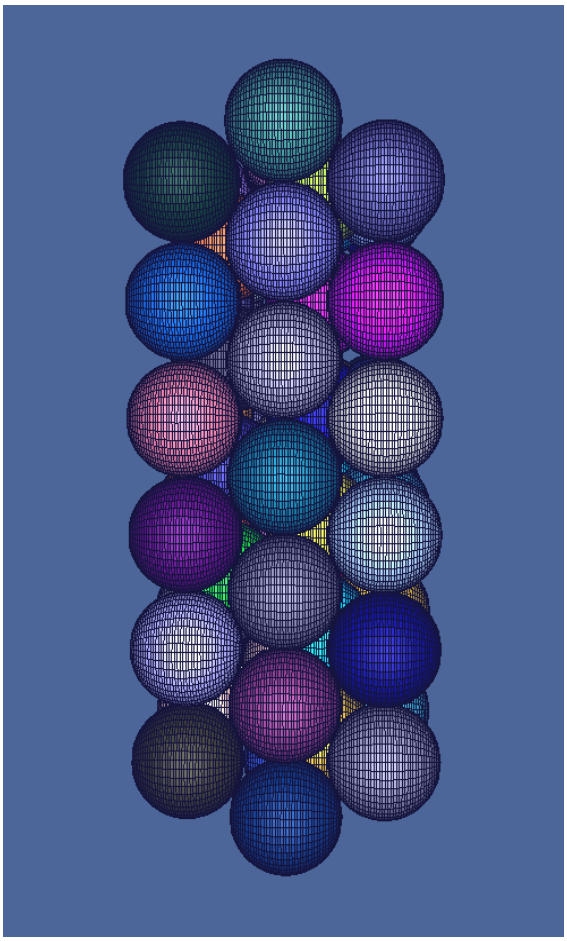

Figure 3.5-A 3D-view of a section of a MCNP5 model showing the cross-section of holmium-loaded microspheres arranged in a sheet-shaped packing configuration inside a cylindrical activation vial. (This figure was generated using VisEd with FORTRAN-90 output.)

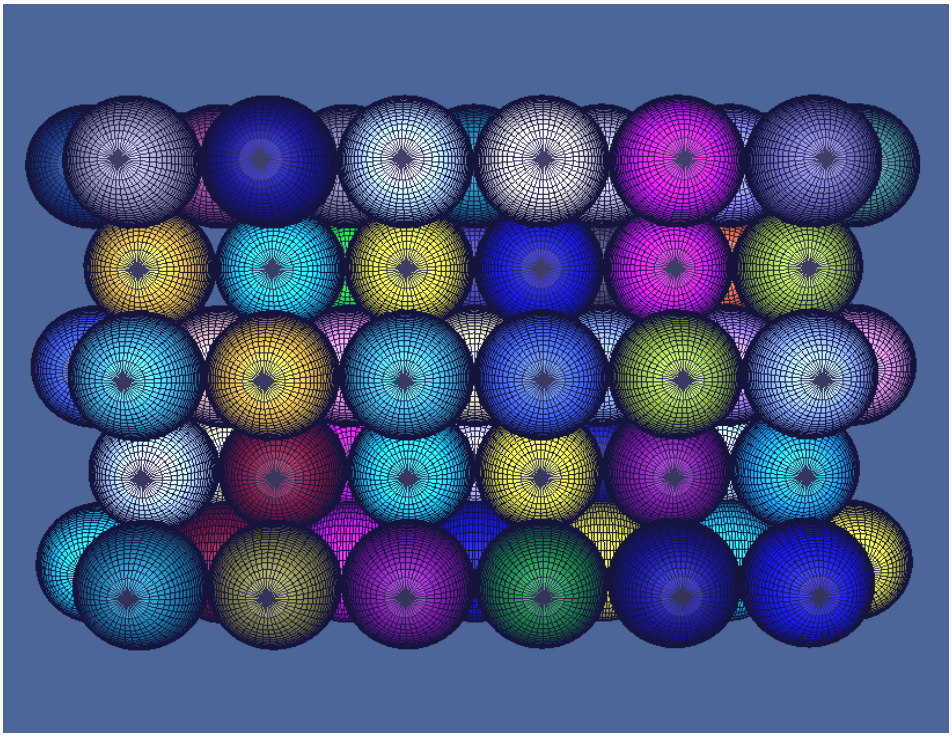

Figure 3.6-A 3D-view of a section of a MCNP5 model showing how layers of holmium-loaded microspheres are arranged in a sheet-shaped packing configuration. (This figure was generated using VisEd with FORTRAN-90 output.)

Whether the microspheres were arranged in a pile-shaped packing configuration or were arranged in a sheet-shaped packing configuration, they were modeled inside an activation vial, which is placed inside another activation vial; procedures require that dry solids must be double encapsulated during neutron activation in a research reactor such as a TRIGA reactor (*Ref. 12*). For this investigation, dimensions from an actual activation vial were used to generate a MCNP5 model of activation vials, as illustrated in *Fig. 3.7*. Various MCNP5 simulations were run after assigning these activation vials different locations in the thermal column and different materials, such as polyethylene, aluminum, polypropylene, and quartz, to determine their effects on neutron activation results, such as neutron and photon fluxes, dose, and neutron and photon energy

depositions. The chemical formulas for polyethylene and quartz are illustrated in *Figs. 3.8* and *3.9*, respectively.

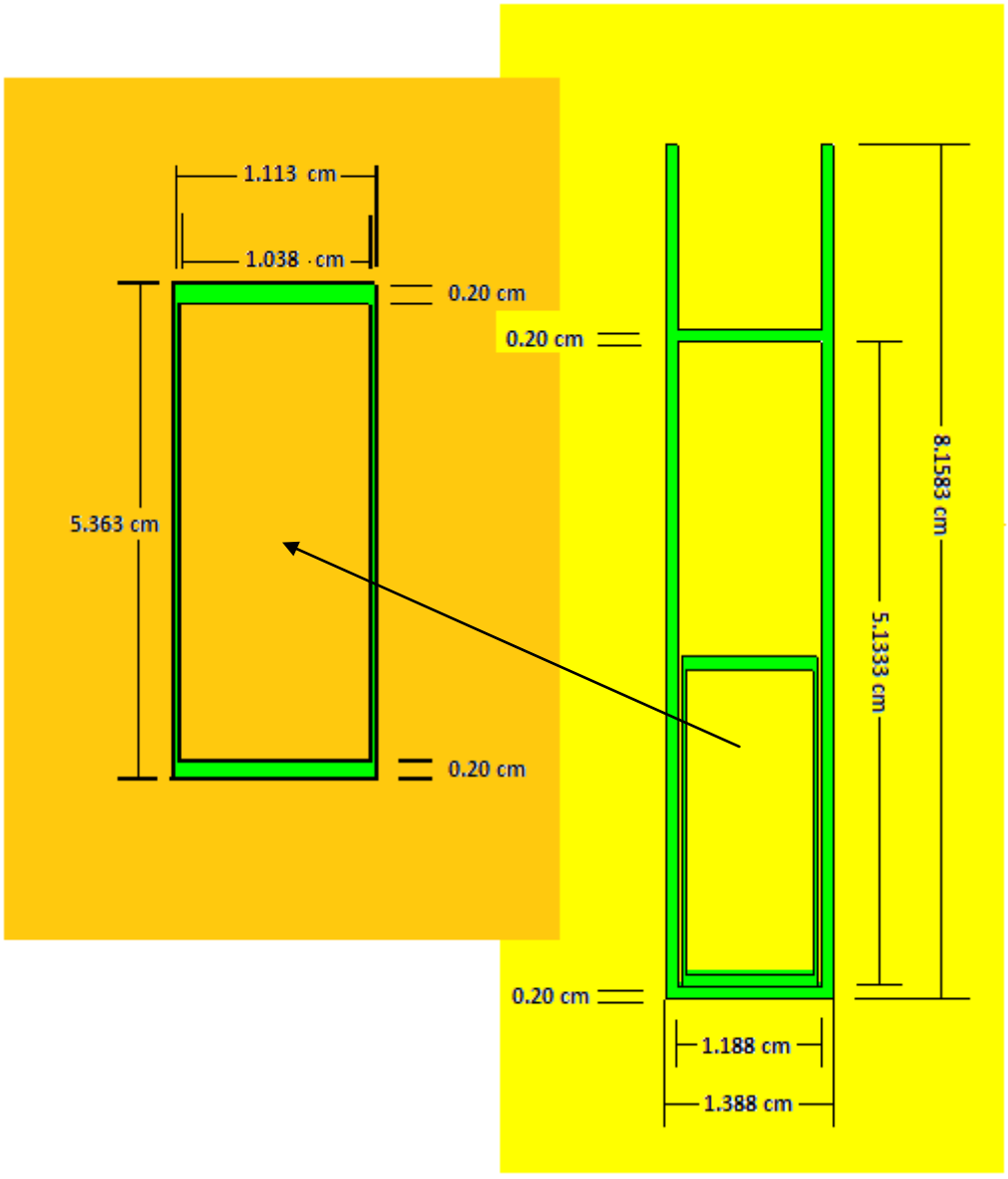

Figure 3.7-Polyethylene activation vials for the neutron activation of holmium-loaded microspheres (dry solids require double encapsulation).

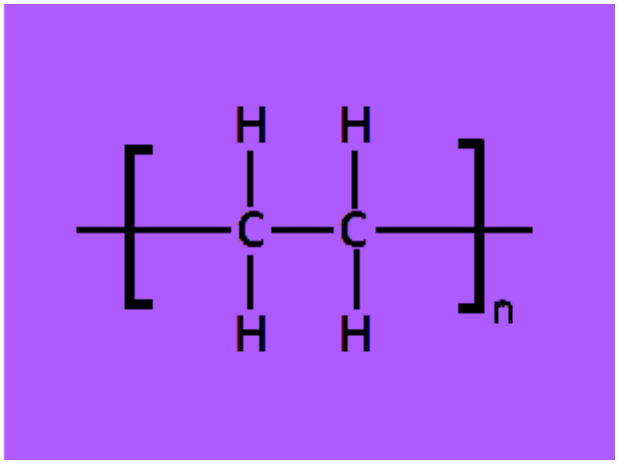

Figure 3.8- Chemical formula for polyethylene polymeric repeat unit. This information was needed for the material section in the MCNP5 model.

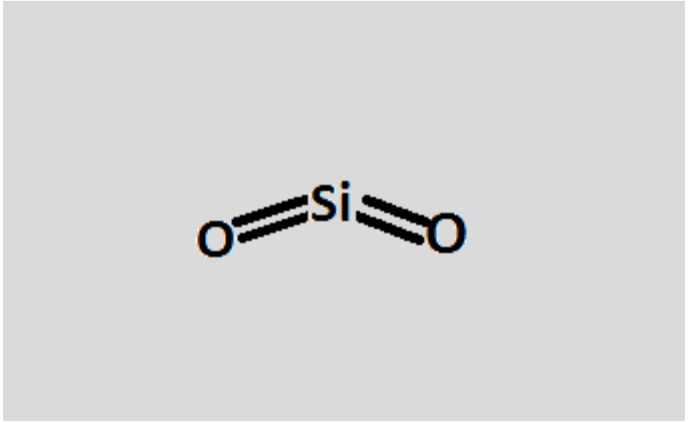

Figure 3.9-Chemical formula for quartz. This information was needed for the material section in the MCNP5 model.

3.2 Synthesis of Polymeric Microspheres Loaded with Holmium-165

To be able to specify values for the cell, the surface, and the material sections in the MCNP5 input decks for various simulations models and to specify the conditions in which the holmium-loaded microspheres were neutron activated, it was necessary to know the chemical components, conditions, and results involved in the synthesis of the microspheres, including their holmium complex and polymeric matrix.

The following background information regarding the chemical components and synthesis of the holmium complex HoAcAc was obtained from *Ref. 5*: acetylacetone (180g) is dissolved in 1080 g water. The pH of this solution ranged between 3.5 and 4.0. Ammonium hydroxide is added to the stirring colorless acetyacetone solution until a pH value of 8.5 is reached and the solution becomes yellow from the formation of acetylacetonate. Then, holmium chloride (10 g in 30 mL water) is stirred into this solution, and HoAcAc crystals are allowed to form, as illustrated in *Fig. 3.10*, at room temperature for at least one day. The crystals are collected by filtration, are washed three times with water, and are dried under nitrogen. For quality assurance purposes, the HoAcAc crystals are examined by infrared spectroscopy, nuclear magnetic resonance, elemental analysis, *x-ray* crystallography, and scanning electron microscopy.

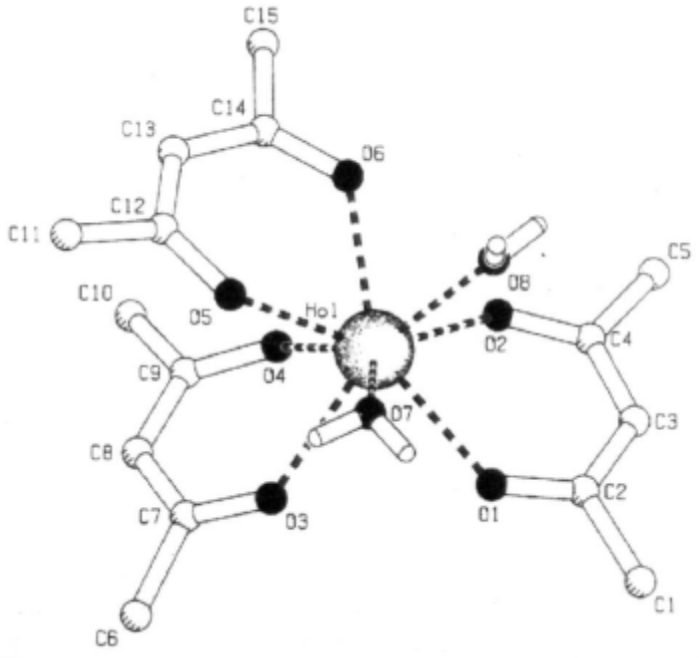

Figure 3.10-Unit cell of holmium-trisacetylacetonate with two coordinated water molecules. (This figure was obtained from *Ref. 2*.) This information was needed for the material section in the MCNP5 model.

The following information regarding the synthesis of the holmium-loaded microspheres was obtained from *Ref. 2*: microspheres loaded with HoAcAc complex in a poly ($_L$-lactic acid) matrix are prepared by dissolving these chemicals in chloroform. The resulting homogenous solution is added to an aqueous solution of polyvinyl alcohol (PVA). The mixture is stirred, and the formed microspheres are collected by centrifugation. Microspheres with a size ranging between 20 and 50 μm are obtained by sieving. Differential scanning calorimetry (DSC) results of this mixture are highly indicative of the HoAcAc being uniformly dispersed throughout the PLLA matrix; the chemical formula for PLLA is illustrated in *Fig. 3.11* (*Ref. 1*).

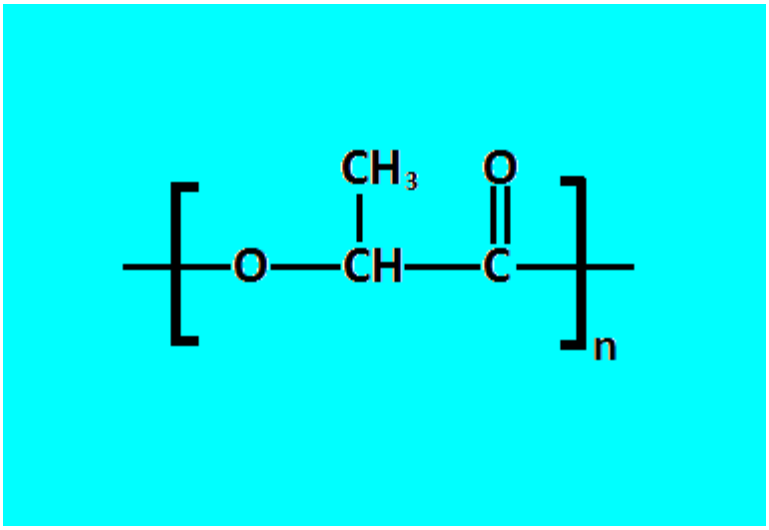

Figure 3.11-Chemical formula for poly ($_{L}$-lactic acid) (PLLA) polymeric repeat unit. This information was needed for the material section in the MCNP5 model. (This figure was obtained from *Ref. 21*)

3.3 Description of the Monte Carlo N-Particle Thermal Column Model

To perform an investigation regarding the neutron-activation of holmium-loaded polymeric microspheres in the thermal column of a TRIGA reactor, various MCNP5 models were built as follows: the overall shape of the thermal column structure was rectangular with a length of 154 cm, a height of 100 cm, and a width of 100 cm. Excluding the aluminum sheets surrounding the reflector and the "cut-out," cylindrical-shaped section where the planar source was located, the entire structure was made of graphite.

The microspheres were modeled as illustrated in *Figs. 3.12* and *3.13*, simulating a conventional pile-shaped packing configuration inside a cylindrical-shaped activation vial. In addition, the microspheres, along with the vials, were placed at various locations in the thermal column, which is a cavity, filled with air, surrounded by rectangular graphite blocks, as

illustrated in *Figs. 3.14* and *3.15*. The thermal column had a rectangular shape that was 125 cm long, 10 cm high and 10 cm wide.

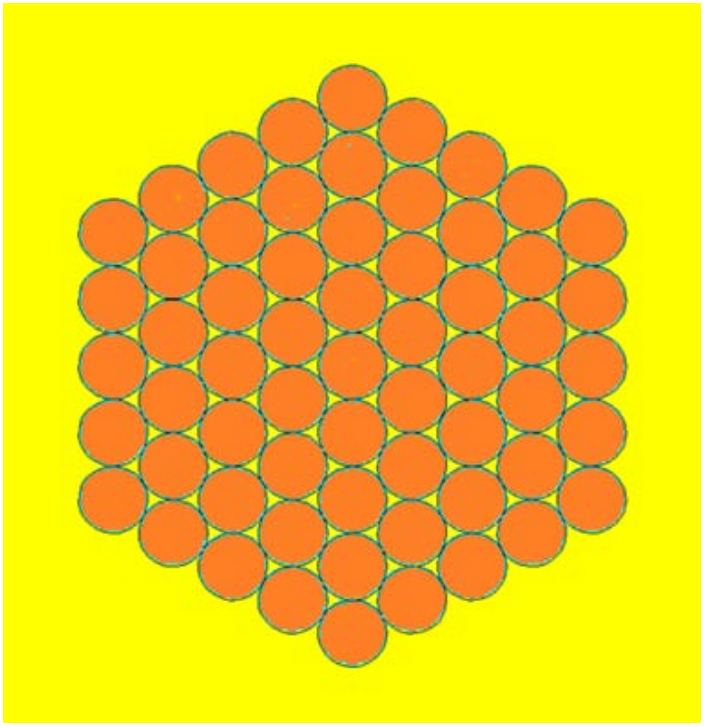

Figure 3.12-A cross-section view of a MCNP5 model showing holmium-labeled microspheres arranged in a pile-shaped packing configuration. (This layer was counted as odd-number when building the model.)

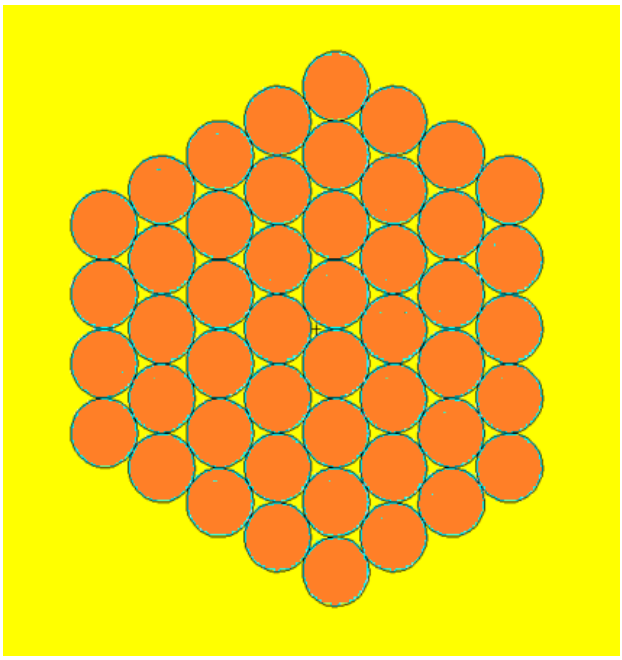

Figure 3.13-A cross-section view of a MCNP5 model showing holmium-labeled microspheres arranged in a pile-shaped packing configuration. (This layer was counted as even-number when building the simulation model.)

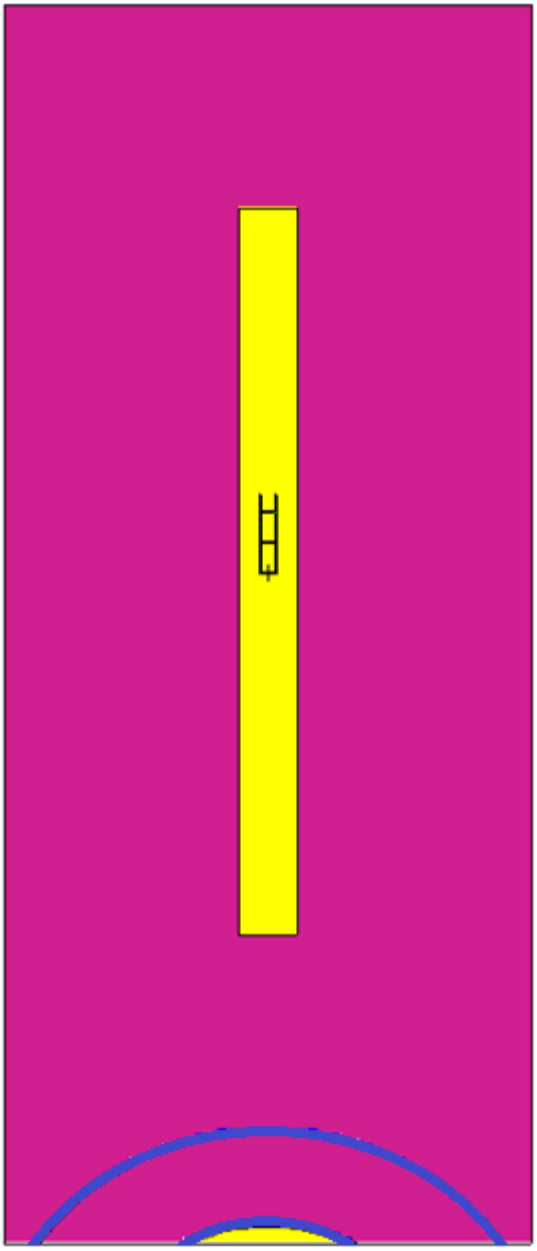

Figure 3.14-"Top view" of a section of the thermal column showing the graphite reflector, the planar source, the aluminum sheets, and the activation vials. The thermal column is modeled in MCNP5 code for the investigation of the neutron activation of holmium-labeled microspheres and the energy deposited by photons and neutrons in them.

Regarding the neutron source for the thermal column, it had a planar shape and was placed at the center of the same location a tubular holder, from the rotating specimen rack, would have been located, which was at 2.25 cm from the aluminum sheet that surrounds the graphite reflector, as illustrated in *Fig. 3.15*. In addition, the source was isotropic, and the neutrons flow only toward the activation vials, with the following initial flux types and magnitudes, as indicated in *Table 3.4*:

Table 3.4-Types of Fluxes provided by the Planar Neutron Source for the thermal column MCNP5 model

Flux Type (Energy range)	Magnitude* ($n\ cm^{-2}\ s^{-1}$)
Thermal	2×10^{12}
Epithermal	1×10^{11}
Fast	1×10^{11}

*These values were obtained from an e-mail sent from the Director of the Radiation Center at Oregon State University.

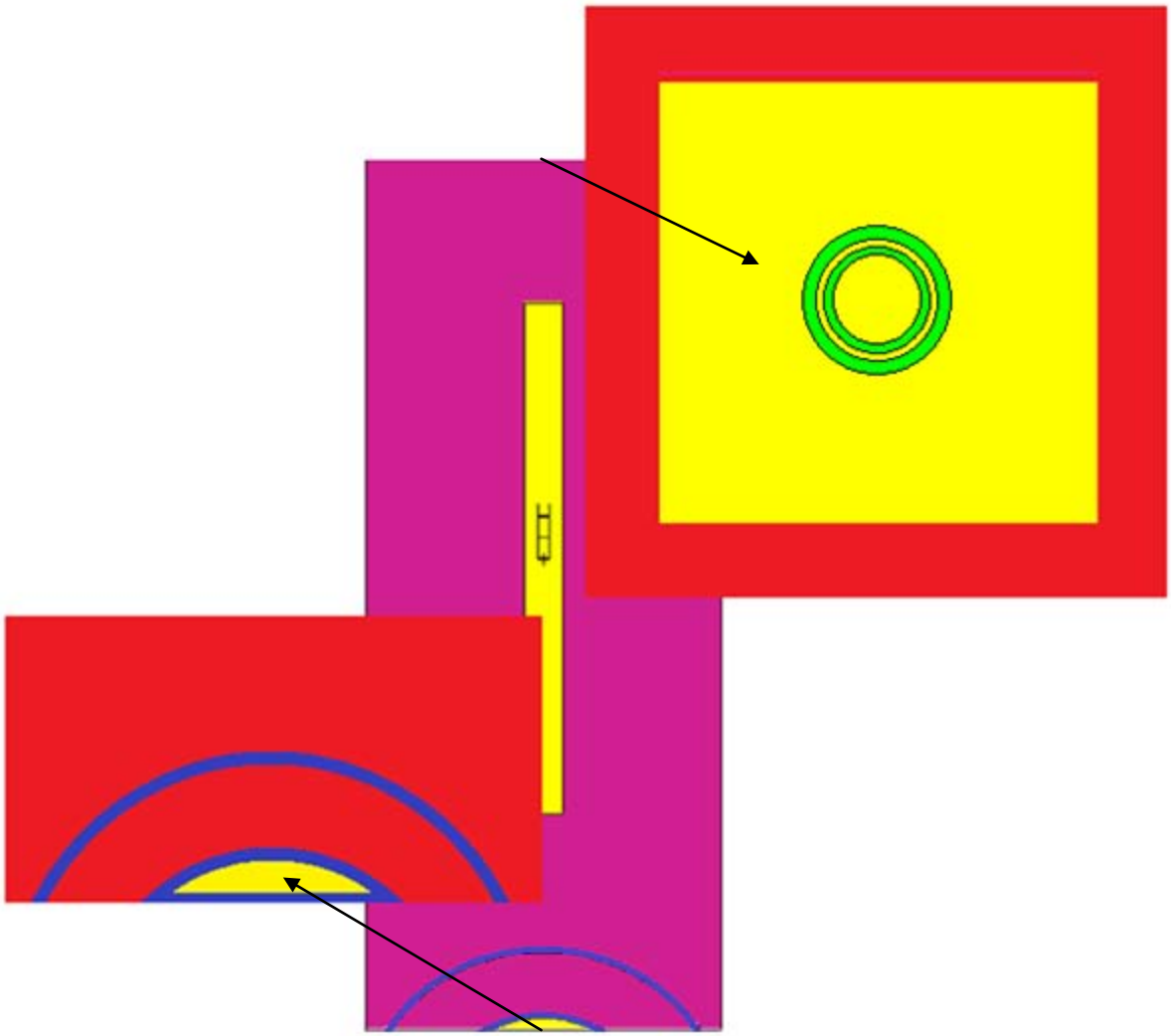

Figure 3.15-A ″cross-section view” of the thermal column MCNP5 model showing the activation vials, the square-shaped thermal column cavity, graphite reflector, planar source, and a section of the square-shaped “front view” of the thermal column structure.

Because the microspheres were modeled as solid and dry, they were double encapsulated, as illustrated in *Fig. 3.16*, in activation vials made of materials that were dependent on the type of simulation performed. As part of this investigation, both the material and the location of these vials were varied in the thermal column to determine their effects on the activation of the microparticles. The following materials, which had been used in previous studies (*Refs. 2 and 14*), were used: polyethylene, aluminum, and quartz.

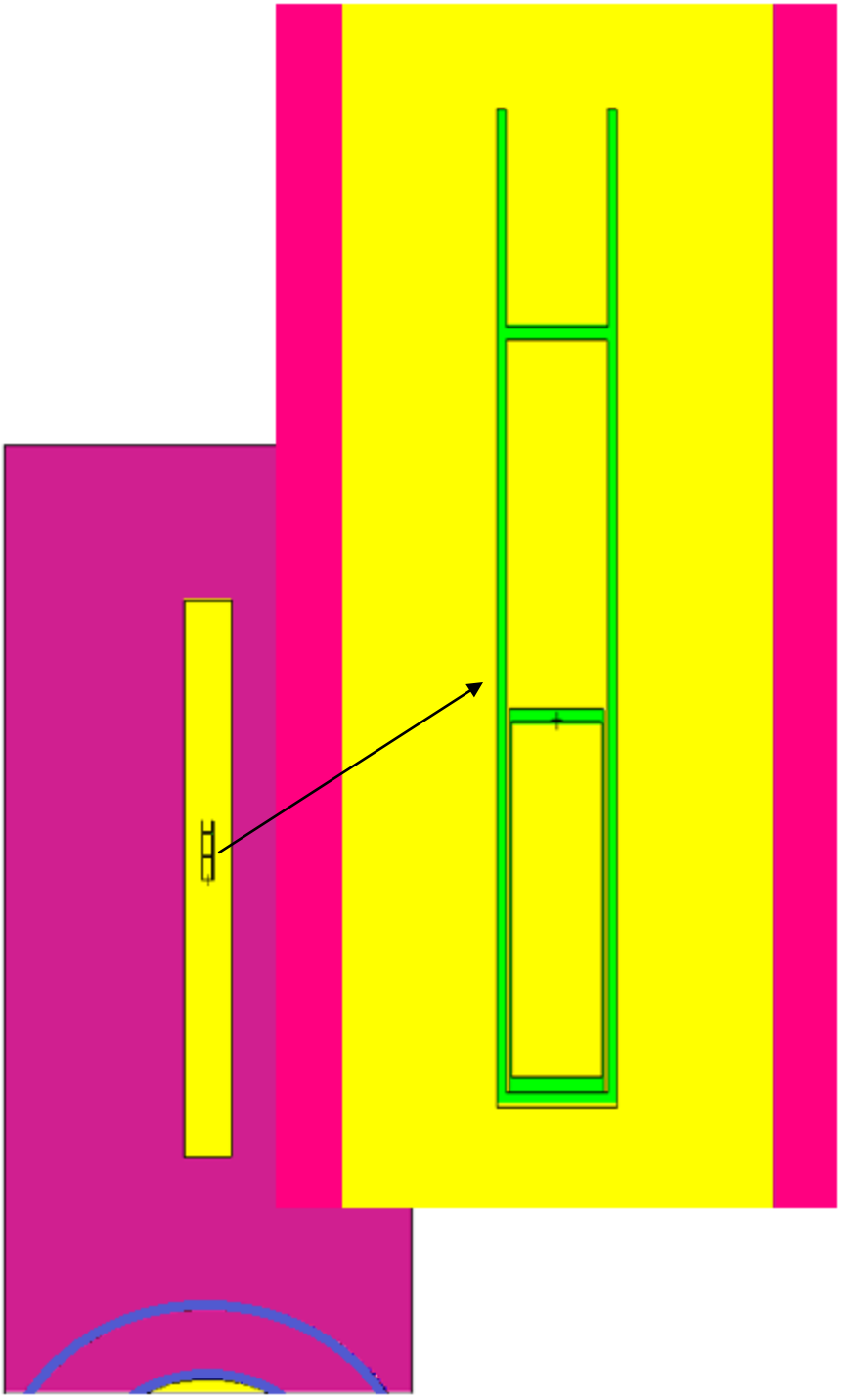

Figure 3.16-A" close view" of the activation vials inside the thermal column. For this investigation, both the material and the location of the activation vials are varied to determine effects on neutron activation and polymer degradation.

Finally, since the leading problem during neutron activation was degradation of the polymeric matrix containing the holmium complex, which may result in deformation, cracking, and melting, the microspheres were arranged in a sheet-shaped packing configuration, as illustrated in *Figs. 3.17* and *3.18*, to investigate its effects on neutron activation results (*Ref. 14)*.

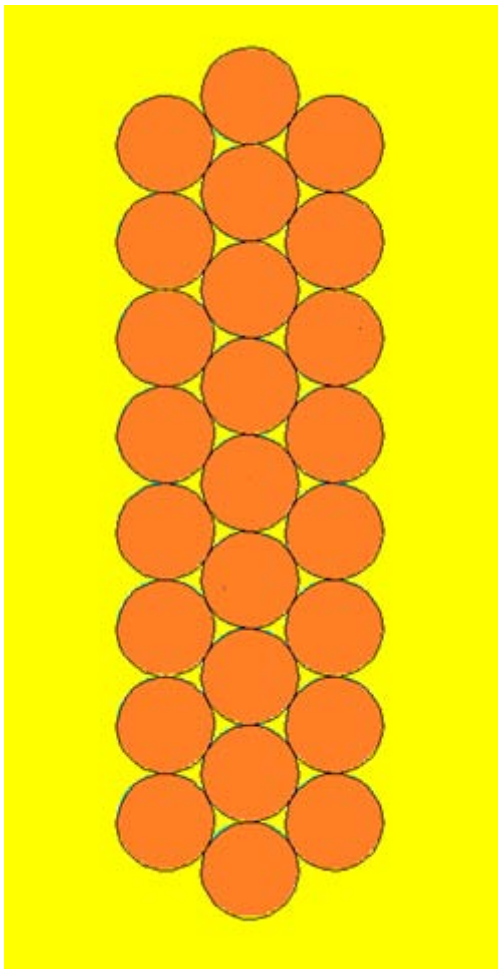

Figure 3.17-A cross-section view of a MCNP5 model showing holmium-loaded microspheres arranged in a sheet-shaped packing configuration. (This layer was counted as odd-number when building the model.)

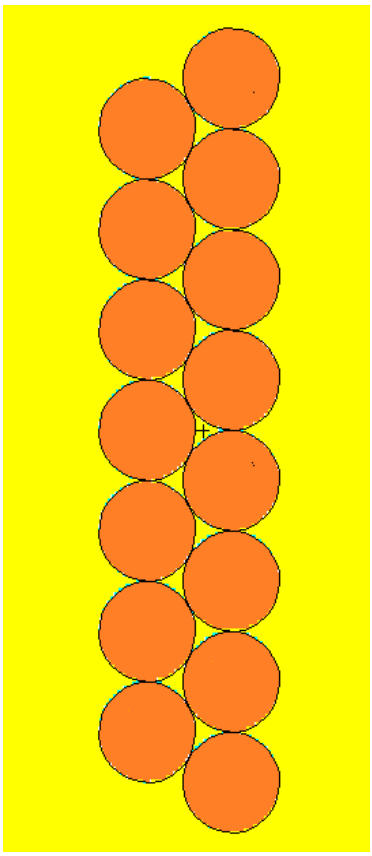

Figure 3.18-A cross-section view of a MCNP5 model showing holmium-loaded microspheres arranged in a sheet-shaped packing configuration. (This layer was counted as even-number when building the model.)

3.4 Assumptions Built into the Thermal Column Simulation Models

To simplify both the neutron activation and energy deposition calculations, the following assumptions were made: the microspheres inside the activation vials did not have a size distribution; all the microspheres were assigned a diameter of 37 μm, meeting one of several therapeutic requirements (*Ref. 2*). In addition, each one of the microsphere contained a holmium acetylacetonate (HoAcAc) mass fraction value of 17 % wt/wt in a poly ($_L$-lactic acid) matrix (*Ref. 2*); and the weight of the microspheres was not taken into account, disregarding a possible

contribution to microspheres deformation and cracking. Finally, only neutron and prompt gamma radiation were considered for the calculation of total energy deposited in both the polymetric matrix and the HoAcAc complex (*Ref. 14*).

3.5 Techniques Used to Investigate the Neutron Activation Simulations of Microspheres

For this investigation, two packing configuration (pile-shaped and sheet-shaped) were modeled inside the thermal column of a TRIGA reactor. As a benchmark, the pile-shaped packing configuration of ten "face layers" and four-diameter-thick "skin layers" placed inside activation vials was used, and skin layers of microspheres were added to it incrementally. Then, either the same amount of microspheres or close to it, as long as complete layers are added, was arranged into a sheet-shaped packing configuration.

Results were subsequently analyzed and compared to the original pile-shaped packing configuration's to determine effects on neutron activation, on temperature change rate (*dT/dt*) at contact points, on changes in enthalpy values for melting and crystallization, on changes in melting temperature, and on energy depositions in the microsphere's polymeric matrix and HoAcAc complex. In addition to changing the packing configuration, the activation vials were placed at different locations in the thermal column; the materials of which the vials were made were changed; and the neutron flux was manipulated to provide an uniform activation pattern throughout the microspheres.

For each MCNP5 simulation run, the following calculations were requested in the output for each microsphere (*Ref. 16*): average neutron flux exposure (*tally F4:N*); average neutron

energy deposition (*tally F6:N*); average photon flux (*tally F4:P*); and average photon energy deposition (*tally F6:P*). The average thermal neutron flux on each microsphere was used to calculate activation, target atom depletion rate, flux attenuation, and the time that it takes to reach therapeutic activity level at a specified neutron flux value.

It should be noted that, after several test runs, it was determined that, regardless of the packing configuration in the activation vials, the microspheres were never exposed to a uniform thermal neutron flux. Therefore, as a corrective action to this problem, the following techniques were performed: a polyethylene spacer, as illustrated in *Fig. 3.19*, of a specified length was modeled and was placed between the microspheres and the face of the thermal column. The objective of the spacer was to attempt to attenuate the thermal neutron flux from a maximum value down to an average value, generating a uniform neutron exposure throughout the microspheres, and consequently, a uniform activation. In addition, another technique involved placing the holmium-loaded microspheres, while arranged in a sheet-shaped packing configuration, in the middle of the activation vials and flanked on both sides by blank, polyethylene microspheres of similar size, as illustrated in *Fig. 3.20*. Simulation cases were run for each technique, as illustrated in the Results section.

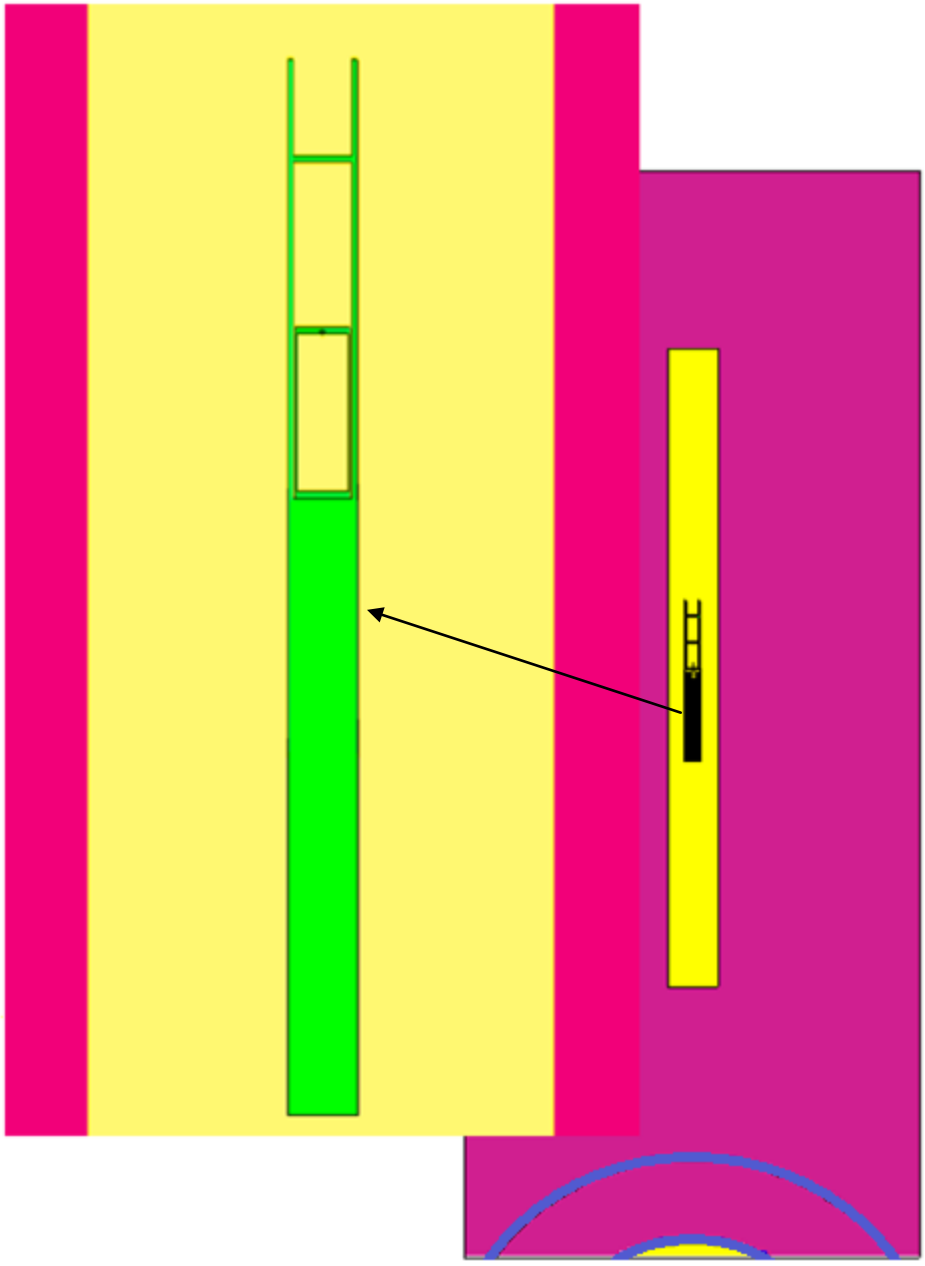

Figure 3.19-A" close view" of modified activation vials inside the MCNP5 model of the thermal column. A polymeric spacer was added to attempt to attenuate the neutron flux from a maximum to an average value throughout the sheet-shaped packing configuration.

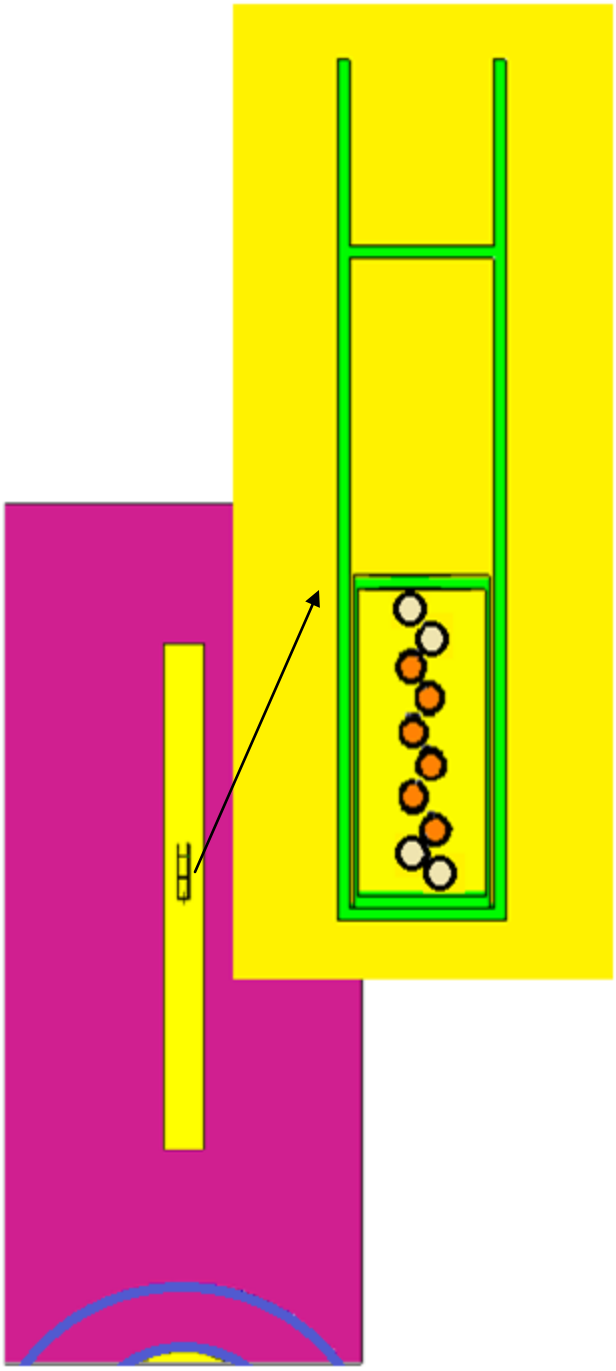

Figure 3.20-To maintain a uniform activation throughout the microspheres arranged in a sheet-shaped packing configuration, holmium-loaded microspheres are activated in the middle of the sheet while being flanked by a set of sacrificial polyethylene microspheres of similar size on each side.

The average photon energy deposition on each microsphere was used to determine the following: since in previous studies (*Refs. 17 and 18*) exposure to photons was used to determine the extent of degradation of the polymeric matrix, average photon energy deposition values were used to determine the effectiveness of minimizing irradiation-induced degradation during neutron activation when holmium-loaded microspheres were arranged in a sheet-shaped packing configuration, as opposed to a pile-shaped packing configuration. In addition, changes in these values, along with neutron-flux exposure results, were used to determine the effects of changing material types of which the activation vials were made, and for this investigation, both the pile-shaped packing configuration and the sheet-shaped packing configuration were modeled inside activation vials made from polyethylene, quartz, and aluminum, as illustrated in *Fig. 3.21*. Simulations were run for each case, and results were compared to determine if the packing configuration had either a positive or a negative effect on the holmium-loaded microspheres during neutron activation.

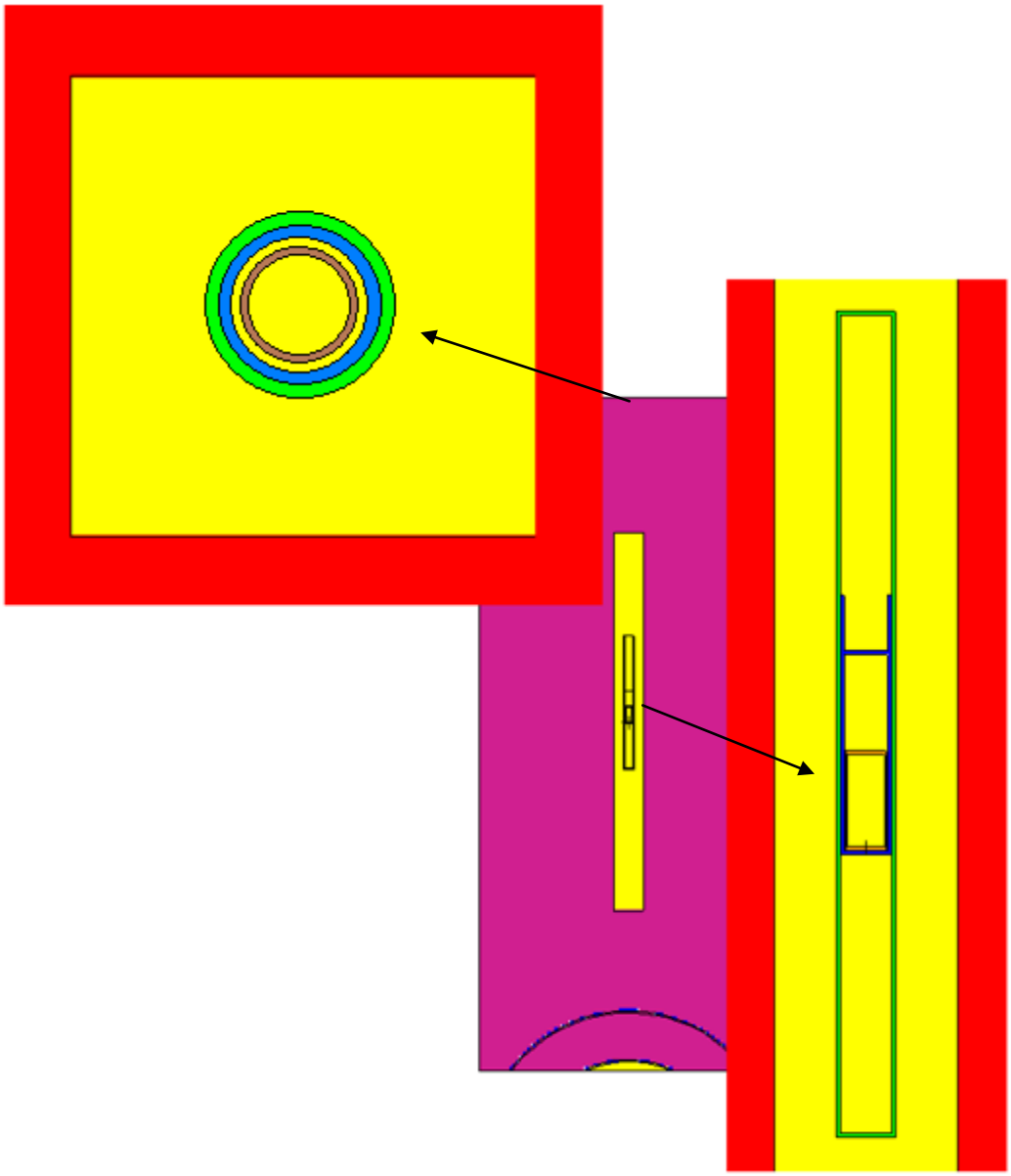

Figure 3.21-A" close view" of the activation vials inside the thermal column. For this study, the materials of which the activation vials were made were varied to determine effects on the neutron activation results.

Both the average neutron energy deposition and the average photon energy deposition not only were used to determine the advantages of arranging the holmium-loaded microspheres in a sheet-shaped, packing configuration over a pile-shaped, packing configuration, but also to

determine if a nuclear reactor was suitable for producing neutron-activated microspheres of acceptable quality for radioembolization therapy (*Ref. 14*). However, for the calculation of the temperature change rate at the contact points among microspheres in both the pile-shaped, packing configuration and the sheet-shaped, packing configuration, only the average-photon energy deposition was used, as stated in *Ref. 1*. Also, related to energy depositions in polymeric matrix was the calculation of dose, for which only average-photon energy deposition were used, as well (*Refs.3, 17, and 18*). Dose was used to determine the extent of degradation of the polymeric matrix that may result in deformation, cracking, or melting. Furthermore, dose, along with extent of degradation, was used to determine both melting point temperature and melting enthalpy values changes, which were material's physical properties that are typically affected by radiation exposure (*Refs.17 and 18*).

Finally, to determine whether the neutron flux generated in the thermal column of a 1 MWt-rated TRIGA reactor, along with other parameters previously mentioned, was sufficient to activate microspheres loaded with holmium-165 in a polymeric matrix (PLLA) to therapeutic levels (7.5-15 GBq, *Ref. 14*), a calculation was performed by using the total activity attained by the amount of microspheres found in both the pile-shaped packing configuration and the sheet-shaped packing configuration. Once this total activity was determined, its value was used to extrapolate the activity that may be attained by the amount of microspheres found in a typical patient dosage of 600 mg. If the extrapolated activity was equal to or higher than the therapeutic activity value found in *Ref. 14*, the neutron flux magnitude generated by a 1 MWt-rated TRIGA reactor was considered acceptable, provided other requirements, such as irradiation time and energy deposition values, are also acceptable (*Ref. 14*).

3.6 Degradation of Polymeric Matrix by High-Energy Radiation

Radiation can alter the physical properties of polymers through main chain scission and cross-linking. Free radicals are formed when macromolecules of polymers are excited under ionizing radiation, and once formed they are free to react with one another or initiate further reactions among polymeric chains, affecting material properties (*Ref. 18*)**.** For example, the combination of two radicals leads to cross-linking or recombination in the amorphous and crystalline regions, respectively, whereas chain transfer and the subsequent splitting results in chain scission. Usually, both these processes take place simultaneously for many polymers (*Ref. 18*)**.**

During neutron activation, the PLLA polymeric matrix of the microspheres loaded with holmium-165 is exposed to the following types of radiation: electron, neutron, and gamma. However, for this investigation, only neutron and gamma radiations were considered for causing the most severe, irradiation-induced degradation effects. Neutron irradiation of PLLA results in similar processes as found in both *e-irradiation* and *γ-irradiation*, namely a decrease in molecular weight and loss in crystallinity. Besides damage to the PLLA, also some damage of the HoAcAc complex occurs as well (*Ref. 17*).

The degree of damage that is inflicted upon the organic PLLA matrix is consequently dependent on both the irradiation characteristics and irradiation time in a particular reactor facility. Therefore, it is paramount to know exactly how long a typical patient dosage (600 mg, 39.68-79.35 Gy) of holmium-loaded microspheres can be irradiated while remaining sufficiently intact for treatment of patients (*Refs. 4 and 14*)**.** In addition, in order to have sufficient time for

transportation from the reactor facilities to the hospital, radioactive, holmium-loaded microspheres must be neutron-irradiated for a certain period of time. The minimum irradiation time is therefore dependent on logistics and the required amount of radioactivity to be instilled, consequently the thermal neutron flux. Conversely, the maximum irradiation time is set by the extent of irradiation damage that occurs (*Ref. 14*)**.**

3.6.1 *Determination of Crystallinity Phase Destruction of Polymeric Matrix*

When subjected to ionizing radiation, PLLA is known to undergo random chain scission on the crystalline state, and the number of damage units in the crystalline region is determined from crystalline and melting temperatures and enthalpy values by absorption of 100 eV energy (*Ref. 17*). However, it is assumed that the polymer is composed of distinct, non-interacting amorphous and crystalline regions where reordering of the structure only occurs at the melting temperature of the crystalline component (*Ref. 17*).

This model was used to determine the % crystallinity of polymers which can be determined by applying the following equation:

$$\% \ Crystallinity = (\Delta_{irr}/\Delta H_{100}) \ x \ 100 \qquad (19)$$

where ΔH_{irr} and ΔH_{100} denote the change in melting enthalpy values of an irradiated sample and of a fully crystallized sample, respectively (*Ref. 17*). To use *Eq. (19)* the value for the change in melting enthalpy of a 100% crystalline *PLLA* is required, and its value was estimated to be 75.57 J/g (*Ref. 17*).

The fraction of undamaged units in the crystalline region *(X)* by radiation was determined as follows:

$$X = \chi_{cf}/\chi_{co} \qquad (20)$$

where χ_{cf} and χ_{co} represent the percent crystallinity of un-irradiated and irradiated samples, respectively (*Ref. 17*). If *X* is substracted from 1, it gives the fraction of damaged units. The *G* value of a polymer is determined by applying the following equation (*Ref. 17*):

$$G \propto N/MD \qquad (21)$$

If *Eq. (21)* is multiplied by *(1-X), the G* value of a polymer can be expressed as the number of units of polymer damaged in crystalline region per 100 eV of energy absorption *(G(-u))* and is determined by applying the following equation:

$$G(-u) = (1-X)N/DM \;\; 10^2/6 \times 10^{18} \qquad (22)$$

where *N*, *M*, and *D* denote the *Avogadro's number*, the molecular weight of repeating units and the dose in terms of kGy, respectively, and the value 6 x 10^{18} corresponds to the conversion factor of kGy to eV (*Ref. 17*). In plotting of the graph *(1-X)* versus *D*, slopes are proportional to the damage in the crystalline regions (*Ref. 17*). As seen in *Table 3.5* and *Fig. 3-22a* and *Fig. 3-22b*, a substantial decrease was observed in the crystallization and melting enthalpy values with increasing dose.

Table 3.5-Crystallization and melting enthalpy data of PLLA irradiated in air and vaccum. (This table was obtained from *Ref. 17*.)

Dose (kGy)	Air		Vacuum	
	Melting (J/g)	Crystalliza-tion (J/g)	Melting (J/g)	Crystalliza-tion (J/g)
0	55.69	43.20	55.69	43.20
10	50.99	41.88	49.17	35.75
25	48.36	38.02	43.30	31.72
50	44.25	34.56	40.13	29.12
80	36.05	29.53	29.78	25.47

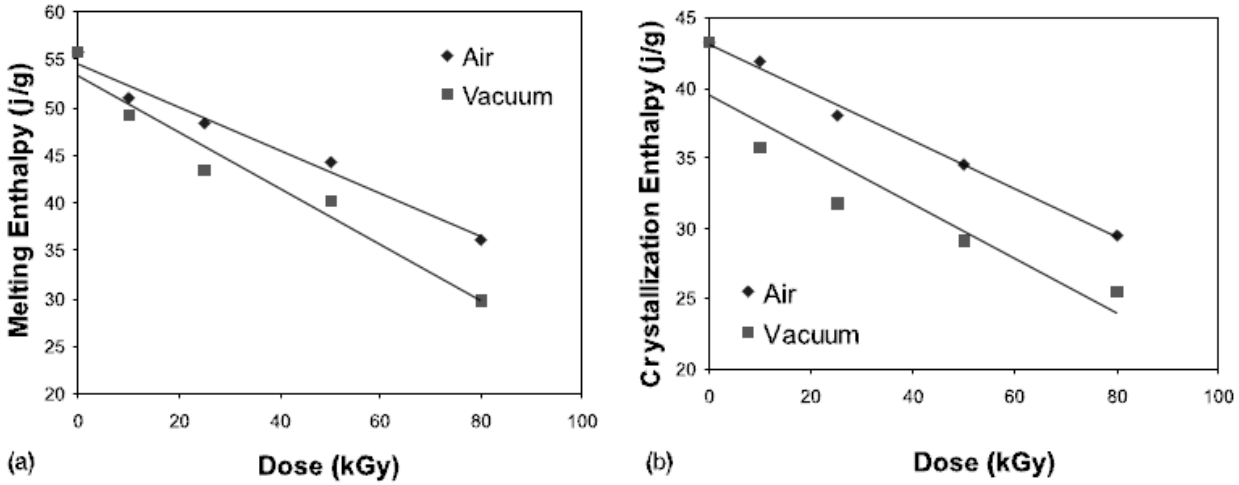

Figure 3.22-(a) Crystallization enthalpy change as a function of dose irradiation. (b) Melting enthalpy change as a function of dose irradiation. (This figure was obtained from *Ref. 17*.)

To find the number of damaged units of PLLA by *γ-rays*, the crystallinity values of PLLA irradiated to various doses in air and vacuum were calculated by using *Eq.(19)* and they are presented in *Table 3.6*. These crystallinity data were plotted in *Fig. 3-23*, and it shows a decrease in the crystallinity with increasing of irradiation dose.

Table 3.6-The crystallinity values of PLLA irradiated in air and vaccum. (This table was obtained from *Ref. 17*.)

Dose (kGy)	Crystallinity (%)	
	Air	Vacuum
0[a]	75.00	75.00
10	68.00	66.00
25	65.00	58.00
50	59.00	54.00
80	48.00	40.00

[a] As received sample.

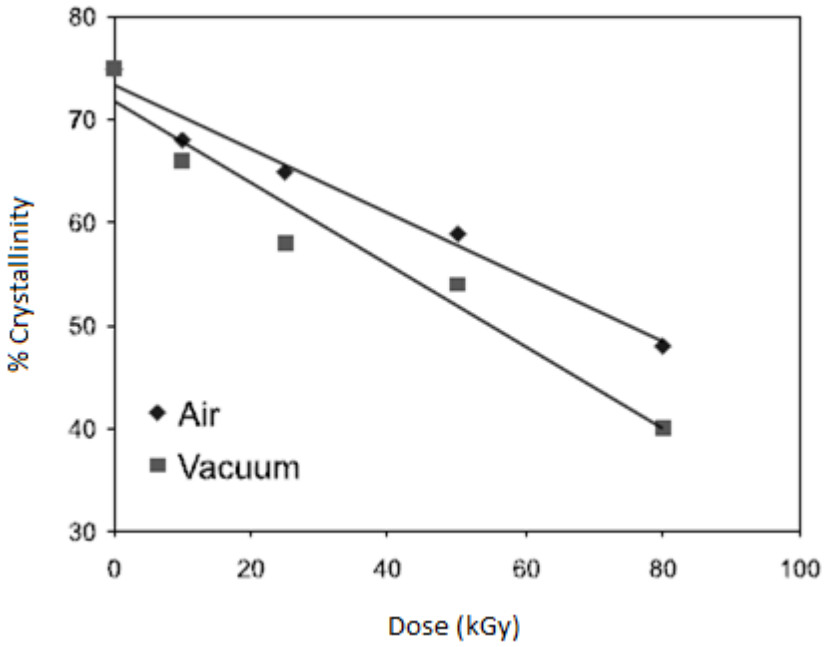

Figure 3.23-Plot of the change in the % Crystallinity as a function of the irradiation dose. (This figure was obtained from *Ref. 17*.)

The fraction of undamaged units *(X)* by irradiation was calculated from the crystallinity data *(χ)* obtained by using *Eq. (20)* and results are presented in *Table 3.7*. On the other hand, the fraction of damaged units of irradiated samples in air and vacuum were plotted versus the dose,

and the results are shown in *Fig. 3.24*. The slope of lines gives *G(-u)* value according to *Eq (22*). In conclusion, PLLA undergoes random main chain scission in the presence of air and in a vacuum, when irradiated with *γ-rays* at ambient temperature, and shows a significant decrease in crystallinity and damage in the crystalline regions (*Ref. 17*).

Table 3.7-The fraction of undamaged *(X)* and damaged *(1-X)* units in crystalline region for PLLA irradiated in air and vacuum. (This table was obtained from *Ref. 17*.)

Dose (kGy)	Air		Vacuum	
	X	$(1-X)$	X	$(1-X)$
0	1.00	0.00	1.00	0.00
10	0.91	0.09	0.88	0.12
25	0.87	0.13	0.77	0.23
50	0.79	0.21	0.72	0.28
80	0.64	0.36	0.53	0.47

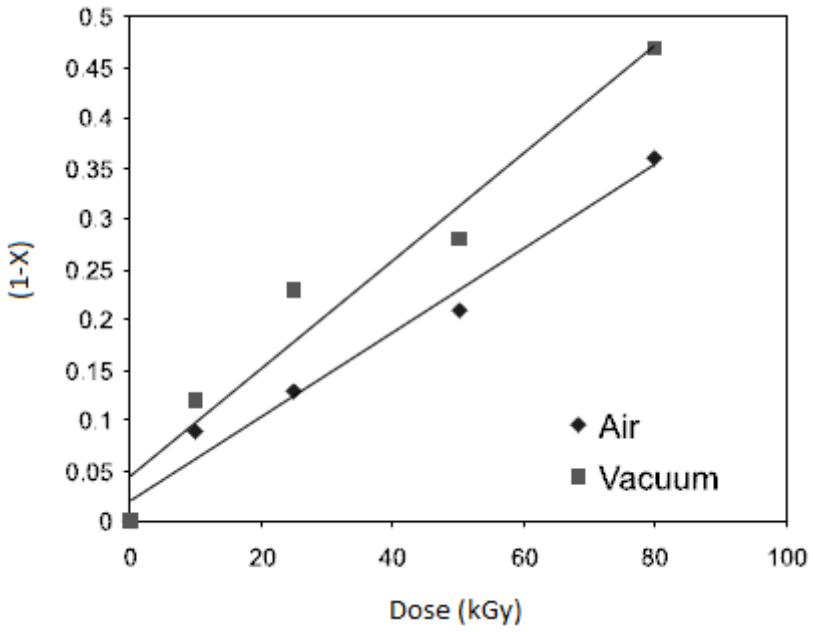

Figure 3.24-The plot of fraction of damaged PLLA units against dose. (This figure was obtained from *Ref. 17*.)

The data, namely for air, contained in *Tables 3.5* through *3.7* were utilized as follows: as an objective to this investigation, it was necessary to determine the extent of damage induced by radiation to which the holmium-loaded microspheres were exposed during neutron activation, while arranged in either a pile-shaped, packing configuration or a sheet-shaped, packing configuration, since it is reflected on product yield, quality, and dose. And the extent of this damage, or degradation, can be assessed by measuring a decrease in magnitude of the material properties for PLLA such as melting point temperature, change in melting enthalpy values, change in crystallization enthalpy values, undamaged unit fraction, and % crystallinity, as opposed to a material property such as damage unit fraction, for which the extent of damage is measured by its increase in magnitude.

To correlate results obtained from the MCNP5 simulations to the irradiation-induced degradation of the microspheres' polymeric matrix, the data included in *Tables 6* through *8* were plotted, and an equation for each curve was generated. Once a correlation for each of the material properties listed above was established, results from both the pile-shaped, packing configuration and the sheet-shaped, packing configuration were analyzed and were compared. As one of the objectives of this investigation, the packing configuration that would indicate the least amount of irradiation-induced damage of the polymeric matrix would be selected for neutron-activating holmium-loaded microspheres in the thermal column of a TRIGA reactor.

3.6.2 *Determination of Crystallinity Destruction and Melting Point and Enthalpy of Fusion Reductions of a Polymeric Matrix*

The relation of the mole fraction, *x*, of crystalline units after irradiation to values of the melting point temperature ($T_{m,o}$) before neutron activation ($x=1$) and to values of the melting point temperature ($T_{m,D}$) after neutron activation ($x<1$) was determined as follows:

$$1/T_{m,D} - 1/T_{m,o} = (-R/\Delta H)\, ln(x) \qquad (23)$$

where R and ΔH denote the gas constant and the change in melting enthalpy per mole of crystalline units, respectively (*Ref. 19*).

Using results from MCNP5 simulations, *Eq.(23)* was applied to determine the advantages and disadvantages presented by both the pile-shaped, packing configuration and the sheet-shaped, packing configuration during neutron activation in the thermal column of a TRIGA reactor. For example, a packing configuration showing the lowest sum of melting point temperatures added from all the holmium-loaded microspheres shows the most radiation-induced degradation of the polymeric matrix, making the microsphere prone to flaws such as melting, deformation, cracking, and surface pores.

3.6.3 *Determination of Melting Point Temperature at Points of Contact between Polymeric Matrices*

A theoretical temperature increase without heat transfer from the activation vial in the simulations was determined by applying the following equation:

$$dT/dt = 1/C(dE/dt) \qquad (24)$$

where *dT/dt* is the temperature increase per second (K s^{-1}), *dE/dt* is the energy deposited per kilogram per second (kJ kg^{-1} s^{-1}), and *C* is the PLLA's specific heat value, which is estimated to be 1.5 kJ kg^{-1} K^{-1} (*Ref. 1*). In the simulations, the polymer melting point was theoretically reached at the points where microspheres touch each other, as illustrated in *Fig. 3.25*, but without a general polymer melting; therefore, a heat transfer certainly occurred from the microspheres out to the activation vial (*Ref. 1*). Furthermore, pore formation may be ascribed to the lower specific heat value of holmium (0.16 kJ kg^{-1} K^{-1}), yielding much higher increasing temperature change rate in the holmium atom than in the PLLA matrix. Therefore, the holmium atoms in the irradiated microspheres may represent some local hot spots in the PLLA matrix that may lead to surface pores (*Ref. 1*).

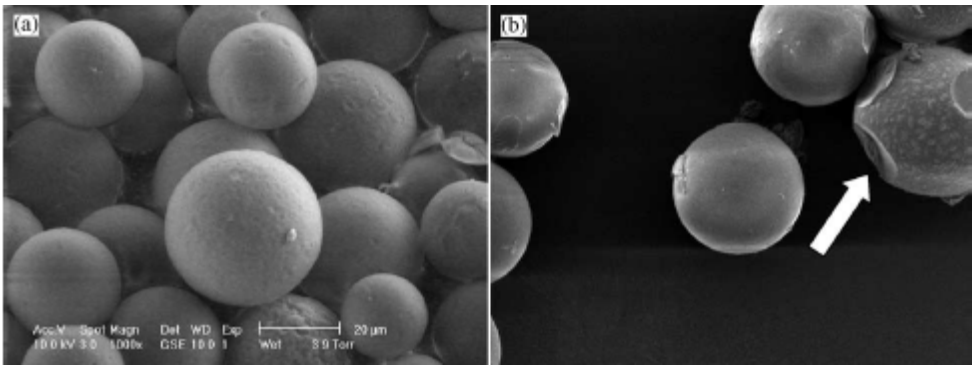

Figure 3.25-Electron micrographs of microspheres with a loading of 17% (wt/wt) ^{165}Ho. Non-irradiated microspheres have a spherical structure and smooth surface (a) After irradiation only small surface changes were seen (white arrow; b). (This figure was obtained from *Ref. 14*.)

This concept was applied to the neutron activation simulations as part of determining the advantages and disadvantages presented by both the pile-shaped, packing configuration and the

sheet-shaped, packing configurations. When using *Eq.(24)*, it was assumed that photons deposited energy in the polymeric matrix, and to make the simulation model calculations as conservative as possible, the energy transferred from these photons was the same as the energy absorbed by the polymeric matrix.

3.6.4 *Determination of Suitability for Neutron Activation of Microspheres Loaded with Holmium-165 in a in Specified Nuclear Reactor*

To determine whether a specified nuclear reactor is suitable for routine production of microspheres loaded with holmium-165 in a polymeric matrix made of PLLA, a ratio of neutron flux to the sum of energies deposited by both neutrons and photons has been established, as indicated in *Ref. 14*, that relates neutron flux to degradation extent of a polymeric matrix. This ratio was represented as follows:

$$Ratio = \frac{Thermal\ Neutron\ Flux}{(Sum\ of\ Neutron\ Energy\ and\ Gamma\ Energy\ Depositions)} \qquad (25)$$

where the thermal neutron flux is in neutrons per cm^2 per h and the total energy deposition is in MeV per g per h. For this investigation, a ratio of 15 was used as a benchmark for comparing the performance of microspheres arranged in a sheet-shaped, packing configuration to the performance of microspheres arranged in a conventional pile-shaped, packing configuration during neutron activation.

A previous study showed that a ratio of 15 implies that holmium-loaded microspheres of acceptable quality can be produced in a nuclear reactor of a specified rated power. Once an

adequate ratio is established, the maximum irradiation time must be determined by carrying out the irradiation of a few samples of microspheres loaded with holmium-165 in a polymeric matrix made of PLLA. For this investigation, a maximum irradiation time of 7 hours was selected for a ratio of 15, as indicated in *Ref. 14*, to determine if holmium-loaded microspheres in the simulations can be activated to therapeutic levels (7.5 to 15 GBq) without damaging both holmium complex and the polymeric matrix; any results showing ratios lower than 15 indicate microspheres prone to damage, lowering both the overall product's yield and quality.

4.0 Results

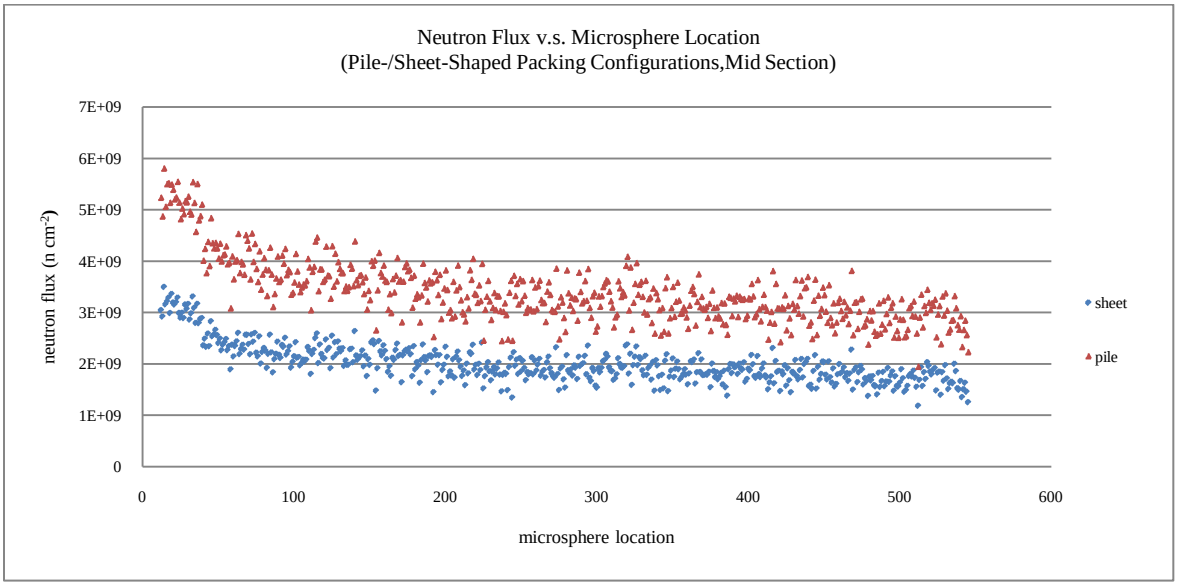

Figure 4.1-A comparison between the neutron flux exposure results from holmium-loaded microspheres arranged in a sheet-shaped, packing configuration and the neutron flux exposure results from holmium-loaded microspheres arranged in a pile-shaped, packing configuration.

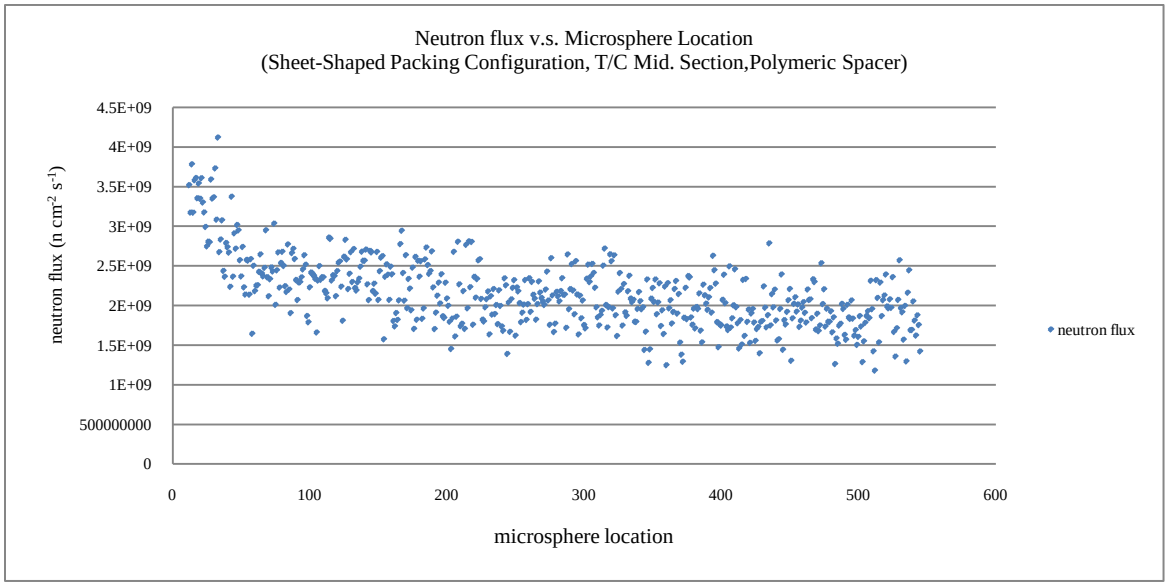

Figure 4.2-Neutron flux exposure results on holmium-loaded microspheres arranged in a sheet-shaped, packing configuration with polymeric spacer attached to activation vials.

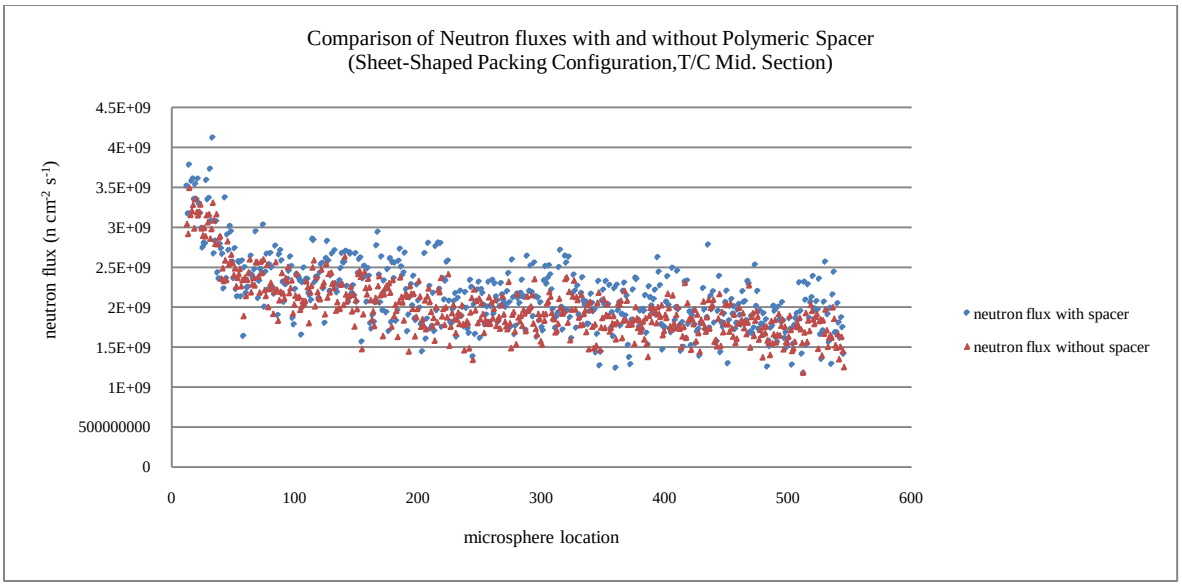

Figure 4.3-A comparison between the neutron flux exposure results from holmium-loaded microspheres arranged in a sheet-shaped, packing configuration with a polymeric spacer attached to the irradiation vials and the neutron flux exposure results on holmium-loaded microsphere arranged in a sheet-shaped, packing configuration without a polymeric spacer attached to the activation vials.

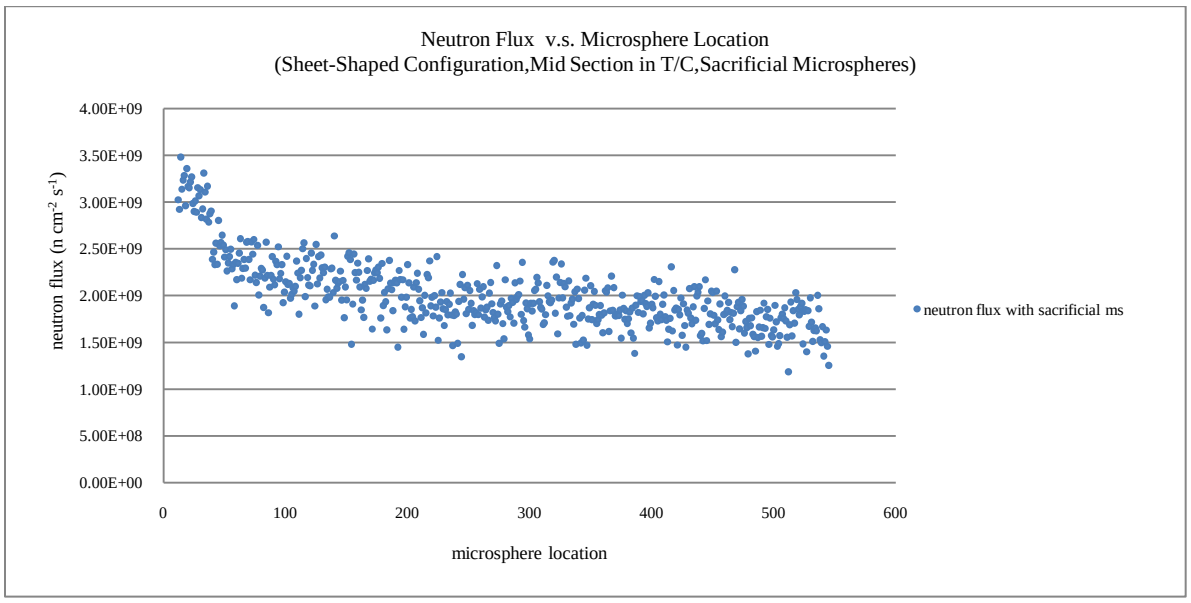

Figure 4.4- Neutron flux exposure results for sheet-shaped, packing configuration containing both blank microspheres and holmium-loaded microspheres. The purpose of the blank microspheres is to maintain an uniform neutron flux exposure pattern on the microspheres loaded with holmium, resulting in an uniform activation throughout.

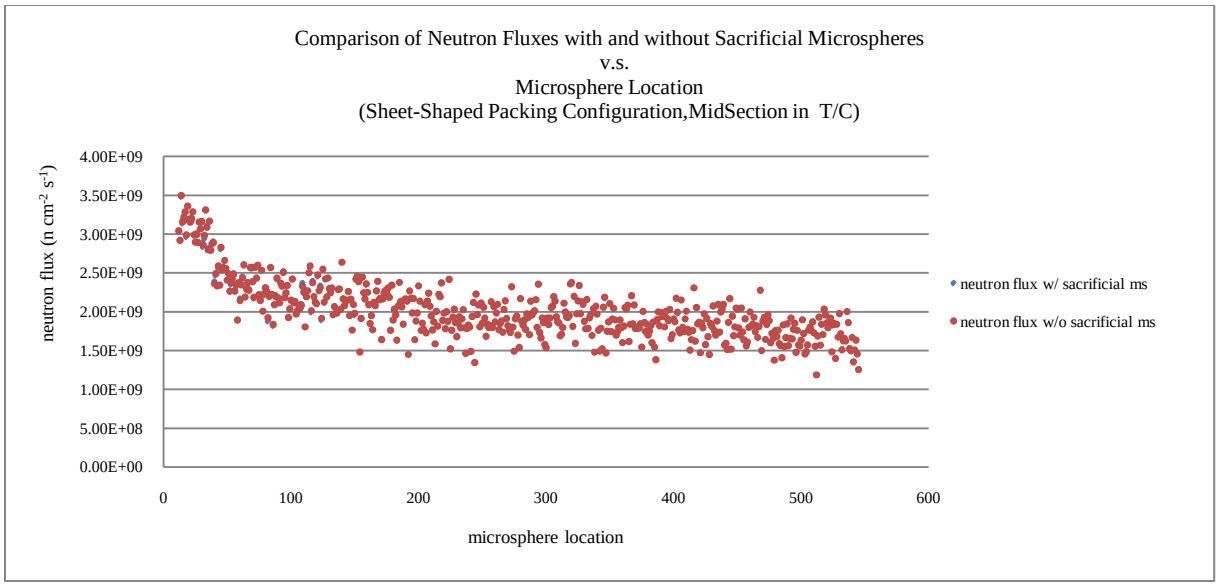

Figure 4.5-A comparison between the neutron flux exposure results from all-holmium-loaded microspheres arranged in a sheet-shaped, packing configuration and the neutron flux exposure results from a sheet-packing, configuration containing both blank sacrificial microspheres and holmium-loaded microspheres.

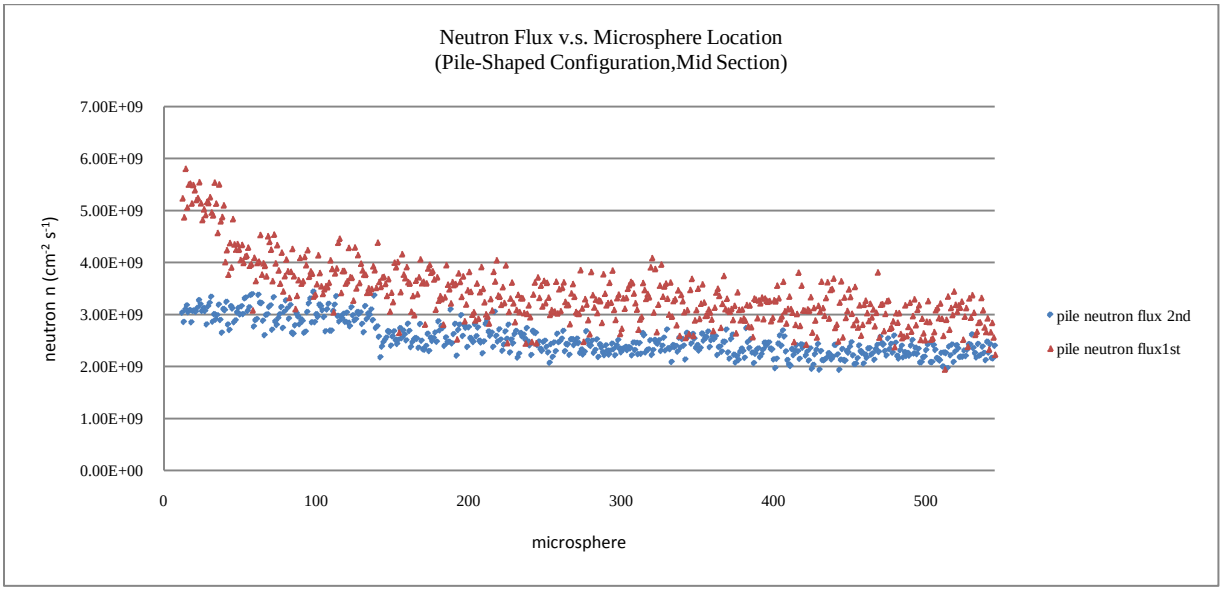

Figure 4.6-A comparison of the neutron flux results between two pile-shaped, packing configurations of different sizes to demonstrate the neutron flux suppression effects on the microspheres located in the inner regions of the pile during neutron irradiation.

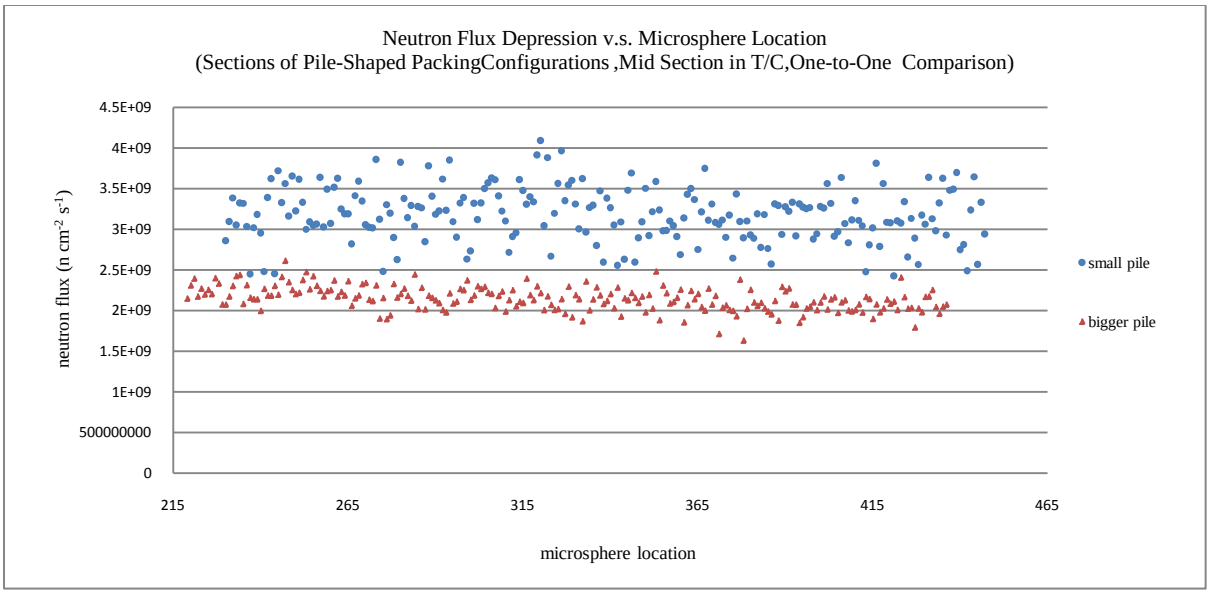

Figure 4.7-Sections of two pile-shaped packing configurations of different sizes to demonstrate the neutron flux suppression effects on the microspheres located in the inner regions of the pile during neutron irradiation.

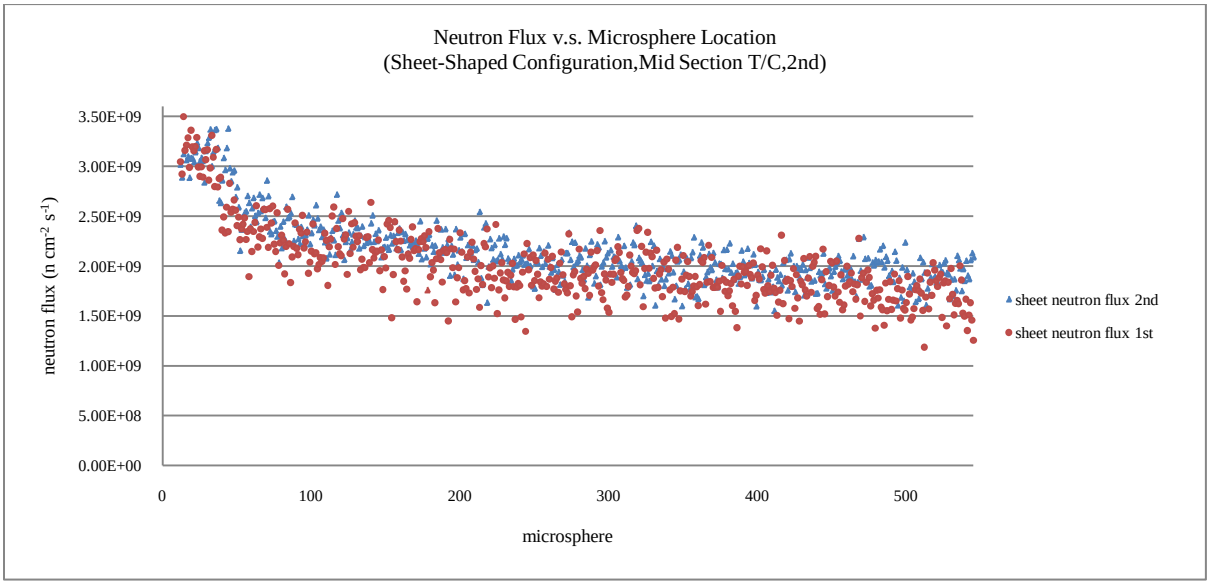

Figure 4.8- A comparison of the neutron flux results between two sheet-shaped, packing configurations of different sizes to demonstrate the lack of neutron flux suppression effects on the microspheres.

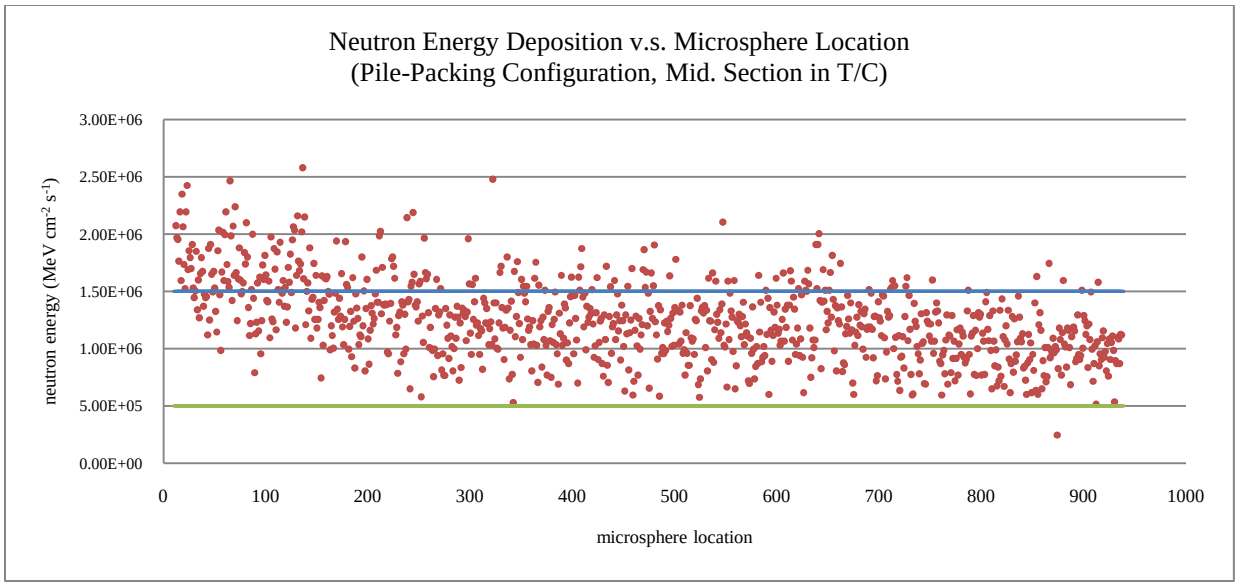

Figure 4.9-Simulation results showing neutron energy deposited per microsphere loaded with holmium in a polymeric matrix (PLLA) arranged in a pile-shaped, packing configuration to determine if a nuclear reactor is suitable for acceptable-quality neutron activation. Lines were generated on the chart to point out differences with other charts.

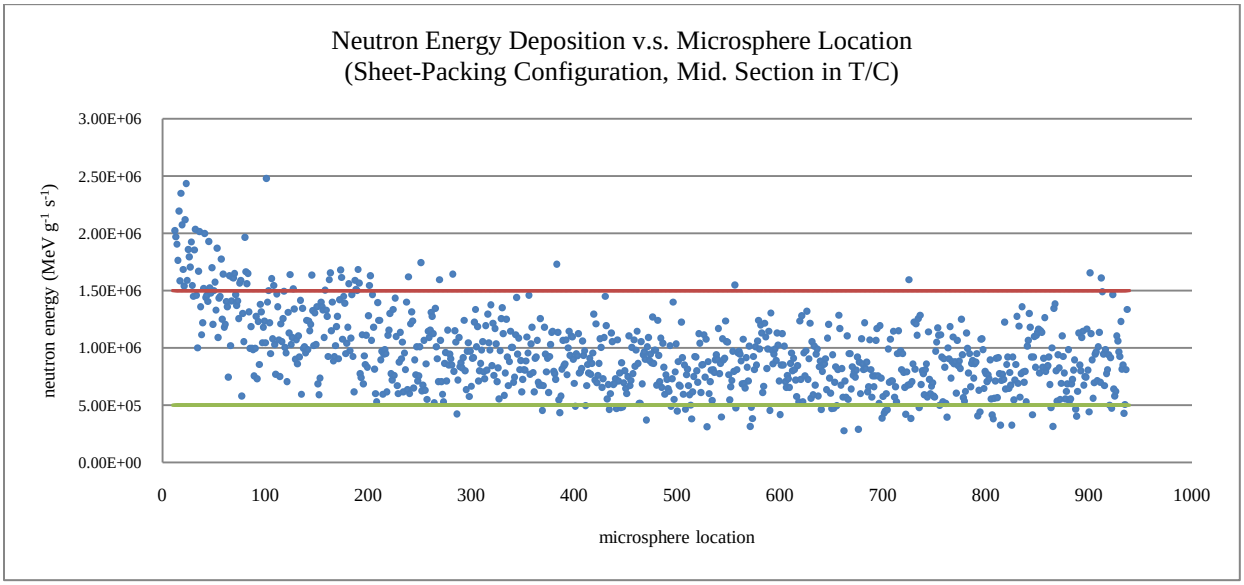

Figure 4.10-Simulation results showing neutron energy deposited per microsphere loaded with holmium in a polymeric matrix (PLLA) arranged in a sheet-shaped packing configuration to determine if a nuclear reactor is suitable for acceptable-quality neutron activation. Lines were generated on the chart to point out differences with other charts.

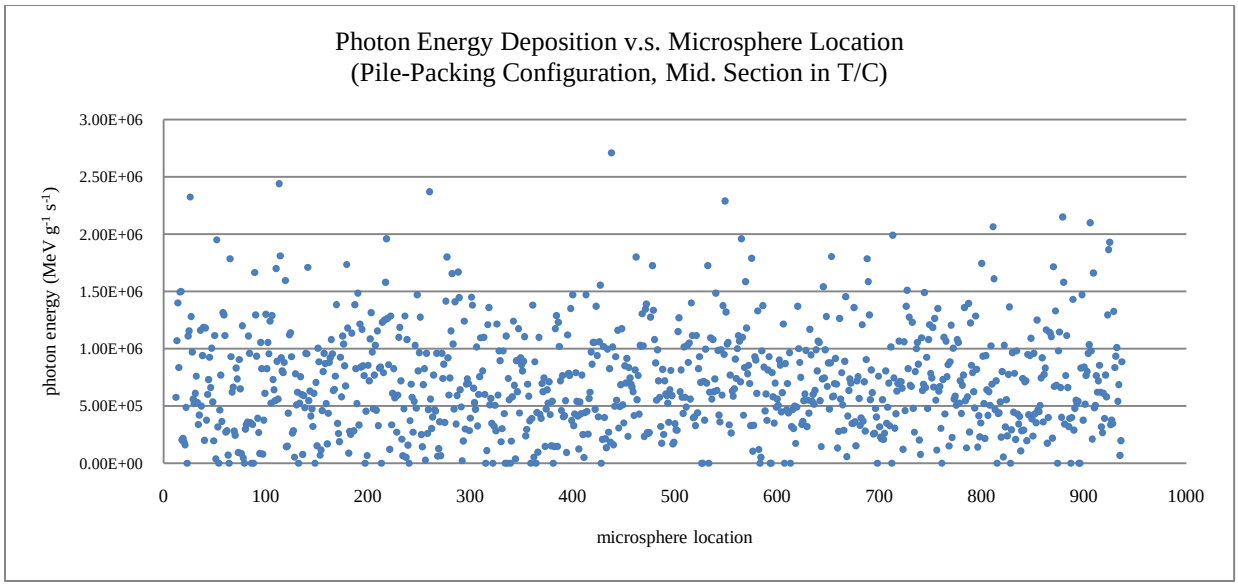

Figure 4.11-Simulation results showing photon energy deposited per microsphere loaded with holmium in a polymeric matrix (PLLA) arranged in a pile-shaped packing configuration to determine if a nuclear reactor is suitable for acceptable-quality neutron activation.

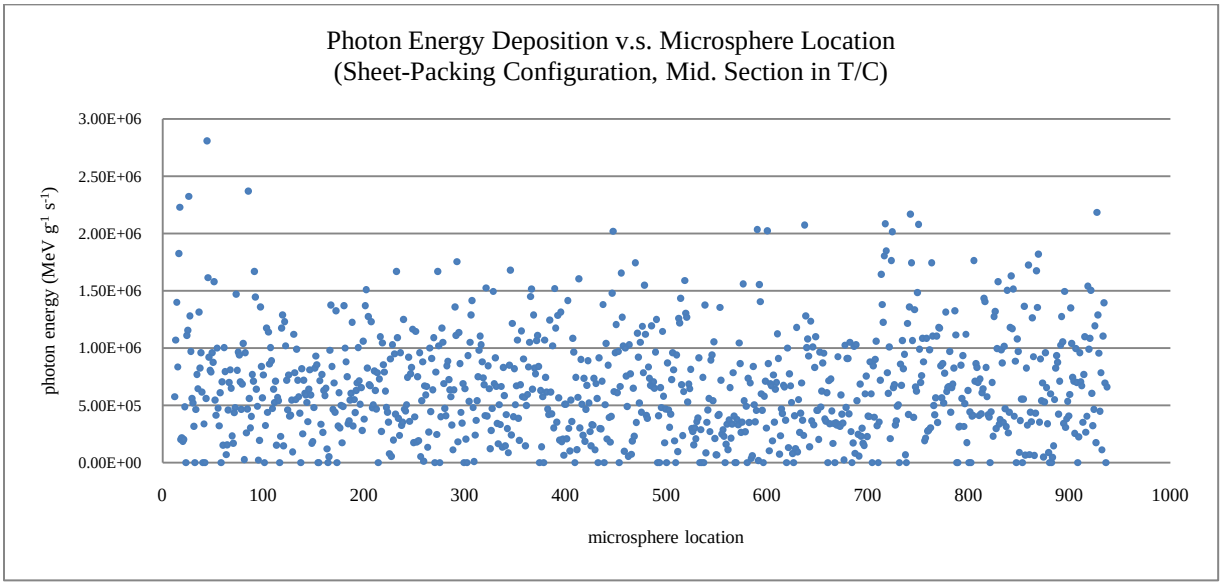

Figure 4.12- Simulation results showing photon energy deposited per microsphere loaded with holmium in a polymeric matrix (PLLA) arranged in a sheet-shaped, packing configuration to determine if a nuclear reactor is suitable for acceptable-quality neutron activation.

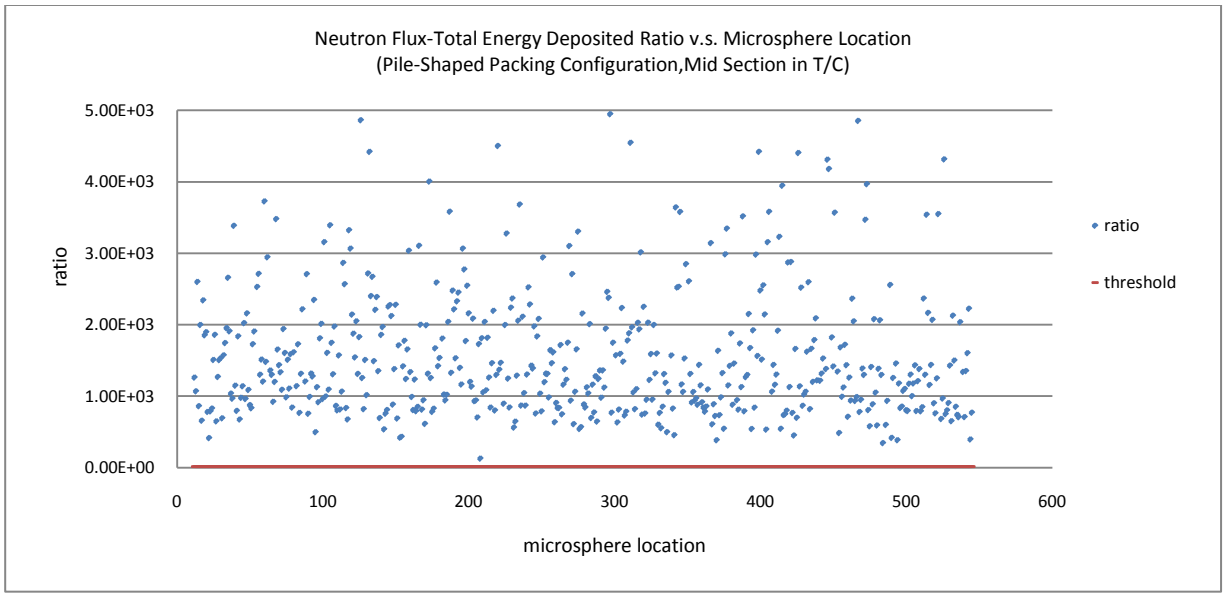

Figure 4.13-Simulation results showing neutron flux-to-total energy deposited per microsphere loaded with holmium in a polymeric matrix (PLLA) arranged in a pile-shaped packing configuration to determine if a nuclear reactor is suitable for acceptable-quality neutron activation.

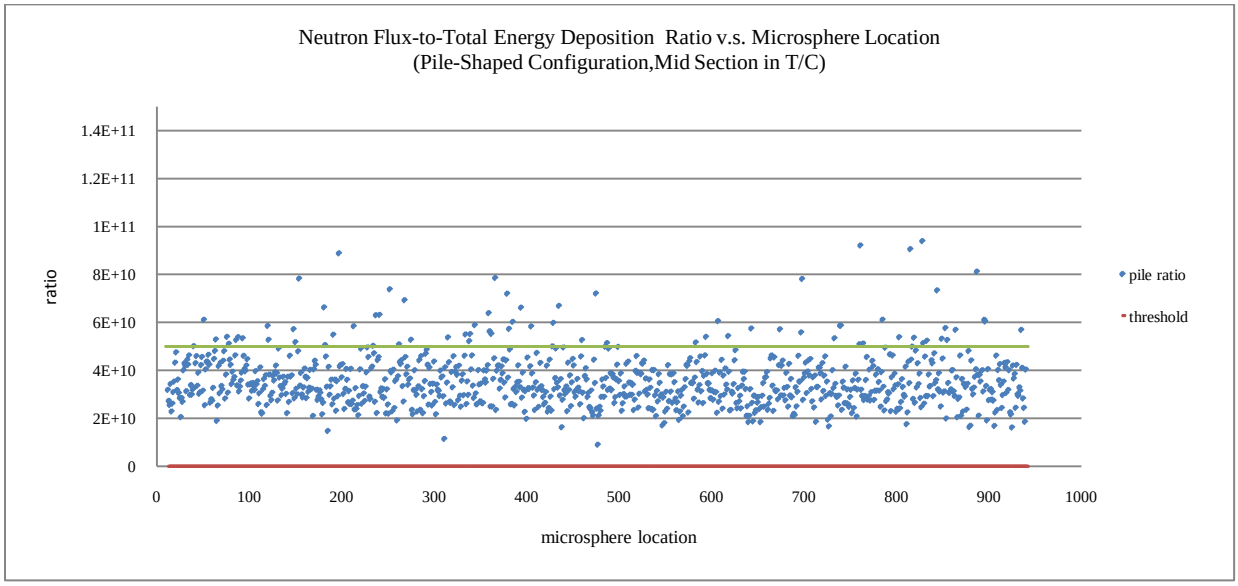

Figure 4.14-Simulation results showing neutron flux-to-total energy deposited per microsphere loaded with holmium in a polymeric matrix (PLLA) arranged in a bigger pile-shaped packing configuration to determine if a nuclear reactor is suitable for acceptable-quality neutron activation. As pile gets bigger, ratio values are not as even as values shown in smaller pile; more ratio values are closer to threshold. A green line was generated on the chart to point out differences with other charts.

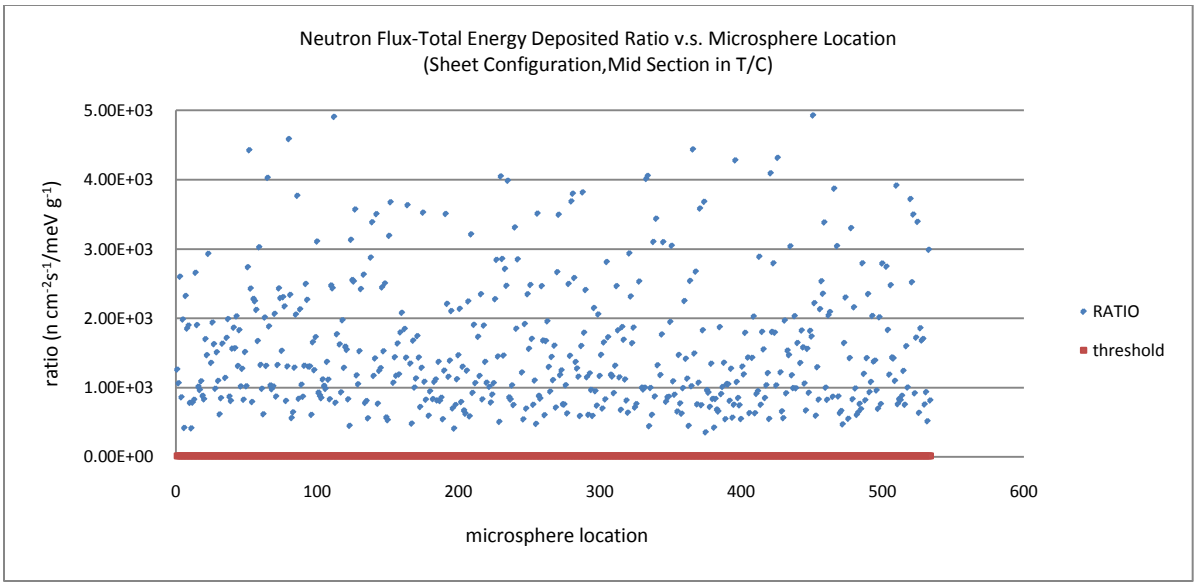

Figure 4.15-Simulation results showing neutron flux-to-total energy deposited per microsphere loaded with holmium in a polymeric matrix (PLLA) arranged in a sheet-shaped packing configuration to determine if a nuclear reactor is suitable for acceptable-quality neutron activation.

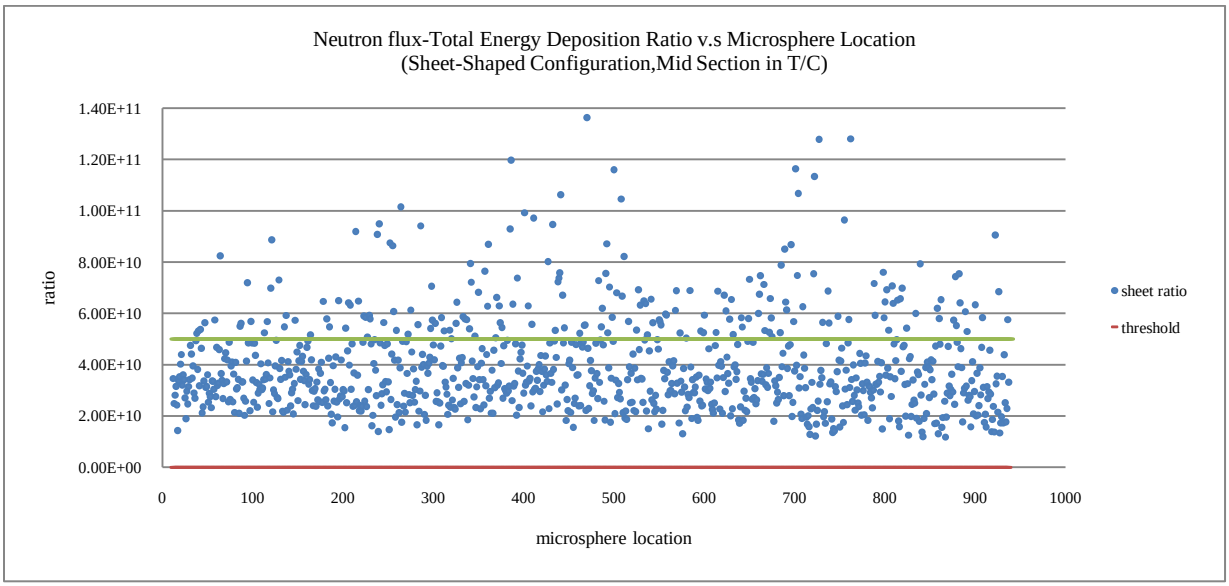

Figure 4.16-Simulation results showing neutron flux-to-total energy deposited per microsphere loaded with holmium in a polymeric matrix (PLLA) arranged in a bigger sheet-shaped packing configuration to determine if a nuclear reactor is suitable for acceptable-quality neutron activation. As pile gets bigger, ratio values have more or less similar distribution as values shown in smaller sheet-shaped configuration. A green line was generated on the chart to point out differences with other charts.

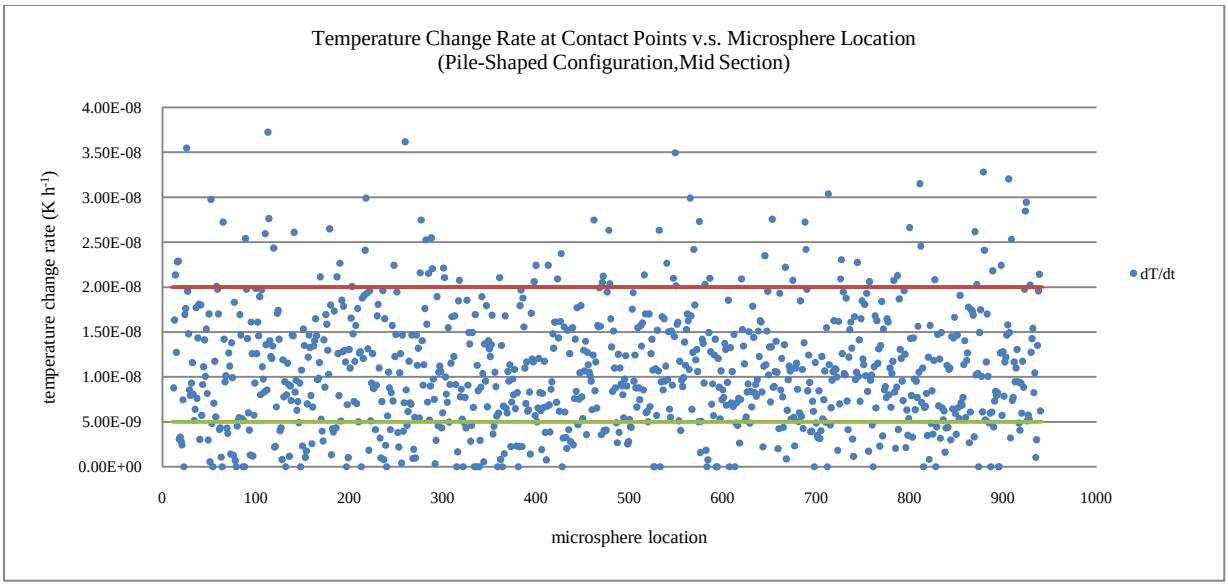

Figure 4.17-Simulation results showing temperature change rates at points where microspheres contact one another in a pile-shaped packing configuration. Lines were generated on the chart to point out differences with other charts.

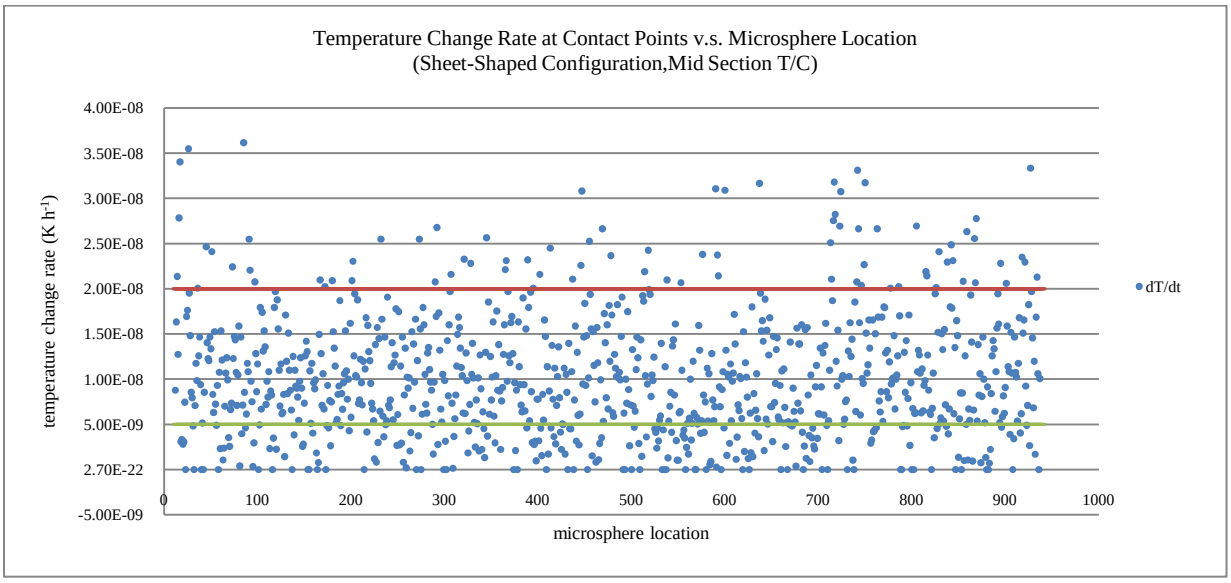

Figure 4.18-Simulation results showing temperature change rates at points where microspheres contact one another in a sheet-shaped, packing configuration. Compared with the results for the pile-shaped, packing configuration, the majority of the temperature change rate values for the sheet-shaped, packing configuration are lower and show a more even distribution. Lines were generated on the chart to point out differences with other charts.

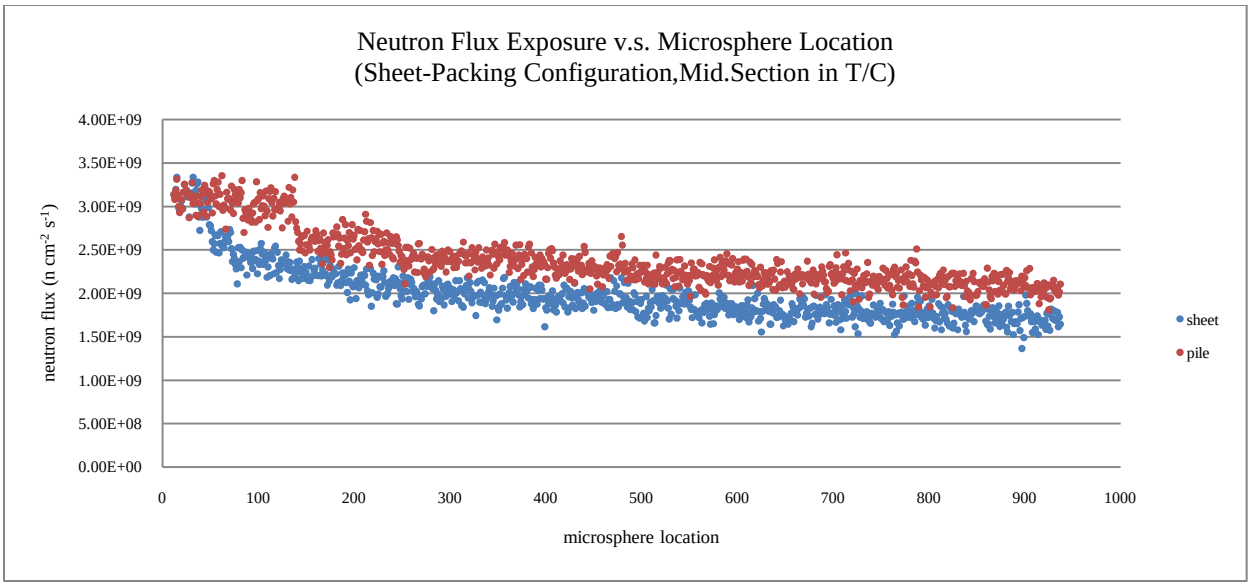

Figure 4.19-A comparison of neutron flux exposure results between an enlarged, pile-shaped, packing configuration and its corresponding sheet-shaped,packing configuration. These results were used to determine effects of packing geometry on activation patterns throughout configurations.

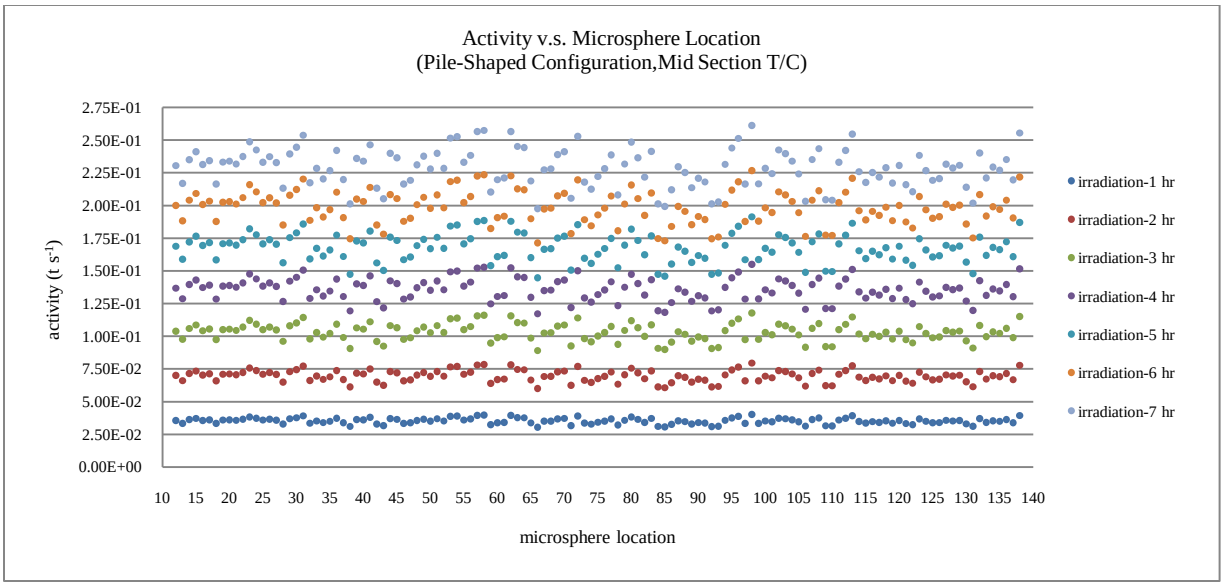

(A)

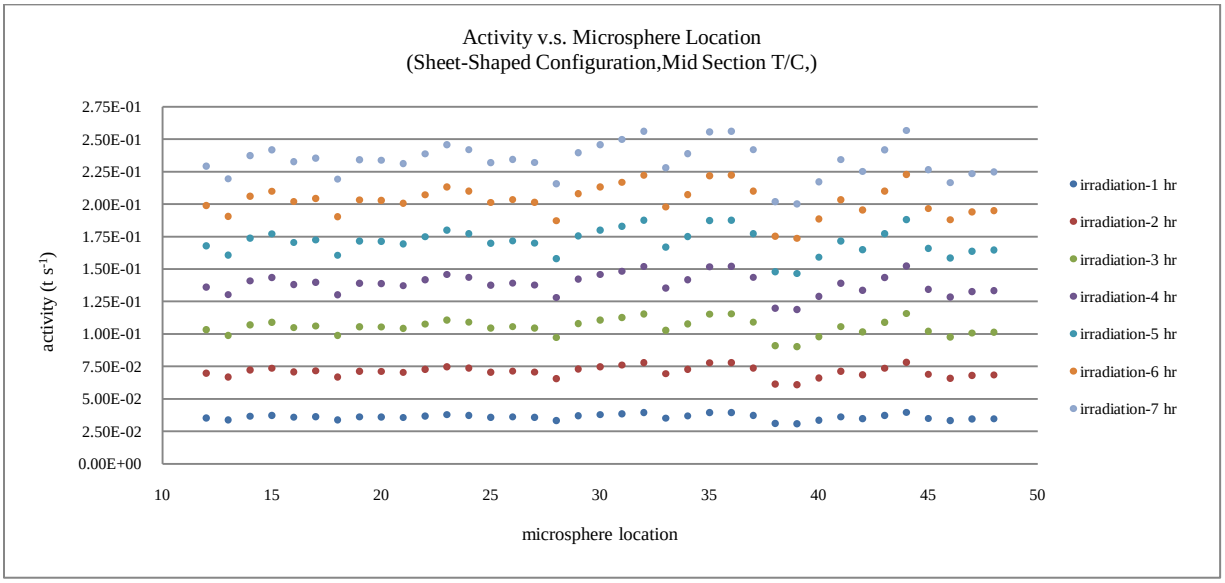

(B)

Figure 4.20- A comparison of activation results between a section of a pile-shaped, packing configuration (A) and its corresponding section in a sheet-shaped, packing configuration (B) both located close to the end of the activation vials facing the face of the thermal column.

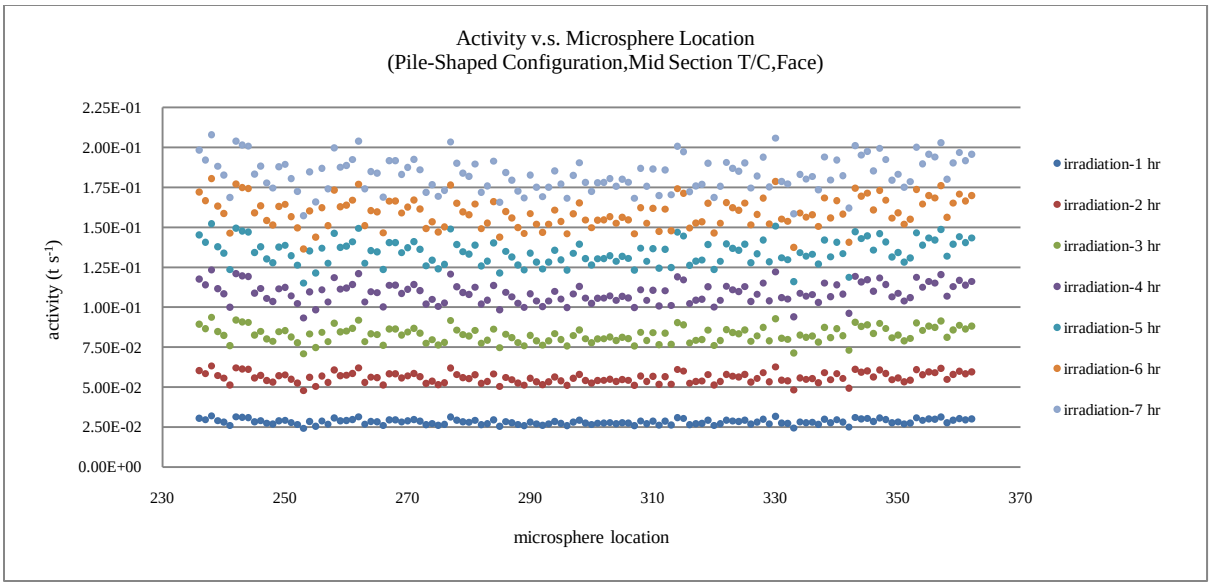

(C)

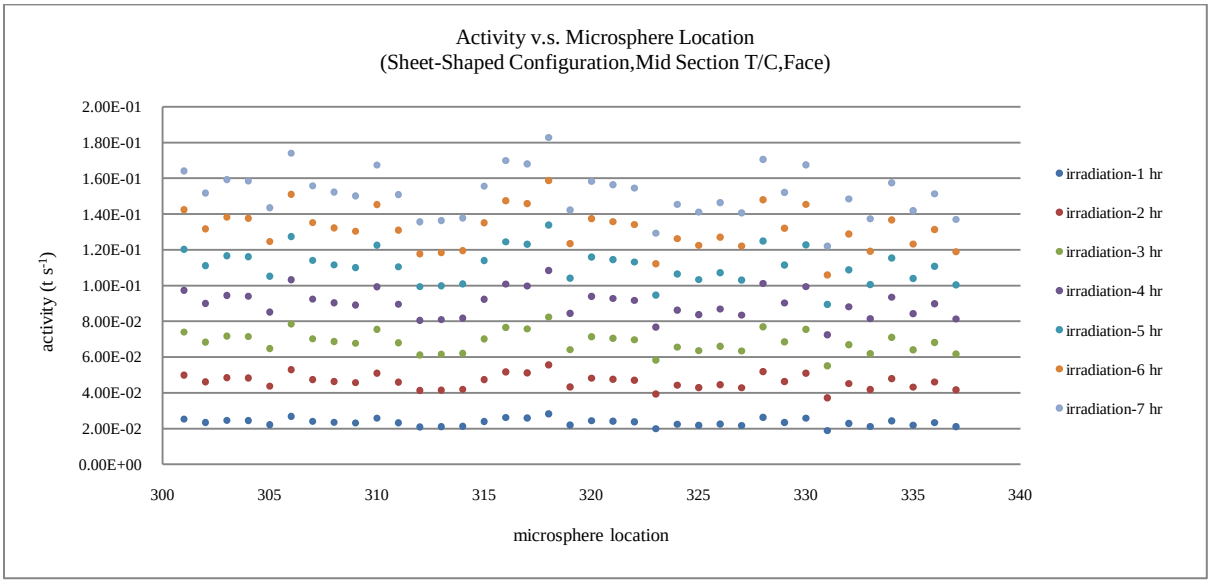

(D)

Figure 4.21-A comparison of activation results between a section of a pile-shaped, packing configuration (C) and its corresponding section in a sheet-shaped,packing configuration (D) both located close to the middle of their configurations.

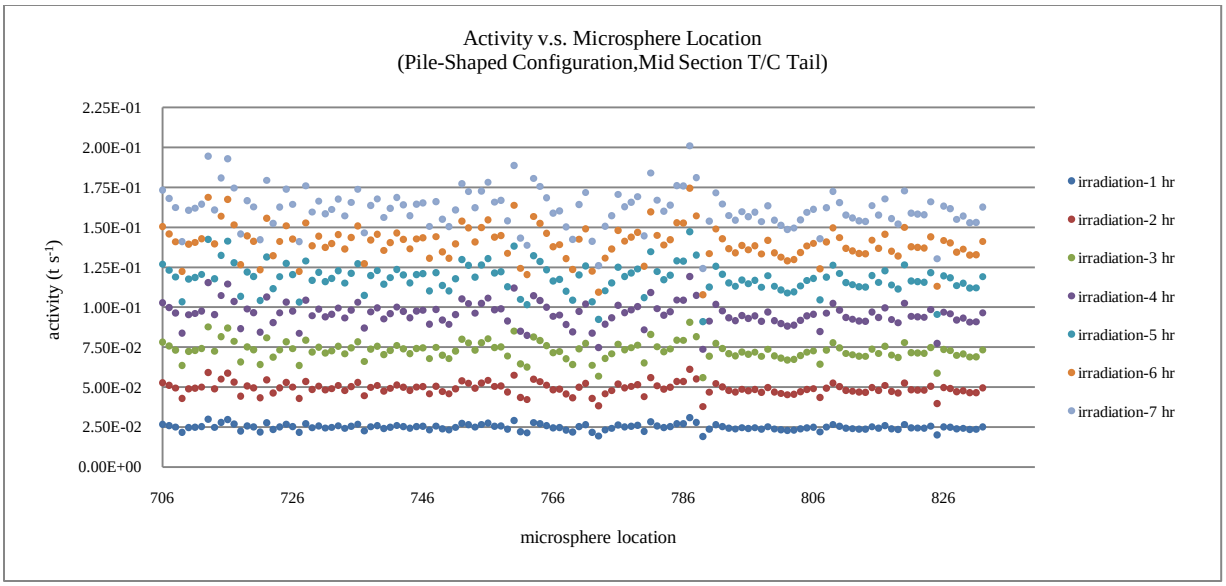

(E)

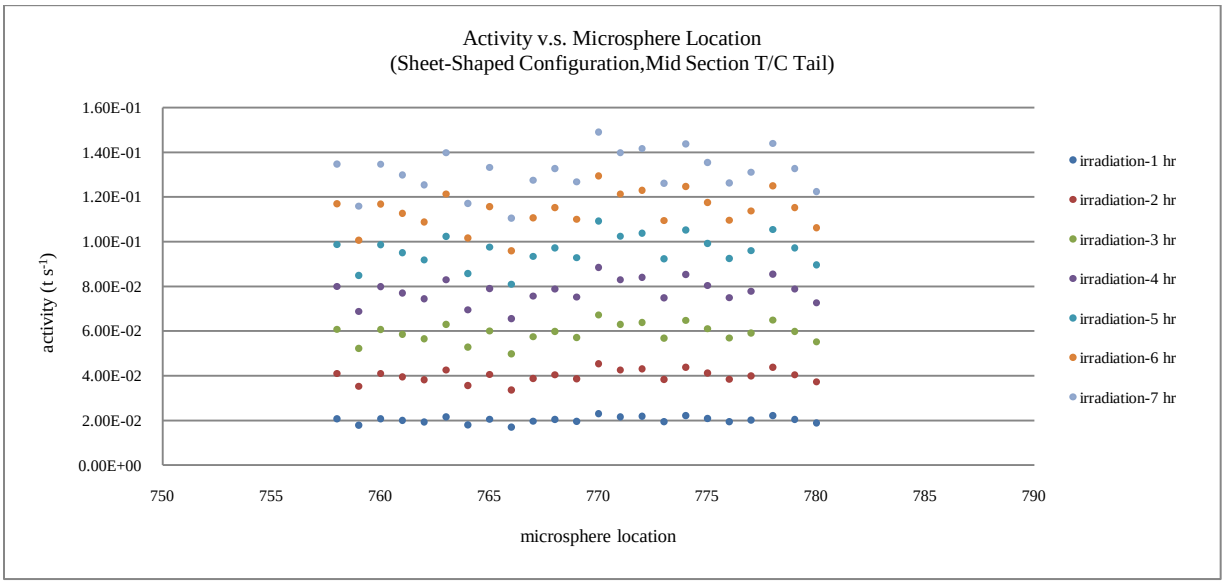

(F)

Figure 4.22-A comparison of activation results between a section of a pile-shaped, packing configuration (E) and its corresponding section in a sheet-shaped, packing configuration (F) both located close to the end of their configurations.

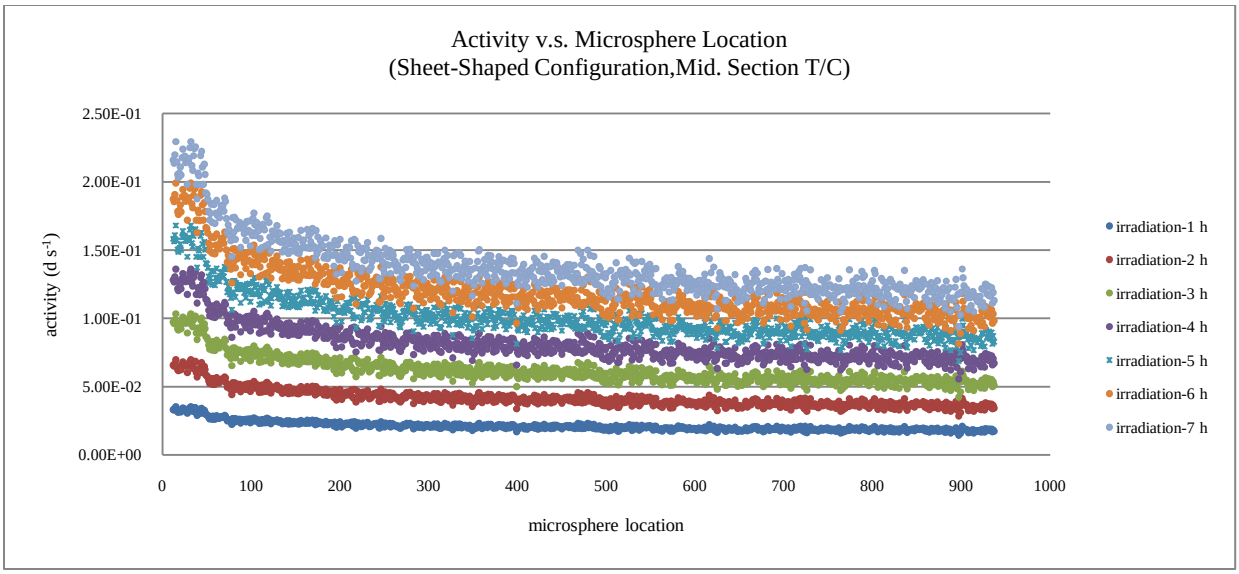

Figure 4.23-Simulation results showing activity per microsphere loaded with holmium in a polymeric matrix (PLLA) arranged in a sheet-shaped, packing configuration at different irradiation times.

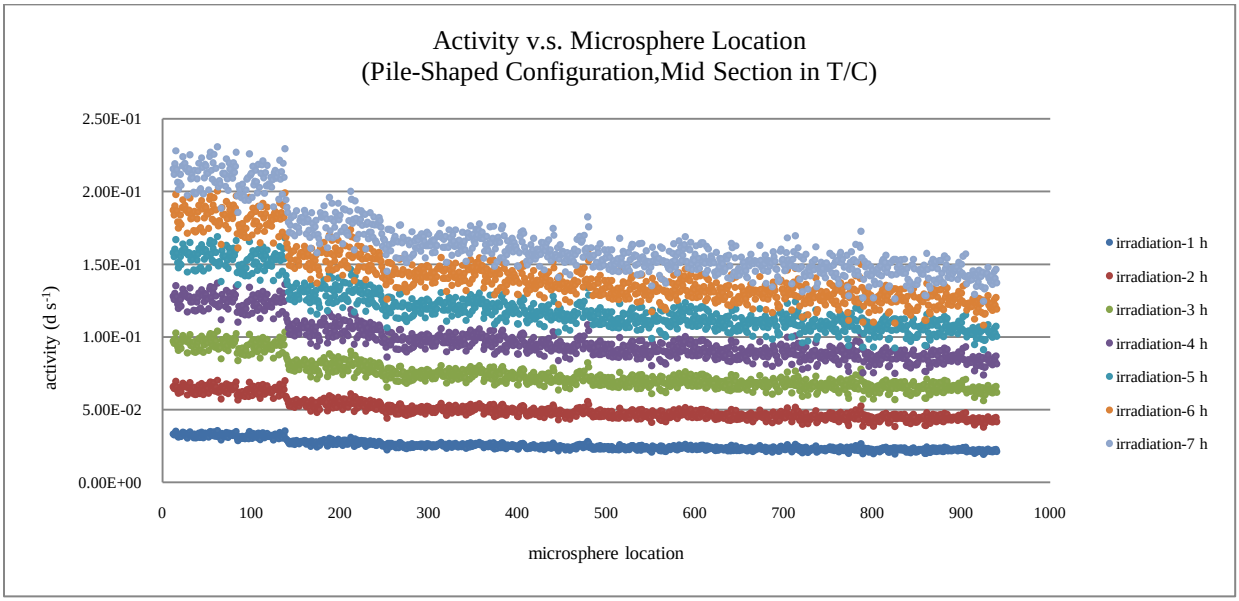

Figure 4.24-Simulation results showing activity per microsphere loaded with holmium in a polymeric matrix (PLLA) arranged in a pile-shaped, packing configuration at different irradiation times.

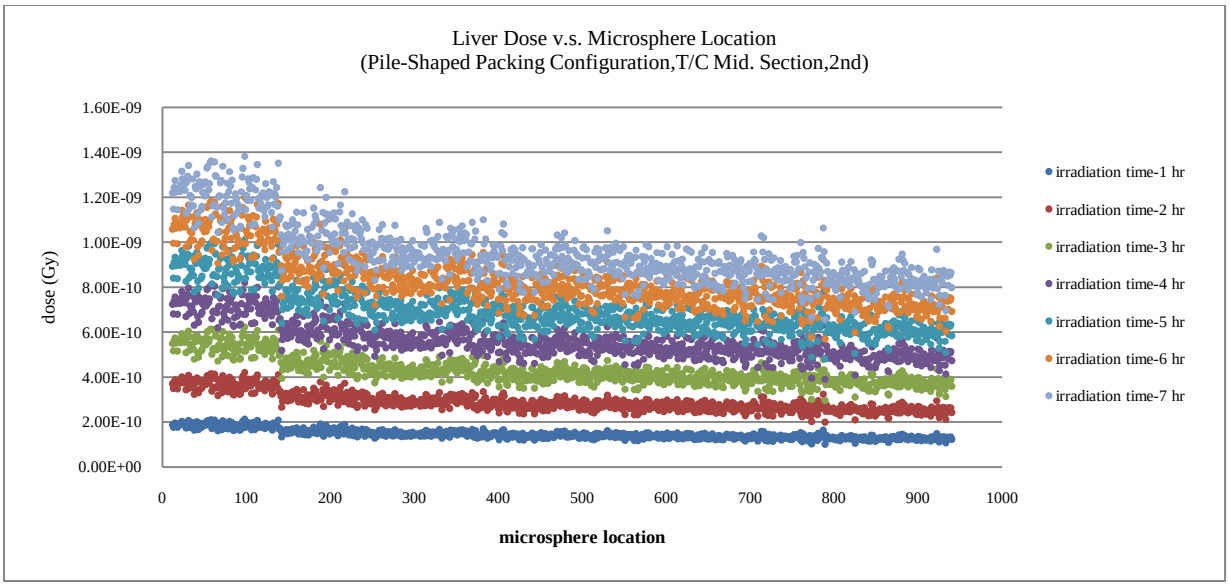

Figure 4.25-Simulation results showing liver dose per microsphere loaded with holmium in a polymeric matrix (PLLA) arranged in a pile-shaped packing configuration at different irradi-adiation times.

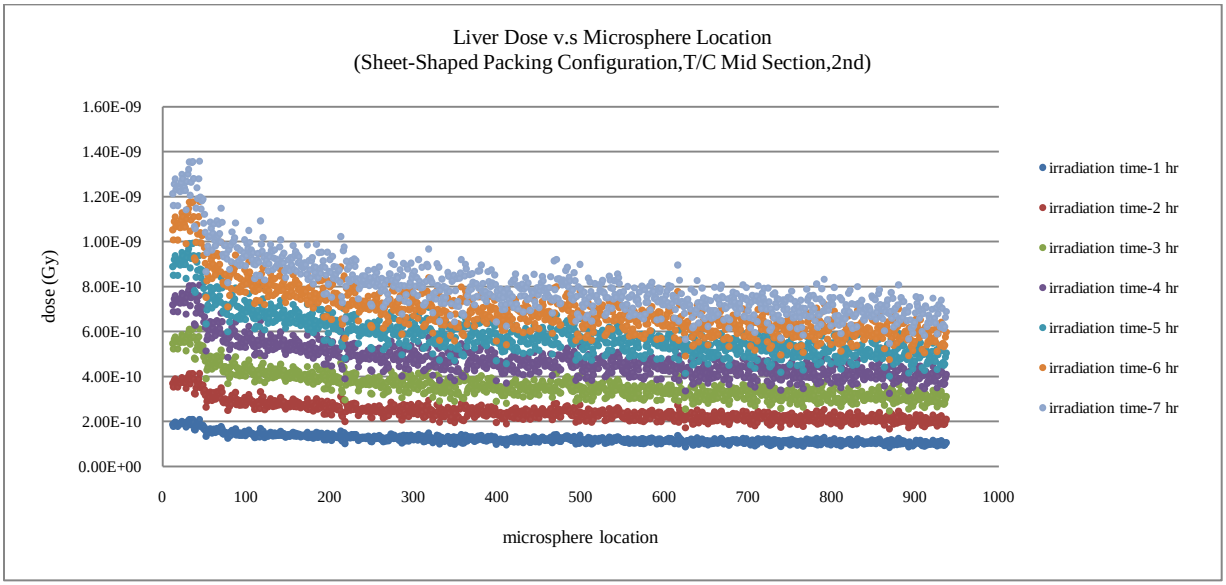

Figure 4.26-Simulation results showing liver dose per microsphere loaded with holmium in a polymeric matrix (PLLA) arranged in a sheet-shaped, packing configuration at different irra-diadiation times.

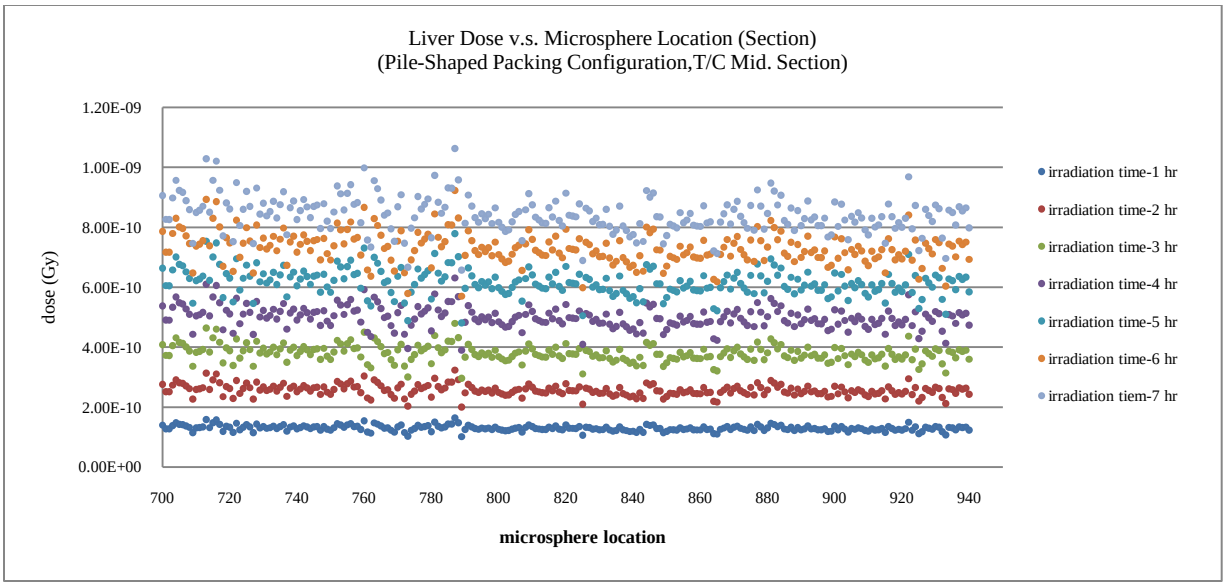

Figure 4.27-Simulation results showing liver dose per microsphere loaded with holmium in a polymeric matrix (PLLA) arranged in a pile-shaped, packing configuration at different irradi-adiation times.

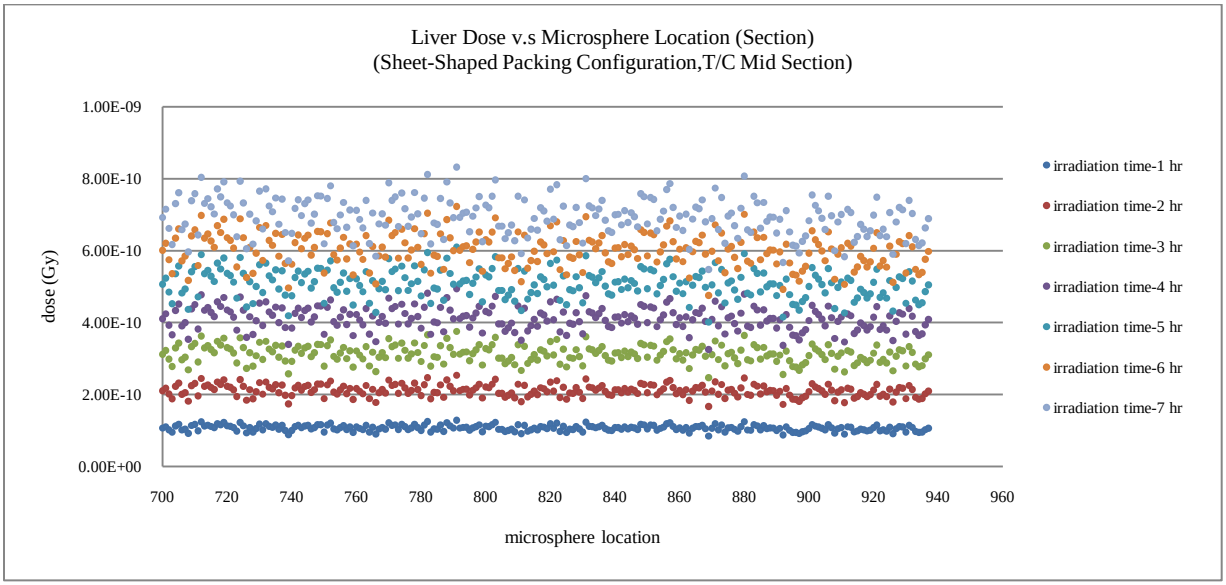

Figure 4.28-Simulation results showing liver dose per microsphere loaded with holmium in a polymeric matrix (PLLA) arranged in a sheet-shaped, packing configuration at different irra-diadiation times.

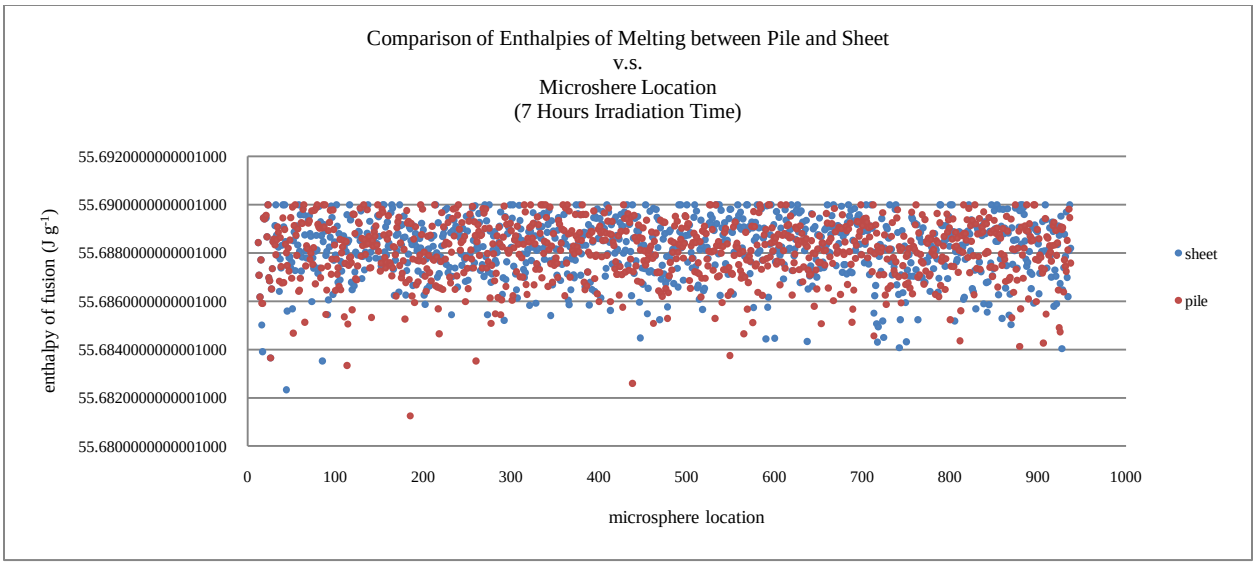

Figure 4.29-Enthalpy of fusion results for pile- and sheet-shaped packing configurations after neutron activation simulation for seven hours. A decrease in the magnitude of this value in each microsphere is the result of radiation-induced degradation of the polymeric matrix.

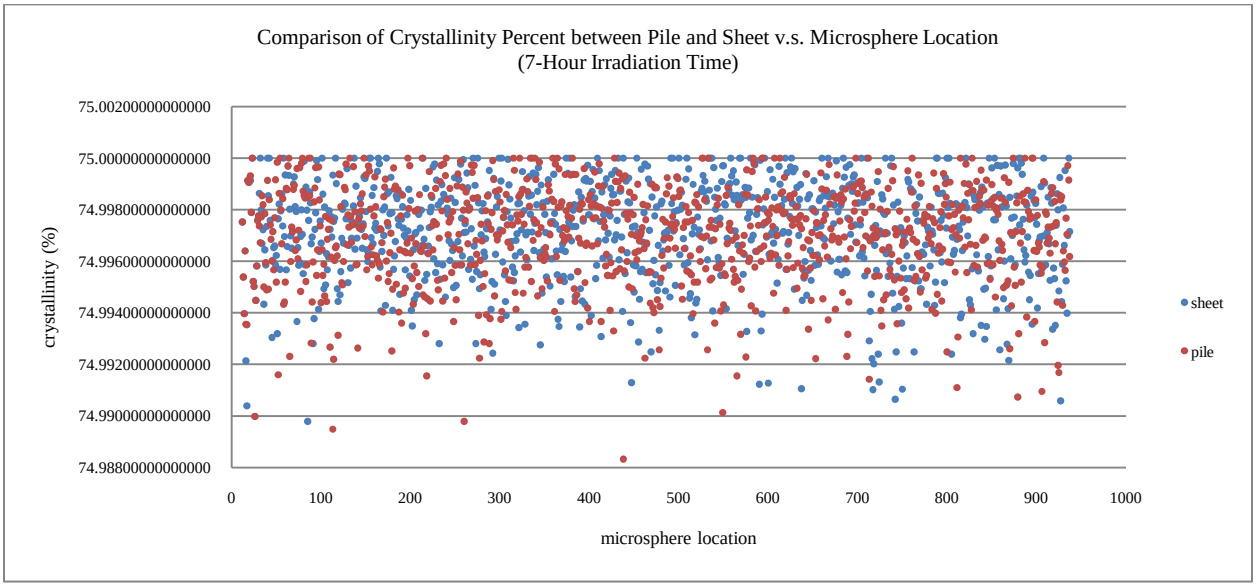

Figure 4.30- % Crystallinity results for pile- and sheet-shaped packing configurations after neutron activation simulation for seven hours. A decrease in the magnitude of this value in each microsphere is the result of radiation-induced degradation of the polymeric matrix.

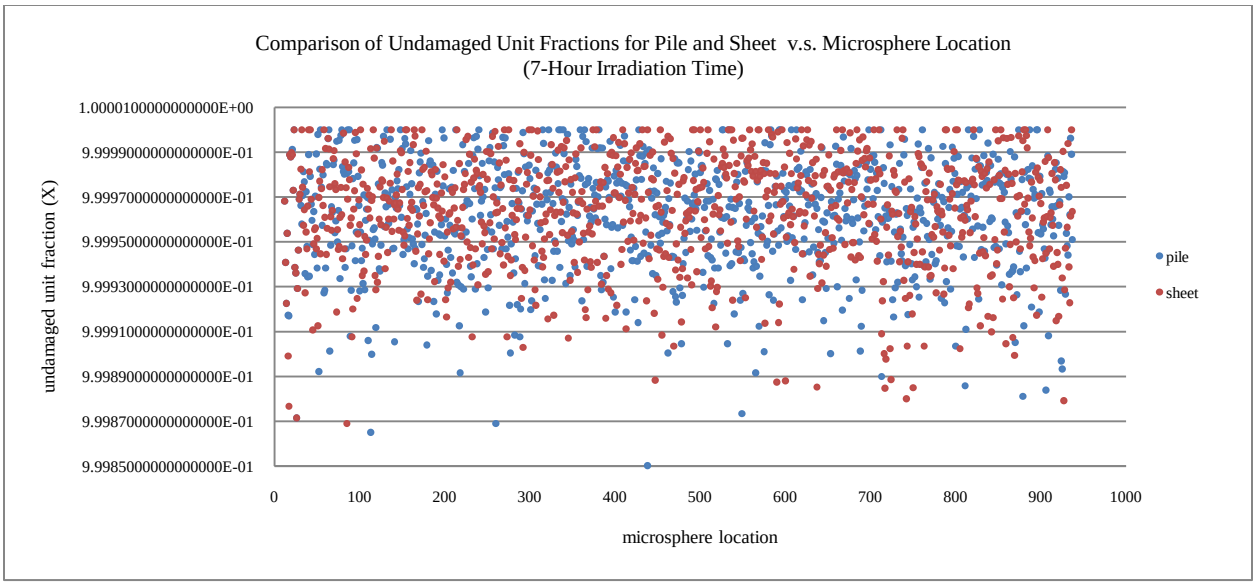

Figure 4.31-Undamaged unit fraction results for pile- and sheet-shaped packing configurations after neutron activation simulation for seven hours. A decrease in the magnitude of this value in each microsphere is the result of radiation-induced degradation of the polymeric matrix.

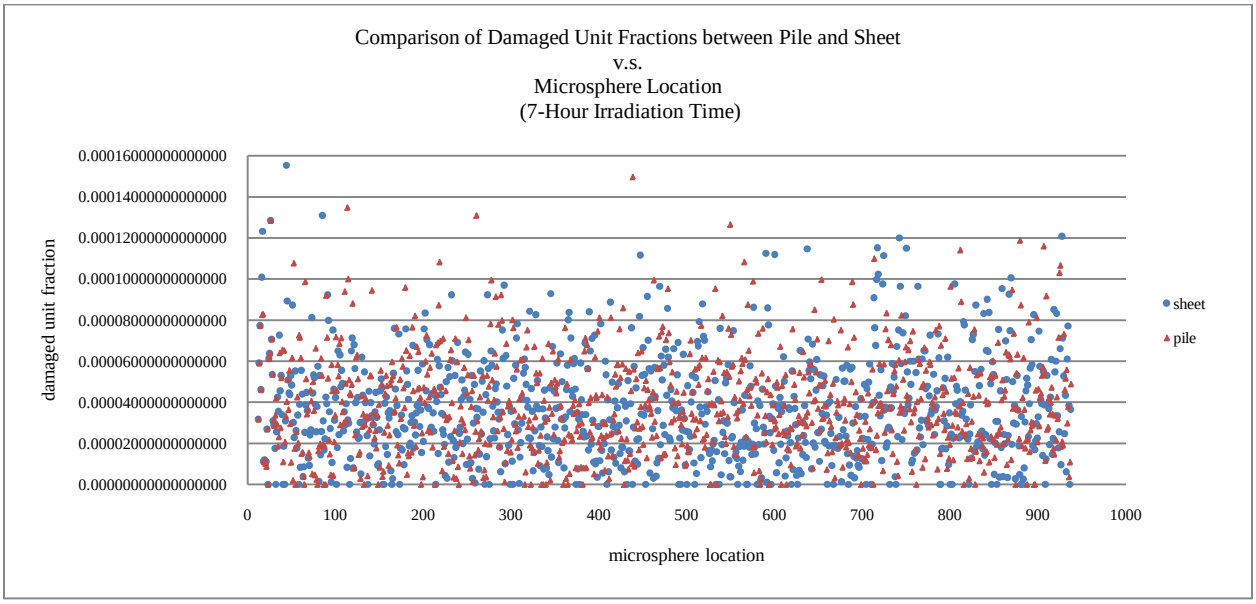

Figure 4.32-Damaged unit fraction results for pile- and sheet-shaped packing configurations after neutron activation simulation for seven hours. An increase in the magnitude of this value in each microsphere is the result of radiation-induced degradation of the polymeric matrix.

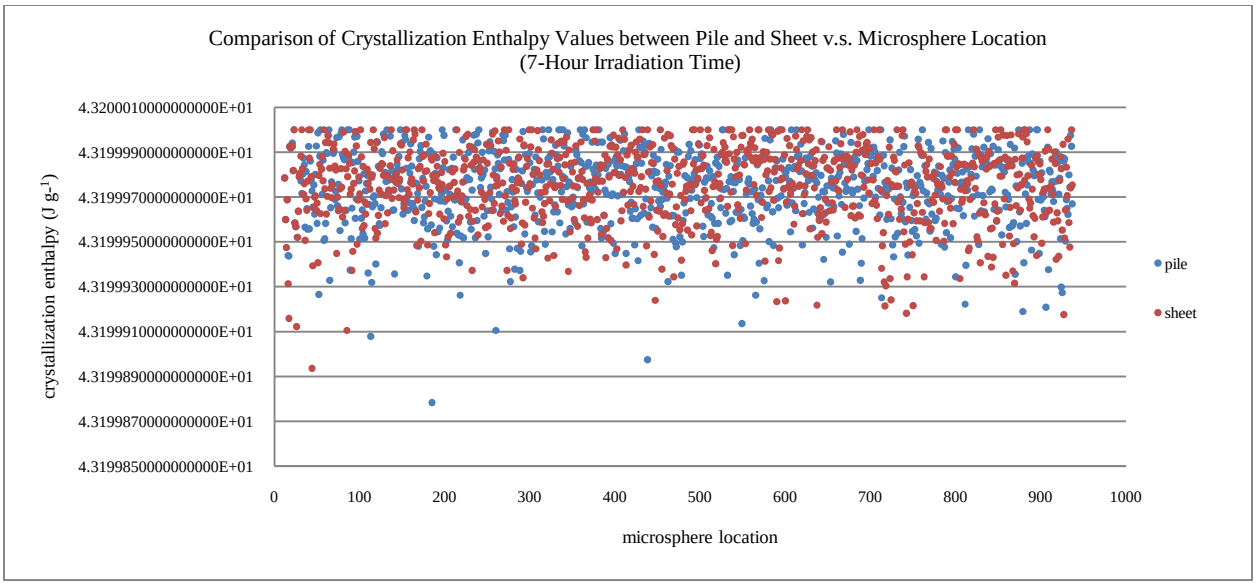

Figure 4.33-Enthalpy of crystallization results for pile- and sheet-shaped packing configurations after neutron activation simulation for seven hours. A decrease in the magnitude of this value in each microsphere is the result of radiation-induced degradation of the polymeric matrix.

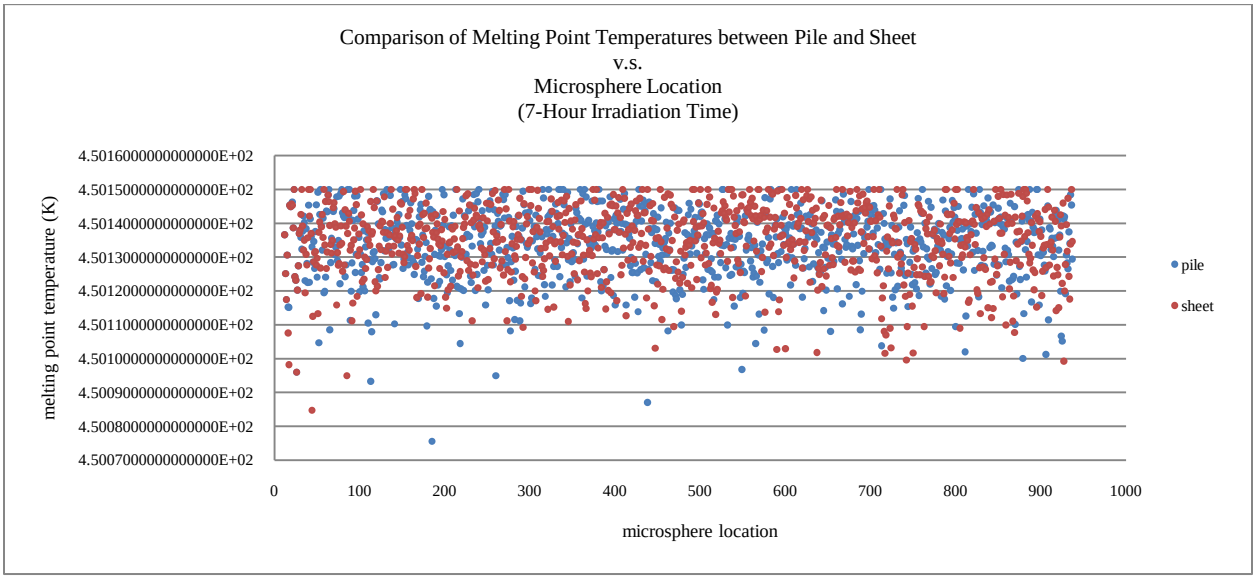

Figure 4.34-Melting point temperature results for pile- and sheet-shaped packing configurations after neutron activation simulation for seven hours. A decrease in the magnitude of this value (450.15 °C, *Ref. 3*) in each microsphere is the result of radiation-induced degradation of the polymeric matrix.

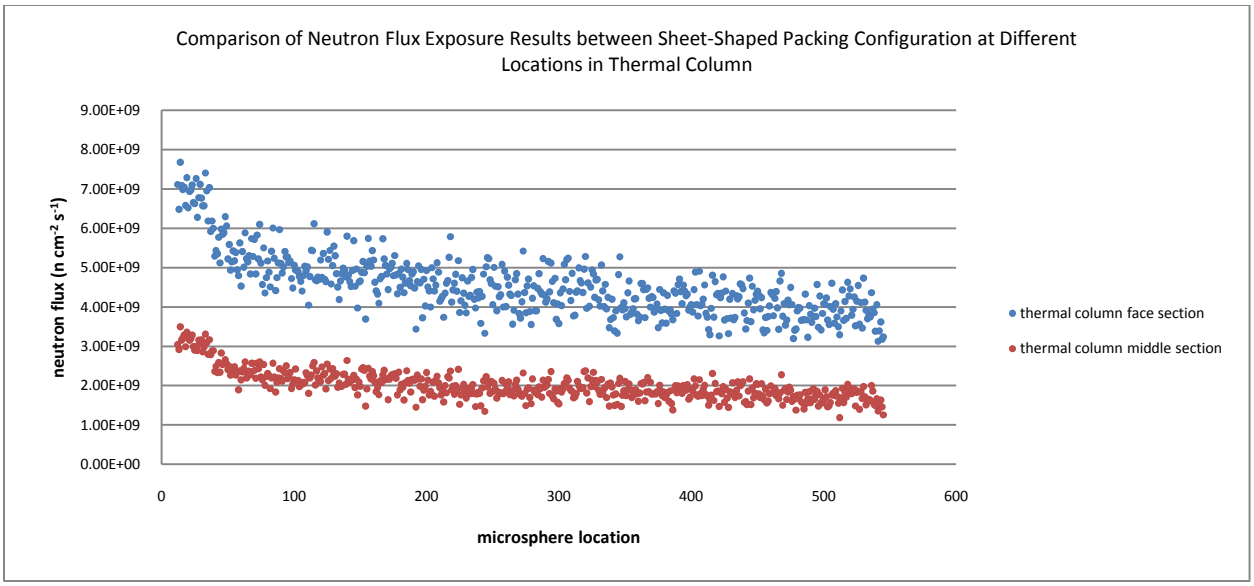

Figure 4.35-Comparison of neutron flux exposure results between microspheres arranged in a sheet-shaped packing configuration located at the face and at the middle of the thermal column.

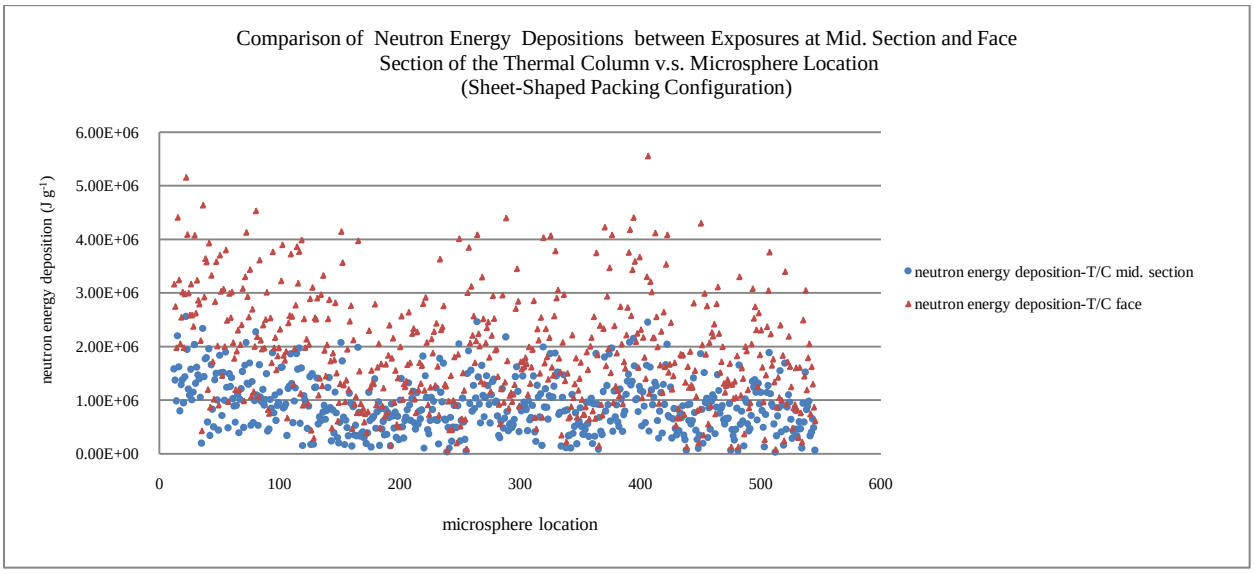

Figure 4.36-Comparison of the neutron energy depositions results between microspheres arranged in a sheet-shaped packing configuration located at the middle of the thermal column and microspheres also arranged in a sheet-shaped packing configuration located at the face of the thermal column, or closest to the reactor.

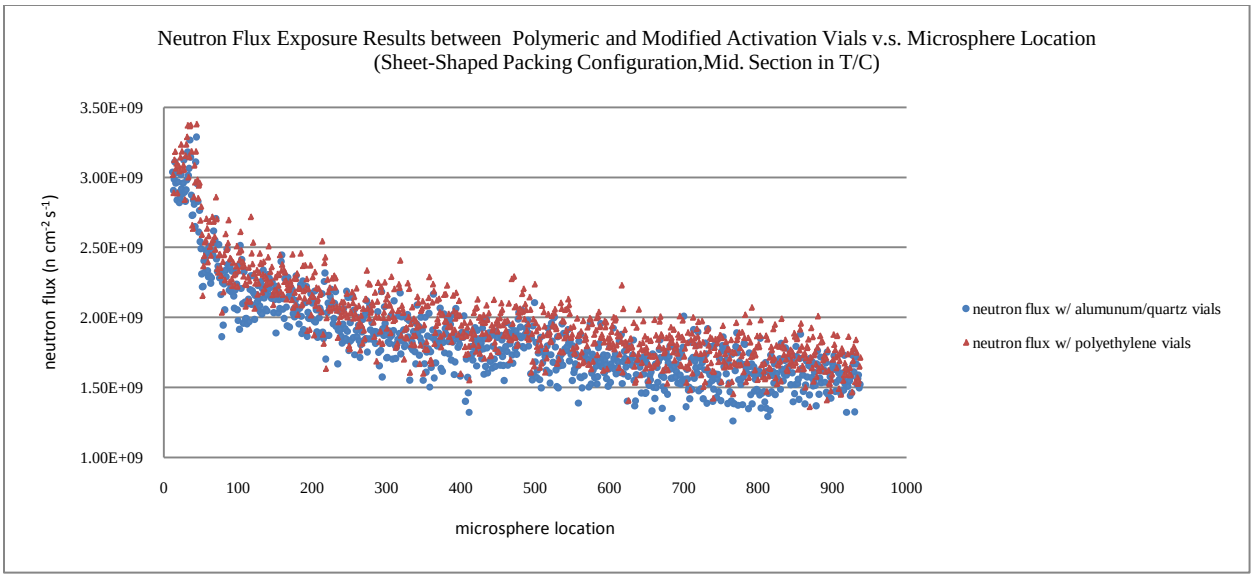

Figure 4.37-Comparison of neutron flux results of microspheres arranged in a sheet-shaped packing configuration inside a quartz vial that is put inside an aluminum container, and the container is enclosed inside a polyethylene vial and microspheres arranged in a sheet-shaped packing configuration inside polyethylene vials.

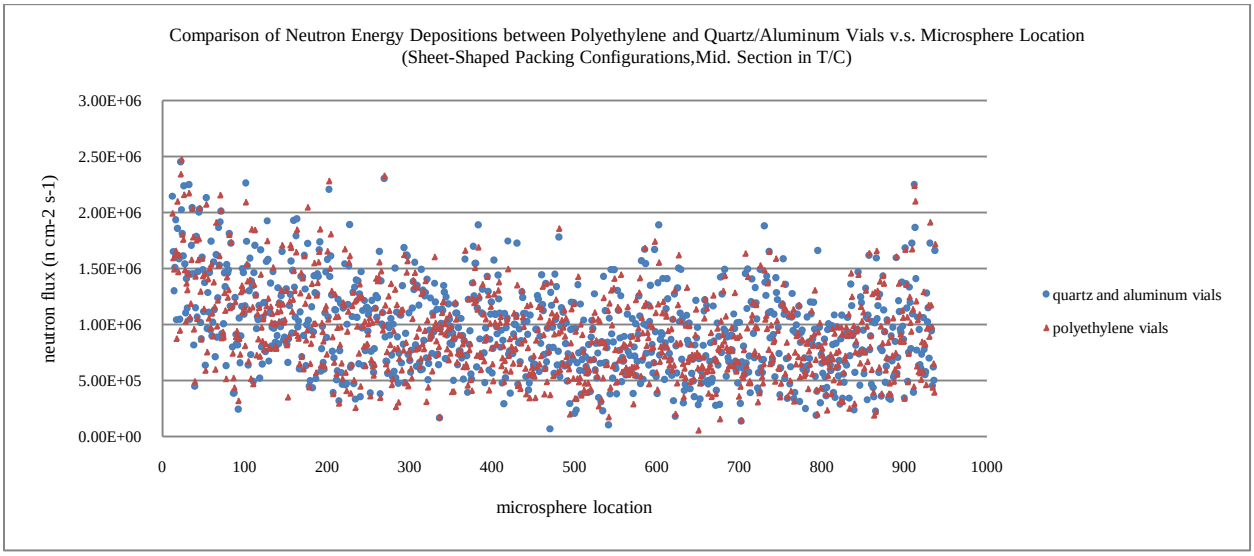

Figure 4.38-Comparison of neutron energy deposition results of microspheres arranged in a sheet-shaped packing configuration inside a quartz vial that is put inside an aluminum container and the container is enclosed inside a polyethylene vial and microspheres arranged in a sheet-shaped packing configuration inside polyethylene vials.

5.0 Discussion

The difference in neutron flux exposure patterns between microspheres arranged in a sheet-shaped, packing configuration and microspheres arranged in a pile-shaped, packing configuration could be the result of the sheet-shaped geometry provided less scattering, shielding, and thermalizing effects than the pile-shaped geometry, which was consistently illustrated throughout the simulation results. However, it should be noted that a point will be eventually reached at which any further addition of microspheres to a sheet-shaped, packing configuration will start producing a neutron flux exposure pattern similar to the one that a pile-shaped packing configuration would produce. In addition, another scattering effects was provided by surfaces perpendicular to the packing configurations, such as the walls at each end of the thermal column and the walls at each end of the activation vials; it should be noted that these wall effects not only affected both packing geometries, as indicated in the simulation results, but also the effects were pronounced for the microspheres placed closer to the them.

Regarding radiation-induced degradation of the polymeric matrix, both the pile-shaped, packing configuration and the sheet-shaped, packing configuration indicated similar extent of degradation. These similar polymeric degradation results may have been caused by the geometry of the thermal column and the material of which it was made; the holmium-loaded microspheres, regardless of their packing configuration, were placed in a sealed cavity, filled with air, and were exposed to a neutron flux that may be considered constant throughout the length of the packing configurations and were exposed to gammas that were either captured by the walls or the polymer. However, longer-history simulations are required to obtain better results for gamma fluxes and energy depositions for both neutrons and gammas.

6.0 Conclusion and Future Work

Holmium-loaded microspheres arranged in a sheet-shaped, packing configuration had indicated a uniform neutron flux exposure, although lower, than the holmium-loaded microspheres arranged in a pile-shaped packing configuration. In addition, while the holmium-loaded microspheres located in the inner regions of the pile-shaped packing configuration had experienced neutron flux suppression as the size of the pile was increased, the neutron flux exposure of the holmium-loaded microspheres located anywhere in the sheet-shaped, packing configuration remained approximately constant regardless of the size increase, excluding the end facing the reactor. Uniform neutron flux exposures during neutron activation produces microspheres with approximately uniform activity values, which translate into approximately uniform dose values on the patient's liver tumor, minimizing the possibilities of either over-dosing or under-dosing, provided the microspheres be distributed uniformly around the tumor. Finally, the possibility of self-shielding are significantly minimized when neutron-activating microspheres arranged in a sheet-shaped packing configuration; previous studies have not indicated signs of self-shielding when neutron-activating dosages up to 1000 mg in a pneumatic rabbit system, exposed to a thermal neutron flux of 5.0×10^{12} n cm^{-2} s^{-1} (*Ref.14*).

Regarding the effects of the location of the activation vials in the thermal column during neutron activation, it was previously assumed that the closer the vials were to the face of the thermal column, or to the reactor, the higher neutron flux would provide both a higher and uniform activation pattern. However, after results from simulations were analyzed and were compared, the closer the activation vials were to the face of the thermal column both the distribution of the neutron exposure values among microspheres became greater and their

neutron energy deposition values became significantly greater than a similar sheet-shaped, packing configuration placed in the middle of the thermal column; higher neutron energy deposition values means more damage being done to both the polymeric matrix and the holmium complex. Therefore, to maintain a uniform neutron exposure pattern, a distance between the microspheres and vertical surfaces, such as the walls from the activation vials and the walls from the thermal column, should be maintained. Blank microspheres could be placed on regions of the activation vials where neutron flux exposure values are significantly higher than the rest, and length of activation vials should be significantly longer than the length of either the pile- or sheet-shaped packing configurations

Regarding radiation-induced damage on the polymeric matrix during neutron activation, both the pile- and sheet-shaped, packing configurations indicated same extent of degradation, as indicated by changes in the material' physical properties such as change in enthalpy of melting and crystallization, melting point temperature, fraction of damaged and undamaged units, and percent of crystallization. However, changes in some material's physical properties for the microspheres arranged in a pile-shaped, packing configuration indicated trends toward more severe irradiation-induced damage after neutron activation than for the microspheres arranged in a sheet-shaped, packing configuration, as indicated by simulation results, such as the temperature change rates, neutron energy depositions, photon energy depositions, and ratios.

Simulation results for activation values indicated that the neutron flux in the thermal column provided by a 1 MWt-rated TRIGA reactor was not high enough to activate holmium-loaded microspheres to therapeutic levels within seven hours; however, these reactors are built

for higher power ratings. In addition, although the sheet-shaped packing configuration has indicated the potential to reducing the variation in individual doses provided by the holmium-loaded microspheres, this investigation was performed using MCNP5 simulation models, which included no size distribution among microspheres, microspheres loaded with a uniform and constant holmium concentration, and only neutrons and photons were taken into account during polymer degradation calculations. Therefore, to improve the quality of current results, more MCNP5 simulations must be performed. It is also critical that MCNP5 simulation must be performed using greater number of histories (e.g. greater than $1x10^9$) and considering electrons.

Finally, regarding future work, research could be done on areas such as the biodistribution of the radioisotope-loaded microspheres around tumors, radiation-resistant polymers used on the synthesis of microspheres, shielding containers, and microdosimetry. A particular area of research that should be noted concerns neutron flux to total energy deposited ratios, which could be used to determined if a nuclear is suitable for neutron activating microspheres of specific size and radioisotope content in their polymeric matrix (*Ref. 14*). It is strongly believed the value of these ratios is not only dependent on both the size of the microsphere and its radioisotope content, but also it is dependent on the irradiation time and on the location of the activation vials in the nuclear reactor. However, it should be noted that research on microspheres for radioembolization therapy, although interesting, it may require expensive equipment and facilities, training, certifications, and qualified physicians (i.e., M.D.).

References

1. Hamoudeh M. Holmium-Loaded PLLA Nanoparticles for Intratumoral Radiotherapy Via the TMT Technique: Preparation, Characterization, and Stability Evaluation after Neutron Irradiation. Drug Development and Industrial Pharmacy 34:796-806; 2008.

2. Nijsen JFW. Holmium-166 poly lactic acid microspheres applicable for intra-arterial radionuclide therapy of hepatic malignancies: effects of preparation and neutron activation techniques. European Journal of Nuclear Medicine 26:699-704; 1999.

3. Nijsen J.F.W. Influence of neutron irradiation on holmium acetylacetonate loaded poly(L-lactic acid) microspheres. Biomaterials 23:1831-1839; 2002.

4. Smits MLJ. Holmium-166 radioembolization for the treatment of patients with liver metastases: design of the phase I HEPAR trial. Journal of Experimental & Clinical Research 29:70: 2010.

5. Bult W. Microsphere radioembolization of liver malignancies: current developments. The Quarterly Journal of Nuclear Medicine and Molecular Imaging 53:325-335; 2009.

6. Homium-166 poly(L-lactic acid) microsphere radioembolization of the liver: technical aspects studied in a large animal model. European Radiology 20: 862-869; 2010.

7. Martin JE, Physics for Radiation Protection, 2nd ed. Germany:Wiley-VCH; 2006.

8. Neutron activation image available at: http://www.google.com/images?rlz=1T4GPCK_enUS375US380&q=neutron+activation+analysis

9. General Atomics Electronics Systems website available at: http://www.ga-esi.com/triga/.

10. Marcum WR. Thermal Hydraulic Analysis for the Oregon State TRIGA Reactor using RELAP5-3D. Nuclear Engineering Department, Oregon State University; 2008.

11. Picture of 3 MWt TRIGA reactor built at the Atomic Energy Research Establishment of the Bangladesh Atomic Energy Commission. This picture is available at: http://www.bing.com/images/search?q=triga+reactor+pictures.

12. Reactor Startup Report for the Oregon State TRIGA Reactor Using LEU Fuel

13. Components of dry air website available at: http://www.engineeringtoolbox.com/molecular-mass-air-d_679.html

14. Nijsen JFW. Neutron activation of holmium poly(L-lactic acid) microspheres for hepatic arterial radioembolization: a validity study. Biomedical Microdevices 11:763-772; 2009.

15. Visual Editor Consultants website vai;able at: http://mcnpvised.com/.

16. X-5 Monte Carlo Team. MCNP-General Monte Carlo N-Particle Transport Code, Version 5, Volume II: User's Guide. New Mexico; Los Alamos National Laboratory: 2003.

17. Kantoglu O., Guven O. Radiation induced crystallinity damage in poly(L-lactic acid). Nuclear Instruments and Methods in Physics Research B 197:259-264; 2002.

18. Loo JSC. Degradation of poly(lactide-*co*-glycolide)(PLGA) and poly(L-lactide) (PLLA) by electron beam radiation. Biomaterials 26:1359-1367; 2005.

19. Jellinek H.H.G. Aspects of Degradation and Stabilization of Polymers. New York: Elsevier Scientific Publishing Company; 1978.

20. Cagle DW. Synthesis, Characterization, and Neutron Activation of Holmium Metallofullerenes. Journal of American Chemical Society 118:8043-8047; 1996.

21. Jin F. Crosslinking of Poly($_L$-lactide) by γ-Irradiation. Journal of Macromolecular Rapid Communications 23:909-912; 2002.

APPENDICES

APPENDIX A – Acronyms and Abbreviations

All of the acronyms and the more complex units of measure are defined and are discussed where they first appeared in the paper. The following is a list is a compilation of these items.

Acronyms and Abbreviations

MCNP	Monte Carlo N-Particle Transport Code
PVA	Polyvinyl Alcohol
DSC	Differential Scanning Calorimetry
MRI	Magnetic Resonance Imaging
CT	Computed Tomography
3D	Three Dimensional
RE	Radioembolization
OSTR	Oregon State Research Reactor
^{99m}Tc–MAA	Technetium-99 Albumin Macroaggragate
FLIP	Fuel Life Improvement Program
PLLA	Poly (L-lactic Acid)
HoAcAc	Holmium Acetylacetonate
VisEd	Visual Editor
TRIGA	Training Research Isotopes General Atomics
LEU	Low Enriched Uranium
HEU	Highly Enriched Uranium

Units of Measure

Bq	becquerel(s)
°C	degree(s) Celsius
cm	centimeter(s)
cm^2	square centimeter(s)
g	gram(s)
Gy	(Gray(s)
keV	kiloelectron volt(s)
kg	kilogram(s)
μm	micrometer(s)
m	meter(s)
m^3	cubic meter(s)
MeV	megaelectron volt(s)
s	second(s)
h	hour(s)
GeV	gigaelectron volt(s)
GBq	gigabecquerel(s)
MWt	megawatt(s) thermal
kGy	kiloGray(s)

APPENDIX B – Mass Fraction Calculations for Holmium Concentration in PLLA Matrix

$V=(4/3)\pi(0.00185\ cm)^3$
$V=2.65218263783333 \times 10^{-8}\ cm^3$

$M_{Total}=(1.4\ g/cm^3)(2.65218263783333 \times 10^{-8}\ cm^3)$
$M_{Total}=3.71305569296667 \times 10^{-8}\ g$
$M_{HoAcAc}=(0.17)(3.71305569296667 \times 10^{-8}\ g)$
$M_{HoAcAc}=6.31219467804333 \times 10^{-9}\ g$

$M_{PLLA}=3.71305569296667 \times 10^{-8}\ g - 6.31219467804333 \times 10^{-9}\ g$
$M_{PLLA}=3.08183622516233 \times 10^{-8}\ g$

$Mole_{PLLA}=3.08183622516233 \times 10^{-8}\ g/72\ g\ mol^{-1}$
$Mole_{PLLA}=4.28032809050324 \times 10^{-10}\ mol$

<u>HoAcAc</u>
$Mass_{C} = (0.349)(6.31219467804333 \times 10^{-9}\ g)$
$Mass_{C} =2.20295594263712 \times 10^{-9}\ g$

$Mass_{O} =(0.2789)(6.31219467804333 \times 10^{-9}\ g)$
$Mass_{O} =1.76047109570629 \times 10^{-9}\ g$

$Mass_{H} =(0.0527)(6.31219467804333 \times 10^{-9}\ g)$
$Mass_{H} =3.32652659532884 \times 10^{-10}\ g$

$Mass_{Ho} =(0.3119)(6.31219467804333 \times 10^{-9}\ g)$
$Mass_{Ho} =1.96877352008172 \times 10^{-9}\ g$

<u>PLLA</u>
$Mass_{C} =(4.28 \times 10^{-10}\ mol)(3\ mol\ C/1\ mol\ PLLA)(12\ g/1\ mol\ C)$
$Mass_{C} =1.5409181125811 \times 10^{-8}\ g$

Mass $_{O}$ =(4.28 x 10^{-10} mol)(2 mol O/1 mol PLLA)(16 g/1 mol O)
Mass $_{O}$ =1.36970498896104 x 10^{-8} g

Mass $_{H}$ =(4.28 x 10^{-10} mol)(4 mol H/1 mol PLLA)(1 g/1 mol H)
Mass $_{H}$ =3.70832154695813 x 10^{-8} g

Mass $_{frac\ C}$=(2.202 x 10^{-9} g + 1.540 x 10^{-8} g)/(3.713 x 10^{-8} g)
Mass $_{frac\ C}$=0.474

Mass $_{frac\ O}$=(1.760 x 10^{-9} g + 1.369 x 10^{-8} g)/(3.713 x 10^{-8} g)
Mass $_{frac\ O}$=0.462

Mass $_{frac\ H}$=(3.326 x 10^{-10} g + 3.708 x 10^{-8} g)/(3.713 x 10^{-8} g)
Mass $_{frac\ H}$=0.055

Mass $_{frac\ Ho}$=(1.96877352008172 x 10^{-9} g)/ (3.713 x 10^{-8} g)
Mass $_{frac\ Ho}$=0.053

APPENDIX C – Neutron Flux Attenuation Calculation

Mid Section of Thermal Column

B=5.0

I_o=3.42 x 10^9 n cm^{-2} (Maximum flux value)

I(x) =1.836 x 10^9 n cm^{-2} (Average flux value)

Σ_{nr}= 0.111cm^{-1} (polyethylene's removal coefficient)

From $I(x) = I_o\, Be^{-\Sigma nrx}$

$\ln I(x) - \ln I_o = \ln B + \ln e^{-\Sigma nrx}$

$\ln I(x) - \ln I_o = \ln B - \Sigma_{nr}\, x$

$\ln I(x) - \ln I_o - \ln B = -\Sigma_{nr}\, x$

$x = \ln I_o + \ln B - \ln I(x) / \Sigma_{nr}$

$x = (\ln I_o + \ln B - \ln I(x)) / 0.111 cm^{-1}$

$x = (\ln(3.42 \times 10^9 \text{ n } cm^{-2}) + \ln(5.0) - \ln I(1.836 \times 10^9 \text{ n } cm^{-2})) / 0.111 cm^{-1}$

x=**20.1 cm** thickness of polyethylene spacer for spheres at mid section of T/C

APPENDIX D – Activity and Irradiation Time Calculation Examples

$T_{1/2}$ = 26.9 h (1614 min)
$\lambda = \ln(2)/ 1614$ min
$\lambda = 429.459 \times 10^{-6}$ min^{-1}
σ_γ = 64 b (64×10^{-24} cm^2)

$V=(4/3)\pi(0.00185\ cm)^3$
$V = 2.65218263783333 \times 10^{-8}$ cm^3
$M_{Total}=(1.4\ g/cm^3)(2.65218263783333 \times 10^{-8}\ cm^3)$
$M_{Total} = 3.71305569296667 \times 10^{-8}$ g
$M_{HoAcAc}=(0.17)(3.71305569296667 \times 10^{-8}\ g)$
$M_{HoAcAc} = 6.31219467804333 \times 10^{-9}$ g
$M_{PLLA} = 3.71305569296667 \times 10^{-8}\ g - 6.31219467804333 \times 10^{-9}\ g$
$M_{PLLA} = 3.08183622516233 \times 10^{-8}$ g

$Mole_{PLLA} = 3.08183622516233 \times 10^{-8}\ g / 72\ g\ mol^{-1}$
$Mole_{PLLA} = 4.28032809050324 \times 10^{-10}$ mol

<u>HoAcAc</u>
$Mass_C = (0.349)(6.31219467804333 \times 10^{-9}\ g)$
$Mass_C = 2.20295594263712 \times 10^{-9}$ g
$Mass_O = (0.2789)(6.31219467804333 \times 10^{-9}\ g)$
$Mass_O = 1.76047109570629 \times 10^{-9}$ g
$Mass_H = (0.0527)(6.31219467804333 \times 10^{-9}\ g)$
$Mass_H = 3.32652659532884 \times 10^{-10}$ g
$Mass_{Ho} = (0.3119)(6.31219467804333 \times 10^{-9}\ g)$
$Mass_{Ho} = 1.96877352008172 \times 10^{-9}$ g

$Atoms_{Ho} = (1.96877352008172 \times 10^{-9}\ g)(1\ mol\ Ho/165\ g)(6.023 \times 10^{23}\ atom/mol)$
$Atoms_{Ho} = 7.18661995 \times 10^{12}$
<u>$N_{Ho} = 7.18661995 \times 10^{12}\ atom\ cm^{-3}$</u>
$\phi = 3.04 \times 10^{9}\ n\ cm^{-2}\ s^{-1}$
$A_2(t) = \phi\sigma N_1 (1-e^{-\lambda 2t}) e^{-\lambda 2T})$
$A_2(420\ min) = (3.04 \times 10^{9}\ n\ cm^{-2}\ s^{-1}) \times (58 \times 10^{-24}\ cm^2) \times (7.18661995 \times 10^{12}\ atom\ cm^{-3})$
$\times (1-e-(429.459 \times 10^{-6}\ min^{-1})(420\ min)) \times e-((429.459 \times 10^{-6}\ min^{-1})(120\ min))$

$A_2(420\ min) =$ <u>$1.97 \times 10^{-1}\ t\ s^{-1}$</u>

APPENDIX E – Target Depletion Calculation Example

Time=7 hr

$N_1(t) = N_o e^{-\phi\sigma 1 t}$

$N_1(t) = N_o e^{-\phi\sigma 1 t}$

$N_1(t) = (7.186619950 \times 10^{12}\ atom/cm^2) \times e - (3.04 \times 10^{9}\ n\ cm^{-2}\ s^{-1} \times 5.8 \times 10^{-23}\ cm^2 \times 2.52 \times 10^{4}\ s)$

$N_1(t) = \underline{7.186619910111 \times 10^{12}\ atom/cm^2}$

$N_2 = \phi\sigma_1 N_1/(\lambda_2 - \phi\sigma_1)\ (e^{-\phi\sigma 1 t} - e^{-\lambda 2 t})$

$N_2 = \underline{(3.44 \times 10^{9}\ n\ cm^{-2}\ s^{-1})(6.4 \times 10\text{-}23cm2)(7.186619950 \times 10^{12}\ atom/cm^2)} \times$

((4.29 x 10-4 min-1/60 s) – 3.44 x 109 n $cm^{-2}\ s^{-1}$ x 6.4 x 10^{-23} cm^2)

(e –(3.44 x 10^9 n $cm^{-2}\ s^{-1}$ x 6.4 x 10^{-23} cm^2 x 2.52 x 10^4 s) – e(-(4.29 x 10-4 min-1/60 s)(2.52 x 104 s)))

$N_2 = \underline{3.6498344603373560 \times 104\ atom/cm^2}$

APPENDIX F – Calculation to Determining if 1 MWt TRIGA Reactor Neutron Flux Magnitude is suitable for Neutron Activation of Microspheres

Sheet-Shaped Packing Configuration:

$V=(4/3)\pi(0.00185\ cm)^3$
$V=2.65218263783333 \times 10^{-8}\ cm^3$

$M_{Total}=(1.4\ g/cm^3)(2.65218263783333 \times 10^{-8}\ cm^3)$
$M_{Total}=(3.71305569296667 \times 10^{-8}\ g) \times (1000\ mg/g)$
$M_{Total}=37.13055693 \times 10^{-6}\ mg$

Typical dosage=600 mg
Total Number of Microspheres=$(600\ mg/37.13055693 \times 10^{-6}\ mg\ microsphere^{-1})$
Total Number of Microspheres=16.15919743×10^6
Total Number of Microspheres=16.0×10^6

Activity ($t\ s^{-1}$)=$(16.0 \times 10^6\ microspheres) \times (1.20 \times 10^2\ t\ s^{-1})/(937\ microspheres)$
Activity ($t\ s^{-1}$)=$2.049 \times 10^6\ t\ s^{-1}$
Activity ($t\ s^{-1}$)=$(2.049 \times 10^6\ Bq) \times (GBq/10^9\ Bq)$
Activity ($t\ s^{-1}$)=0.002049 GBq << 7.5-15 GBq ∴ **Neutron Flux not High Enough**
Activity attained only 0.027% of minimum required therapeutic value.

Pile-Shaped Packing Configuration:

$V=(4/3)\pi(0.00185\ cm)^3$
$V=2.65218263783333 \times 10^{-8}\ cm^3$

$M_{Total}=(1.4\ g/cm^3)(2.65218263783333 \times 10^{-8}\ cm^3)$
$M_{Total}=(3.71305569296667 \times 10^{-8}\ g) \times (1000\ mg/g)$
$M_{Total}=37.13055693 \times 10^{-6}\ mg$

Typical dosage=600 mg
Total Number of Microspheres=$(600\ mg/37.13055693 \times 10^{-6}\ mg\ microsphere^{-1})$
Total Number of Microspheres=16.15919743×10^6
Total Number of Microspheres=16.0×10^6

Activity ($t\ s^{-1}$)=$(16.0 \times 10^6\ microspheres) \times (1.44 \times 10^2\ t\ s^{-1})/(940\ microspheres)$
Activity ($t\ s^{-1}$)=$2.451 \times 10^6\ t\ s^{-1}$
Activity ($t\ s^{-1}$)=$(2.451 \times 10^6\ Bq) \times (GBq/10^9\ Bq)$
Activity ($t\ s^{-1}$)=0.002451 GBq << 7.5-15 GBq ∴ **Neutron Flux not High Enough**
Activity attained only 0.033% of minimum required therapeutic value.

APPENDIX G – Mass Fraction Calculations for Air Mass Component Concentrations inside irradiation vials and Thermal Column

Component (Dry Air)	Volume Ratio	Molecular Mass (kg/kmol)	Molecular Mass in Air (kg/kmol)
Oxygen	2.095×10^{-1}	32	6.704
Nitrogen	7.809×10^{-1}	28.02	21.88
Carbon Dioxide	3×10^{-4}	44.01	0.013
Hydrogen	5×10^{-7}	2.02	0
Argon	9.33×10^{-3}	39.94	0.373
Neon	1.8×10^{-5}	20.18	0
Helium	5×10^{-6}	4	0
Krypton	1×10^{-6}	83.8	0
Xenon	9×10^{-8}	131.29	0
Total Molecular Mass			28.97

Carbon

(1 kmol *C*/1 kmol CO_2) x (1 kmol CO_2/44.01 kg) x (12 kg/1 kmol *C*) = 0.272665 kg *C*/kg CO_2
(0.272665 kg *C*/kg CO_2) x (0.013 kg CO_2/kmol Air) = 0.00354465 kg *C*/kmol Air
0.013-0.00354465 = 0.00945536 kg O_2/Kmol Air
C mass fraction = (0.00354465 kg *C*/ kmol Air) x (1 kmol Air/28.97 kg)
C mass fraction = 0.00012236

Oxygen

O_2 mass fraction = (0.00945536 kg O_2/kmol Air) x (kmol Air/28.97 kg)
O_2 mass fraction = 0.00032638
O_2 mass fraction = (6.704 kg O_2/kmol Air) x (kmol Air/28.97 kg)
O_2 mass fraction = 0.23141181
O_2 mass fraction = 0.23141181 + 0.00032638
O_2 mass fraction = 0.23173819

Nitrogen

N_2 mass fraction = (21.88 kg N_2/kmol Air) x (kmol Air/28.97 kg)
N_2 mass fraction = 0.75526407

Argon

Ar mass fraction = (0.373 kg N_2/kmol Air) x (kmol Air/28.97 kg)
Ar mass fraction = (0.373 kg N_2/kmol Air) x (kmol Air/28.97 kg)
Ar mass fraction = 0.012875388

Check:

Ar mass fraction =	0.01287539
O_2 mass fraction =	0.23173819
C mass fraction =	0.00012236
N_2 mass fraction =	0.75526406
	1.0

APPENDIX H – Material's Physical Property Degradations after Neutron Activation

The following charts were generated using information found in *Ref. 17*. Once generated, equations for the curves were used to determined specific values of material properties such as melting point, enthalpy of fusion, and enthalpy of crystallization, at specified dose values within the range of 0 and 80 kGy:

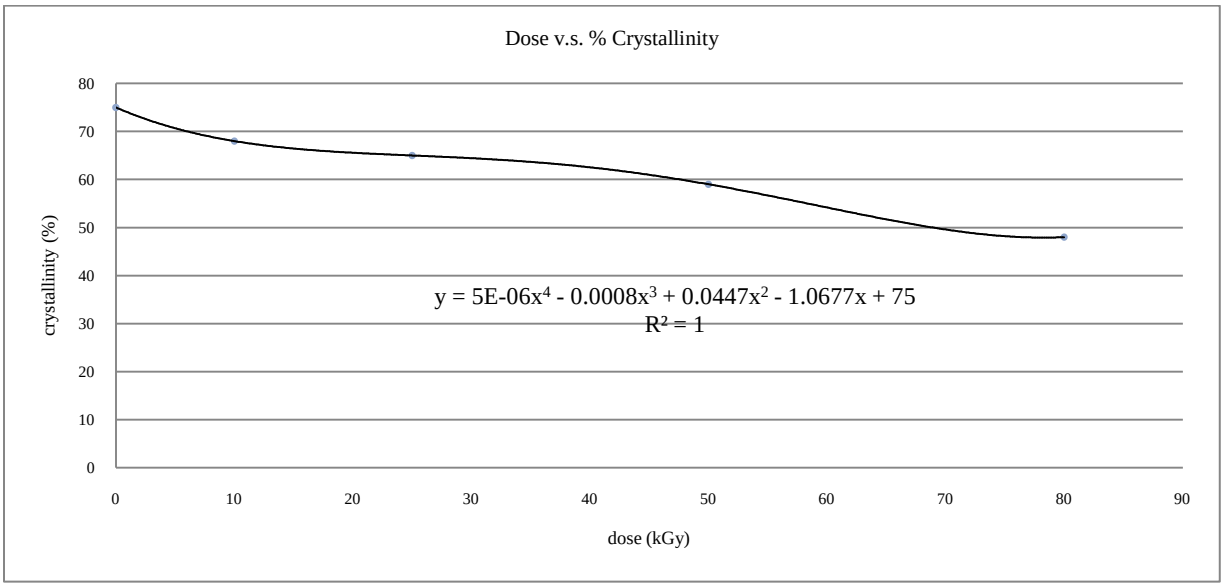

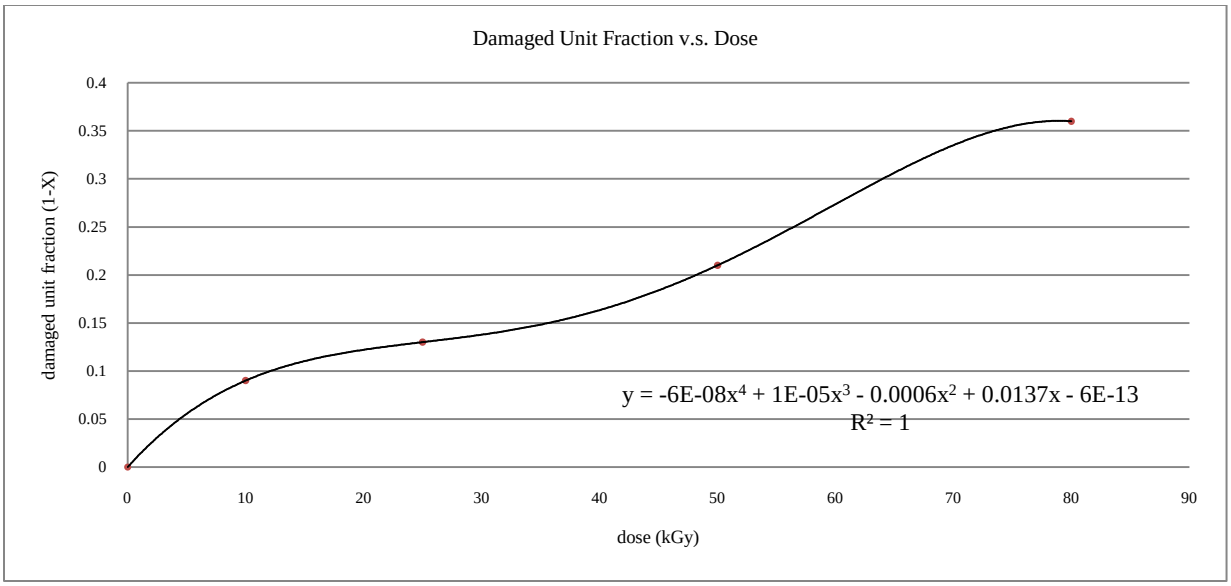
Damaged Unit Fraction v.s. Dose
damaged unit fraction (1-X)
0.4
0.35
0.3
0.25
0.2
0.15
0.1
0.05
0
0
10
20
30
40
50
60
70
80
90
dose (kGy)
y = -6E-08x4 + 1E-05x3 - 0.0006x2 + 0.0137x - 6E-13
R² = 1

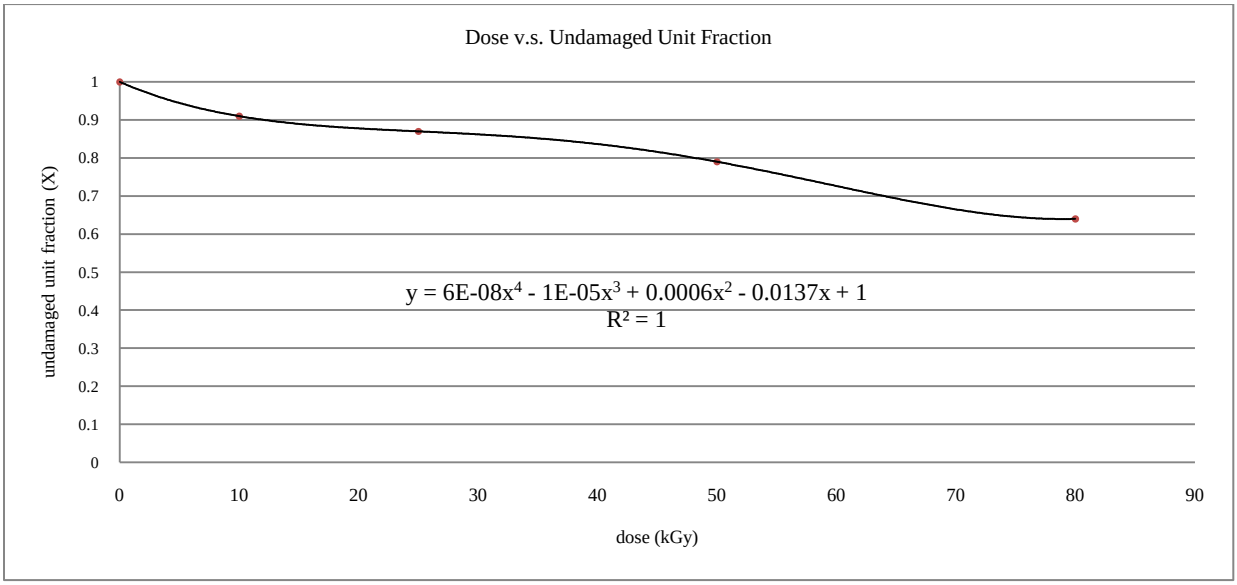
Dose v.s. Undamaged Unit Fraction
undamaged unit fraction (X)
1
0.9
0.8
0.7
0.6
0.5
0.4
0.3
0.2
0.1
0
0
10
20
30
40
50
60
70
80
90
dose (kGy)
y = 6E-08x4 - 1E-05x3 + 0.0006x2 - 0.0137x + 1
R² = 1

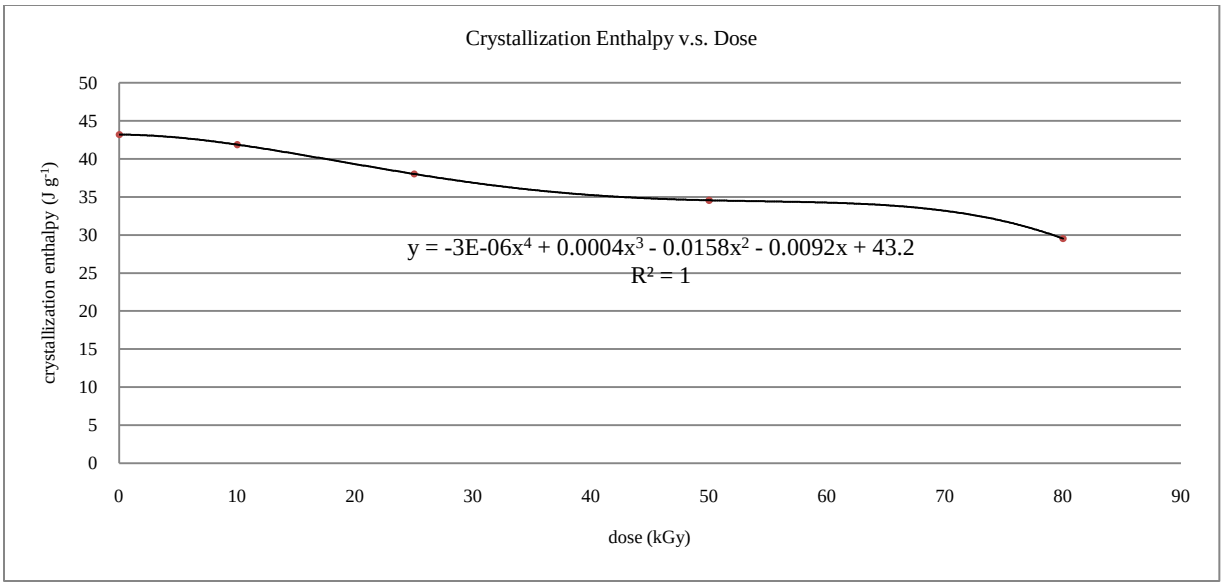

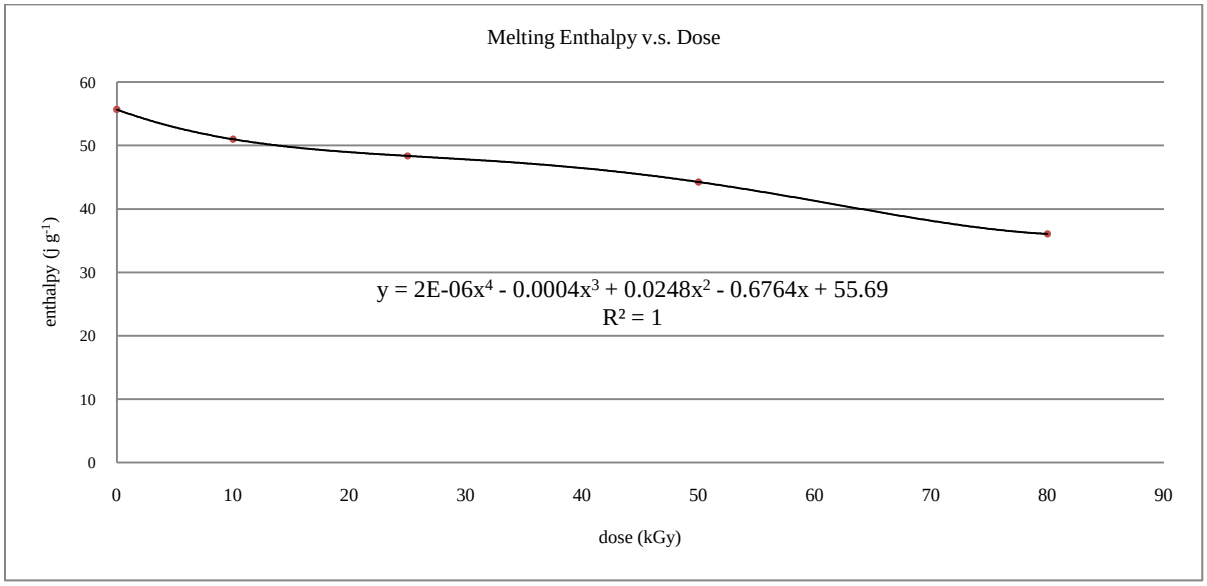

The charts generated below were used to compare the overall performance of both the sheet-shaped configuration and the pile-shaped configuration as a function of neutron-activation time. For example, if the summation of the melting point temperature of each microsphere in the sheet-

shaped configuration is greater than the summation of the melting point temperature of each microsphere in the pile-shaped configuration, then pile-shaped configuration experienced less degradation to its polymeric matrix than the pile-shaped configuration; the melting point temperature values for each microsphere in the sheet-shaped packing configuration were greater than the pile's. Similarly, other charts were generated for values such as % crystallinity, undamaged unit fraction, damaged unit fraction, enthalpy of fusion, and enthalpy of crystallization.

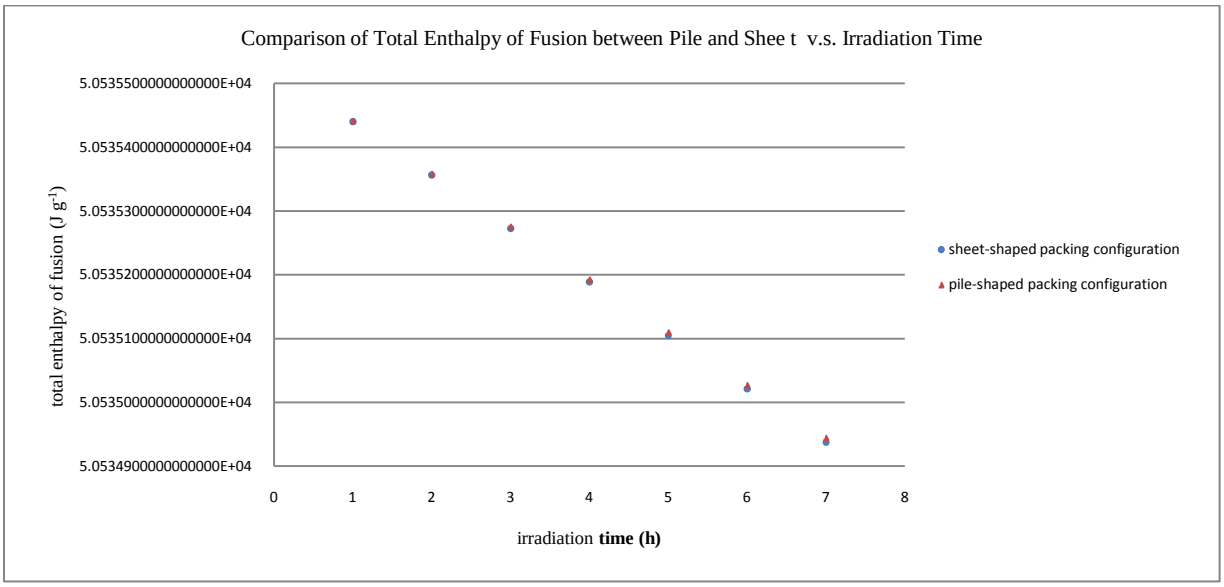

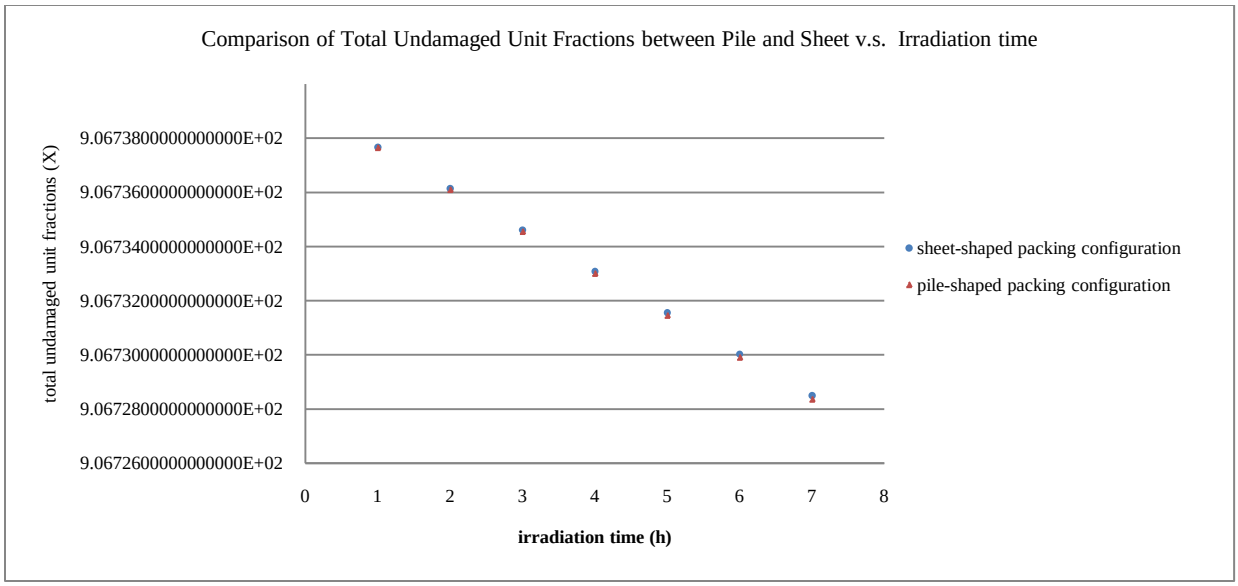
Comparison of Total Undamaged Unit Fractions between Pile and Sheet v.s. Irradiation time
total undamaged unit fractions (X)
9.0673800000000000E+02
9.0673600000000000E+02
9.0673400000000000E+02
9.0673200000000000E+02
9.0673000000000000E+02
9.0672800000000000E+02
9.0672600000000000E+02
0
1
2
3
4
5
6
7
8
irradiation time (h)
sheet-shaped packing configuration
pile-shaped packing configuration

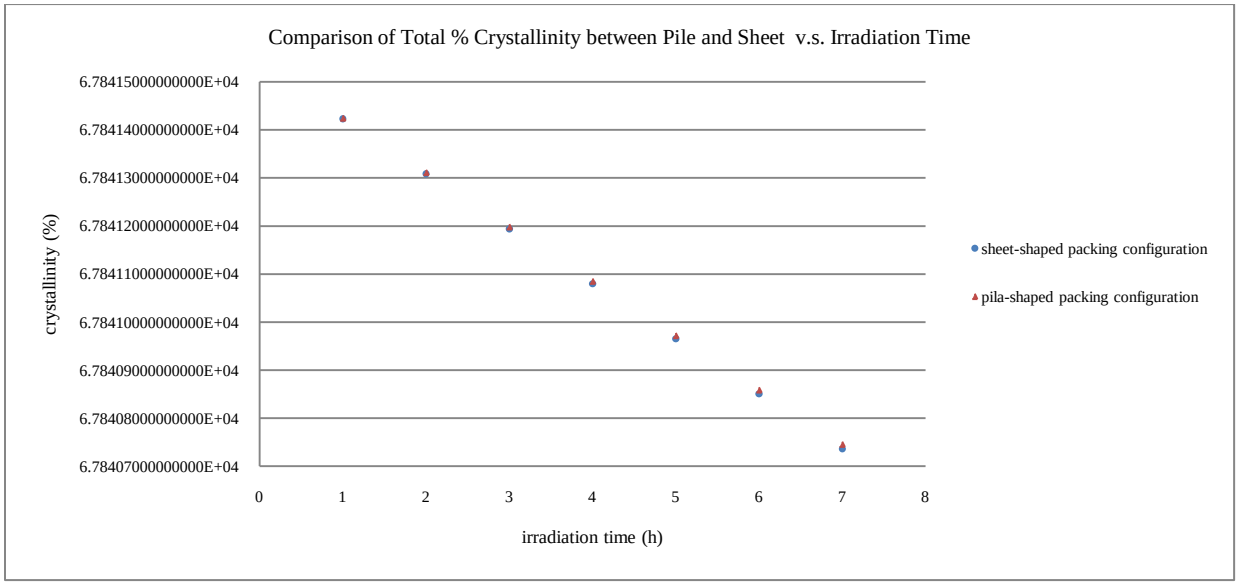
Comparison of Total % Crystallinity between Pile and Sheet v.s. Irradiation Time
crystallinity (%)
6.78415000000000E+04
6.78414000000000E+04
6.78413000000000E+04
6.78412000000000E+04
6.78411000000000E+04
6.78410000000000E+04
6.78409000000000E+04
6.78408000000000E+04
6.78407000000000E+04
0
1
2
3
4
5
6
7
8
irradiation time (h)
sheet-shaped packing configuration
pila-shaped packing configuration

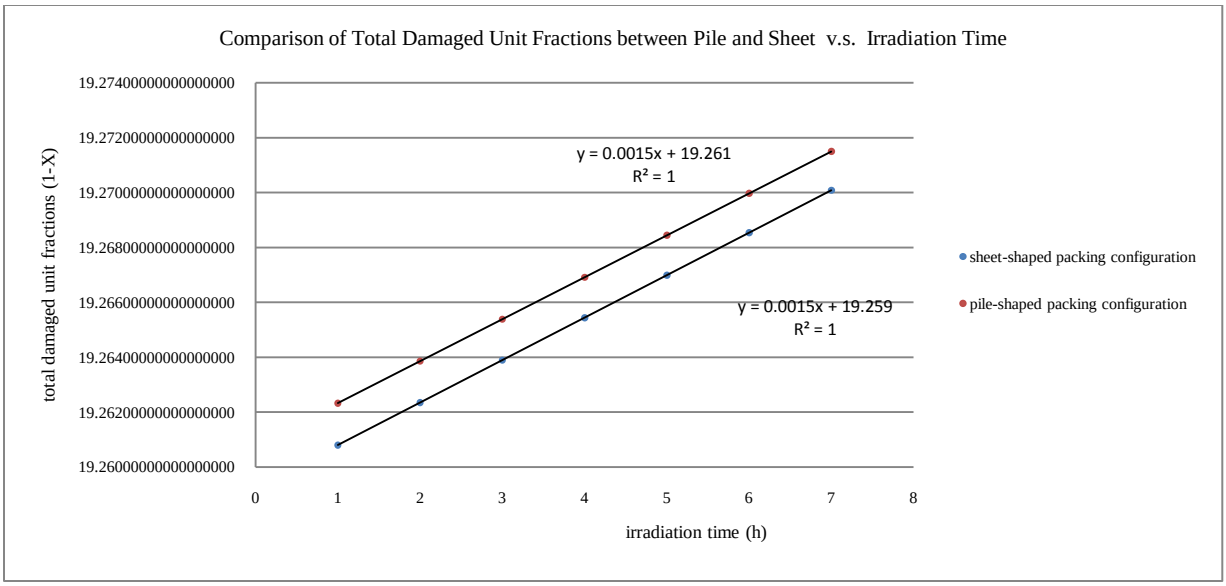
Comparison of Total Damaged Unit Fractions between Pile and Sheet v.s. Irradiation Time
total damaged unit fractions (1-X)
19.27400000000000000
19.27200000000000000
19.27000000000000000
19.26800000000000000
19.26600000000000000
19.26400000000000000
19.26200000000000000
19.26000000000000000
y = 0.0015x + 19.261
R² = 1
y = 0.0015x + 19.259
R² = 1
0
1
2
3
4
5
6
7
8
irradiation time (h)
sheet-shaped packing configuration
pile-shaped packing configuration

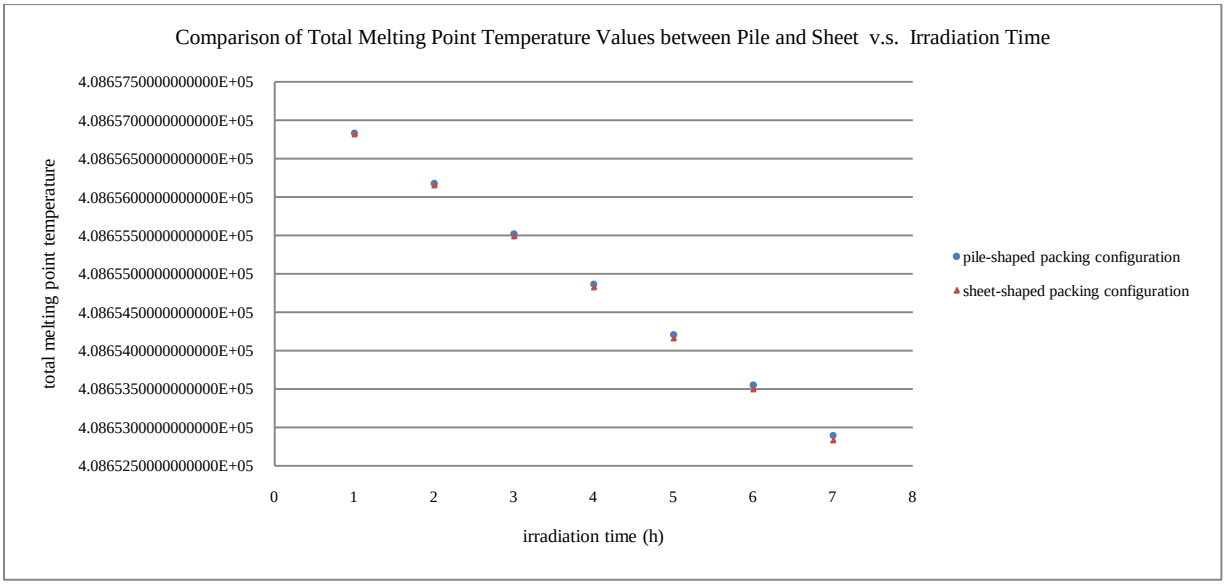
Comparison of Total Melting Point Temperature Values between Pile and Sheet v.s. Irradiation Time
total melting point temperature
4.08657500000000E+05
4.08657000000000E+05
4.08656500000000E+05
4.08656000000000E+05
4.08655500000000E+05
4.08655000000000E+05
4.08654500000000E+05
4.08654000000000E+05
4.08653500000000E+05
4.08653000000000E+05
4.08652500000000E+05
0
1
2
3
4
5
6
7
8
irradiation time (h)
pile-shaped packing configuration
sheet-shaped packing configuration

APPENDIX I – Potential Sheet-Shaped Packing Configuration Polymeric Inserts for Neutron Activating Microspheres Loaded with Holmium-165 in a PLLA Matrix